

# Radial velocity variability and evolution of hot subdwarf stars

S. Geier<sup>1</sup>, M. Dorsch<sup>2</sup>, I. Pelisoli<sup>3,1</sup>, N. Reindl<sup>1</sup>, U. Heber<sup>2</sup>, and A. Irrgang<sup>2</sup>

<sup>1</sup> Institut für Physik und Astronomie, Universität Potsdam, Haus 28, Karl-Liebknecht-Str. 24/25, D-14476 Potsdam-Golm, Germany

<sup>2</sup> Dr. Karl Remeis-Observatory & ECAP, Astronomical Institute, Friedrich-Alexander University Erlangen-Nuremberg, Sternwartstr. 7, D-96049 Bamberg, Germany

<sup>3</sup> Department of Physics, University of Warwick, Coventry, CV4 7AL, UK

Received Accepted

## ABSTRACT

Hot subdwarf stars represent a late and peculiar stage in the evolution of low-mass stars, because they are likely formed by close binary interactions. Here we performed a radial velocity (RV) variability study of a sample of 646 hot subdwarfs with multi-epoch radial velocities from Sloan Digital Sky Survey (SDSS) and Large Sky Area Multi-Object Fibre Spectroscopic Telescope (LAMOST) spectra. Atmospheric parameters and RVs were taken from the literature. For stars with archival spectra but without literature values, we determined the parameters by fitting model atmospheres. In addition, we redetermined the atmospheric parameters and RVs for all the He-enriched sdO/Bs. This large sample allowed us to study RV-variability as a function of the location in the  $T_{\text{eff}} - \log g$ - and  $T_{\text{eff}} - \log n(\text{He})/n(\text{H})$  diagrams in a statistically significant way. As diagnostics we used the fraction of RV-variable stars and the distribution of the maximum RV variations  $\Delta RV_{\text{max}}$ . Both indicators turned out to be quite inhomogeneous across the studied parameter ranges. A striking feature is the completely different behaviour of He-poor and He-rich hot subdwarfs. While the former have a high fraction of close binaries, almost no significant RV variations could be detected for the latter. This led us to the conclusion that there likely is no evolutionary connection between these subtypes. Intermediate He-rich- and extreme He-rich sdOB/Os on the other hand are likely related. We conclude further that the vast majority of this population is formed via one or several binary merger channels. Hot subdwarfs with temperatures cooler than  $\sim 24\,000$  K tend to show less and smaller RV-variations. These objects might constitute a new subpopulation of binaries with longer periods and late-type or compact companions. The RV-variability properties of the extreme horizontal branch (EHB) and corresponding post-EHB populations of the He-poor hot subdwarfs match and confirm the predicted evolutionary connection between them. Stars found below the canonical EHB at somewhat higher surface gravities show large RV-variations and a high RV-variability fraction, which is consistent with most of them being low-mass EHB stars or progenitors of low-mass helium white dwarfs in close binaries.

**Key words.** stars: subdwarfs – stars: horizontal branch – stars: binaries

## 1. Introduction

Hot subdwarf stars (sdO/Bs) constitute a prominent population of faint blue stars at high Galactic latitudes (Heber 2009, 2016). With masses around  $0.5 M_{\odot}$  and radii between  $0.1 R_{\odot}$  and  $0.3 R_{\odot}$  they are much smaller and of lower mass than hot main sequence stars of similar spectral types. Hot subdwarfs can form after main sequence stars such as the Sun expand and become red giants. This expansion stops as soon as helium burning starts in the red giant cores. Most of the observed subluminescent B stars (sdBs) have been identified as extreme horizontal branch (EHB) stars burning helium in their cores (Heber 1986). Although sdBs and sdOs occupy neighboring regions in the Hertzsprung-Russell diagram, they are quite different with respect to their chemical compositions. The atmospheres of sdBs are mostly helium poor and their helium abundances can be extremely low. Subluminescent OB and O stars, on the other hand, show a large variety of helium abundances and can be divided in helium-poor sdOB/Os ( $\log n(\text{He})/n(\text{H}) \leq -1.0$ ), intermediate helium-rich iHe-sdOB/Os ( $\log n(\text{He})/n(\text{H}) = -1.0 \dots 0.6$ ), and extreme helium-rich eHe-sdOB/Os ( $\log n(\text{He})/n(\text{H}) > 0.6$ ).

Hot subdwarfs can only be formed if the progenitor loses its envelope almost entirely after passing the red-giant branch (RGB) or if the ignition of He-burning occurs in an evolutionary

stage late enough for the star to be already devoid of hydrogen. This is very difficult to explain in the context of single-star evolution, although single-star scenarios are still discussed. The attention shifted to binary evolution, when systematic surveys for radial velocity (RV) variable stars revealed a significant fraction (about one third) of the sdB stars to be members of close binaries (see Appendix A). A similarly large fraction of the observed hot subdwarfs showed spectral features of cool main-sequence companions in wide binaries (see Stark & Wade 2003 and references therein).

Motivated by these discoveries, binary evolution scenarios were worked out (see Han et al. 2002, 2003 and references therein). Stable mass transfer to a main sequence companion via Roche lobe overflow (RLOF) has been proposed as major formation scenario for hot subdwarfs by Han et al. (2002, 2003) and composite sdB binaries with the predicted properties have later been discovered and studied (Vos et al. 2018 and references therein; Chen et al. 2013; Vos et al. 2020). The envelope stripping of intermediate and high-mass stars might lead to the formation of core helium-burning stars with higher masses as well (Götberg et al. 2018).

To form close hot subdwarf binaries common envelope (CE) ejection is the only likely channel (see Han et al. 2002, 2003 and references therein). Several studies discovered and analysed hot subdwarfs in close binaries ( $P \simeq 0.03 - 30$  d) both with time-resolved spectroscopy and photometry (e.g. Copperwheat et al.

Send offprint requests to: S. Geier,  
e-mail: sgeier@astro.physik.uni-potsdam.de

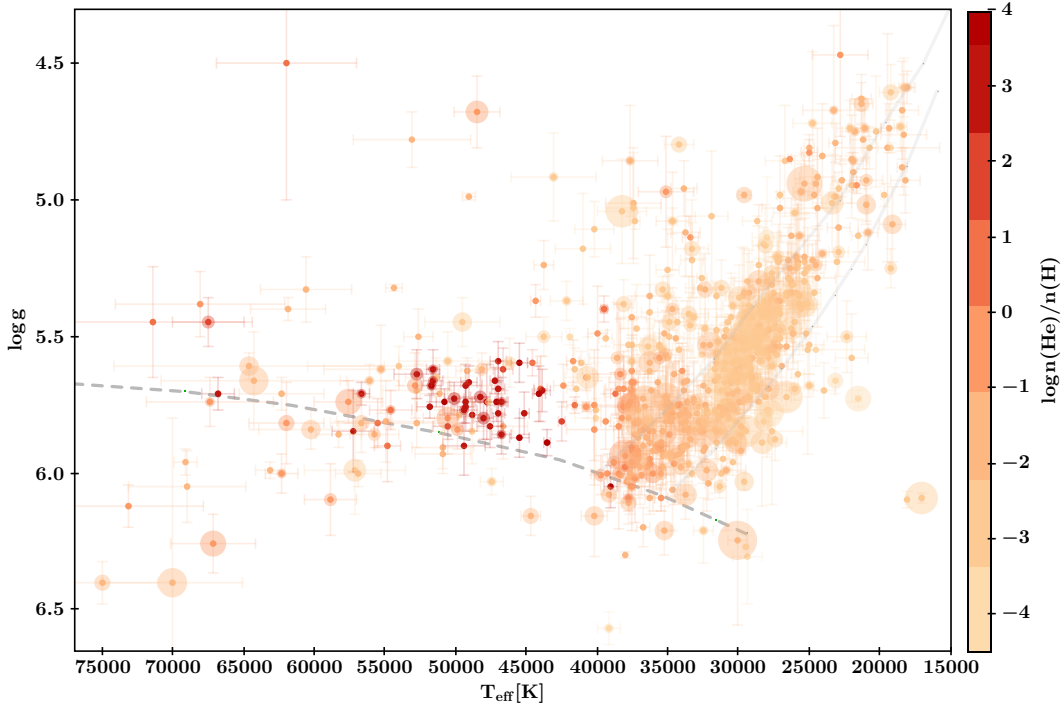


**Fig. 1.**  $T_{\text{eff}} - \log g$  diagram of the full sample of hot subluminescent stars. The size of the symbols scales with  $\Delta RV_{\text{max}}$ , the colour with the helium abundance from light orange to red. The EHB band (solid lines) is based on evolutionary tracks with subsolar metallicity ( $\log z = -1.48$ ) from Dorman et al. (1993). The helium main sequence (dashed line) is taken from Paczynski (1971).

2011; Kawka et al. 2015; Kupfer et al. 2015; Schaffenroth et al. 2019). The majority of the mostly unseen companions are low-mass white dwarfs (WDs) and late main-sequence stars of spectral type M. A significant fraction of the sdBs are orbited by brown dwarfs (Schaffenroth et al. 2018 and references therein) and some have more massive compact companions (e.g. Geier et al. 2007, 2010). Even three close double hot subdwarf binaries have been found (Sener & Jeffery 2014; Finch et al. 2019; Reindl et al. 2020), some of which likely formed via double-core CE evolution (Justham et al. 2011). Also the stripping by massive planets has been studied (Soker 1998; Nelemans & Tauris 1998; Kramer et al. 2020).

About one third of the hot subdwarfs in the field show no indication for binarity and the fraction of those stars turns out to be much higher in globular clusters (GCs, Latour et al. 2018). The merger of two helium white dwarfs (Webbink 1984) was proposed to explain the existence of those objects in the framework of binary evolution as well as mergers of a low-mass star or brown dwarf with a red-giant core (Soker 1998; Politano et al. 2008; Kramer et al. 2020). Politano et al. (2008) predicted that this would lead to rapidly rotating single sdB stars. While the large majority of single sdBs are very slow rotators (Geier & Heber 2012), Geier et al. (2011a, 2013b) discovered two single sdBs, which are indeed fast rotators. Clausen et al. (2011), however, propose that the coalescence of a helium white dwarf with a low-mass, hydrogen-burning star would create a star with a helium core and a thick hydrogen envelope that evolves into an sdB star after a few Gyrs, which would also naturally explain the sdBs' slow rotation rates.

Mixing processes during the merger of He-WDs are more consistent with the helium-rich composition of the He-sdOs. The location of the He-sdOs slightly blueward of the EHB (Ströer et al. 2007; Nemeth et al. 2012) matches with theoretical He-WD

merger tracks (Zhang & Jeffery 2012). In addition, the population of He-sdOs seems to consist mostly of single stars (see Appendix A). Justham et al. (2011) proposed a merger channel involving a core-helium burning sdB and a He-WD for the formation of He-sdOs.

Most recently, more evidence for the diverse types of merger formation channels has been found. Vos et al. (2021) discovered a hydrogen-rich sdB star surrounded by a gas disc indicative of a young merger product, Dorsch et al. (2022) presented a magnetic He-sdO perfectly consistent with the predictions of the He-WD merger channel, and finally Werner et al. (2022) reported the discovery of a whole new class of helium-rich sdOs showing extreme enrichments in carbon and oxygen, which are explained as the mergers of CO and He-WDs (Miller Bertolami et al. 2022).

Hot subdwarf stars might also form by mixing processes inside a single star without any binary interactions. Castellani & Castellani (1993) showed that sufficient mass loss on the RGB can lead to a delayed helium core flash (e.g. D'Cruz et al. 1996; Brown et al. 2001). The flash drives convection and mixes the H-rich envelope into interior layers, where it is burned (Sweigart 1997a, 1997b). The later the flash, the deeper the mixing leading to a higher helium abundance on the surface (Cassisi et al. 2003; Lanz et al. 2004; Miller Bertolami et al. 2008). An early hot flasher might explain single hydrogen-rich sdB stars, while late hot flashers might produce sdO/Bs enriched in helium (Naslim et al. 2013; Dorsch et al. 2019). The deep mixing variant of a hot flasher scenario is most promising to explain the origin of the carbon-rich He-sdO stars (Heber et al. 2010; Schindewolf et al. 2018). To explain EHB stars in globular clusters and elliptical galaxies, the enrichment of their parent population with helium has been proposed (e.g. Yi 2008 and references therein).

The general features visible in the  $T_{\text{eff}} - \log g$  plane seem to be consistent with the main evolutionary channels and evolution-

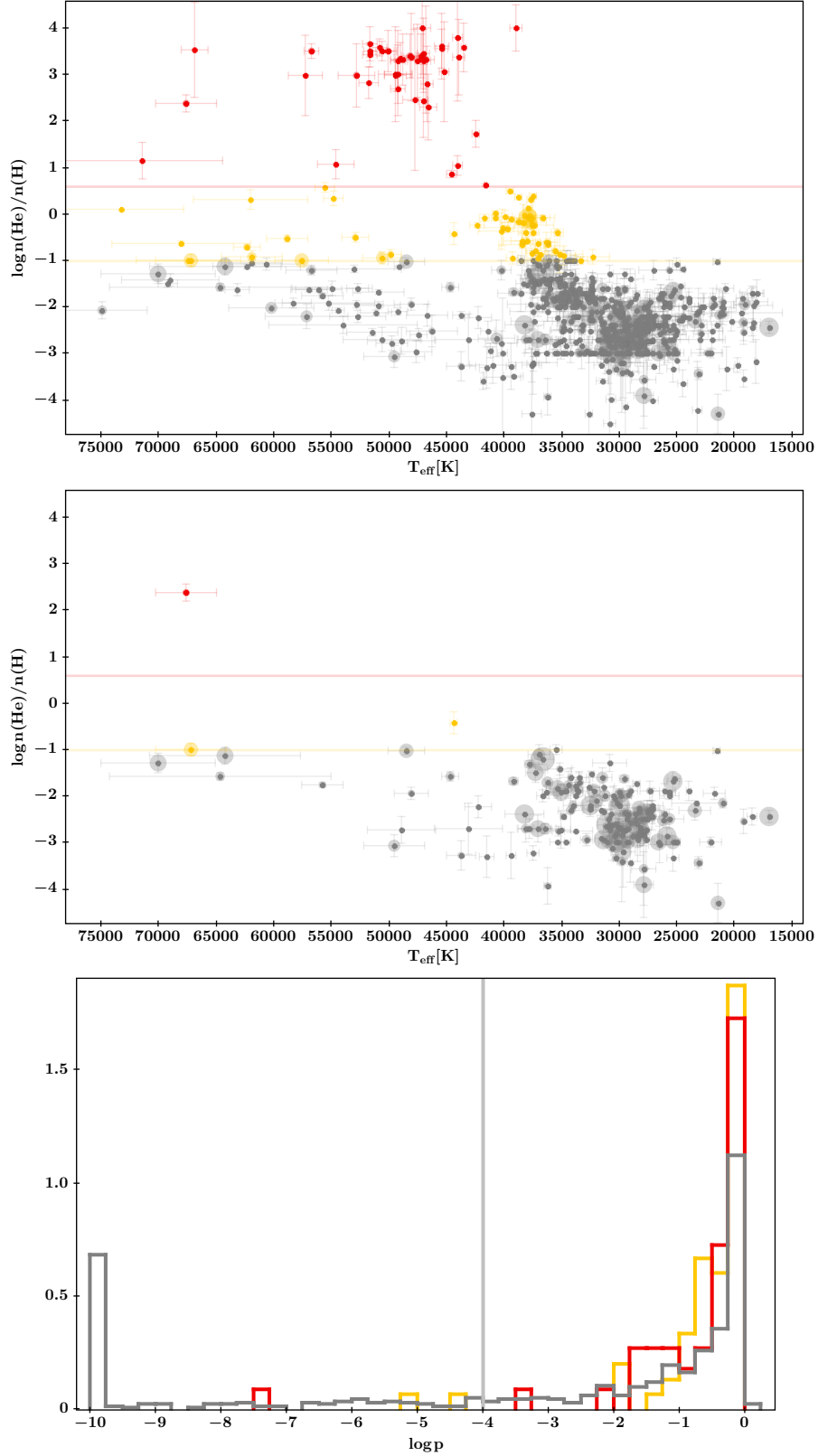


**Fig. 2.** Upper panel:  $T_{\text{eff}} - \log n(\text{He})/n(\text{H})$  diagram of the full sample. Helium-poor stars are marked in grey, intermediate helium-rich ones in orange and extreme helium-rich ones in red. The size of the symbols scales with  $\Delta RV_{\text{max}}$ . Solar helium abundance is marked by the orange horizontal line, while the red line marks the transition between intermediate and extreme helium abundance. Middle panel: The same diagram for the stars showing significant RV variability ( $\log p < -4.0$ ). Lower panel:  $\log p$  distribution of the sample using the same colour-coding as in the upper panels. The significance level  $\log p < -4.0$  is marked by a vertical line. The distribution has been limited to  $\log p > -10$  and all objects with smaller  $\log p$  have been stacked in the first bin for visualisation.

ary tracks (Dorman et al. 1993; Han et al. 2002, 2003; Bloemen et al. 2014; Xiong et al. 2017). Most sdBs are situated on the canonical EHB corresponding to a mass of  $\sim 0.47 M_{\odot}$ , while the sdOB and sdO stars are located in the region of the post-EHB tracks, indicating an evolutionary link between those subclasses such that sdB stars will evolve to become sdOB and finally sdO stars before entering the WD cooling tracks.

The He-sdO stars are concentrated in a region close to the helium main sequence where both the hot-flasher and merger tracks intersect. After the core helium-burning phase they evolve through a shell burning phase to hotter temperatures. Some of them might evolve to become very rare O(He) type stars and finally cool down as helium-rich WDs (Reindl et al. 2014).

Only few sdBs are found to lie below the canonical EHB. All of them seem to be pre-He-WD objects in close binaries, which got stripped before the helium burning started in the core (e.g. Heber et al. 2003). Those stars cross the EHB region while cooling down to become He-WDs and the evolutionary timescale for this process depends on their masses (Driebe et al. 1998; Althaus et al. 2013; Istrate et al. 2016).

Binary evolution scenarios also predict substructures to be present on the EHB (e.g. Han et al. 2002, 2003; Xiong et al. 2017), due to the different formation channels. Hot subdwarfs from the CE-channel are predicted to occupy a region different from the hot subdwarfs formed via the RLOF- or merger-channels. However, those regions partly overlap and the observed samples are affected by selection effects (Han et al. 2003). In addition, Naslim et al. (2012) proposed intermediate He-sdOBs with very peculiar metal-rich abundance patterns to be pre- instead of post-EHB objects, creating another degeneracy in the  $T_{\text{eff}} - \log g$  plane.

The degeneracies between the diverse evolutionary models make it difficult to link the various types of hot subdwarfs. Using other characteristic observable properties seems to be a way forward. Usually the chemical composition is used for that purpose. However, the abundance patterns of hot subdwarfs are strongly affected by diffusion processes (O’Toole & Heber 2006; Hu et al. 2011; Michaud et al. 2011; Geier 2013; Schneider et al. 2018; Byrne et al. 2018). Miller Bertolami et al. (2008) argue that He-sdO stars might even turn into sdBs due to gravitational settling in their atmospheres (see also Nemeth et al. 2012; Luo et al. 2016). For the hottest stages of post-EHB evolution also fractionated stellar winds are predicted to change the abundances (Unglaub 2008; Krticka et al. 2016).

Since binary interactions play an important role for the formation of hot subdwarfs, we find many sdO/Bs in binary systems. In contrast to the chemical composition of the atmosphere, the properties of those binary systems are almost unaffected by the evolution in the sdO/B stage. Only the closest known sdB binaries will shrink significantly due to the emission of gravitational waves while evolving on and off the EHB and might even undergo another phase of mass transfer (see Kupfer et al. 2020 and references therein). For all other hot subdwarf binaries, the orbital parameters and the properties of the companions remain essentially unchanged.

Most previous studies of the RV variability of hot subdwarf stars (Maxted et al. 2001; Napiwotzki et al. 2004a; Morales-Rueda et al. 2003; Copperwheat et al. 2011; Kawka et al. 2015) found that He-sdO/Bs and sdBs with composite spectra usually do not show significant RV variability (indications for significant RV variations of He-sdOs have been found by Green et al. 2008 and Geier et al. 2015b, 2017a), while the variability fractions of stars in the EHB and post-EHB region were rather inconsistent ranging from 30 – 70%. Selection effects such as preferential

selection of the closest binaries or a biased mix of objects from different Galactic populations were proposed as possible reasons for these inconsistencies (see Appendix A for details).

Recently, Pelisoli et al. (2020) compared the fraction of wide, non-interacting hot subdwarf binaries with the respective fraction of the progenitor population of low-mass main sequence stars. The lack of such systems among the hot subdwarfs allowed the authors to provide observational evidence that pure single star evolution is very unlikely to result in the formation of sdO/B stars and that binary interactions are likely always required.

Here we aim at using the close binary properties of hot subdwarf stars, which affect their RV variability, to put constraints on their formation and study their evolutionary links.

## 2. A sample of hot subdwarfs with multi-epoch radial velocities

### 2.1. Sample selection

The sample studied here was compiled from the catalogue of spectroscopically classified hot subdwarfs (Geier et al. 2017a) Data Release 2 (Geier 2020).<sup>1</sup> The catalogue was crossmatched with the catalogues of the Sloan Digital Sky Survey Data Release 12 (SDSS DR12, Alam et al. 2015) and the Large Sky Area Multi-Object Fibre Spectroscopic Telescope Data Release 5 (LAMOST DR5, Luo et al. 2019) and stars with spectra taken at two or more epochs separated by a at least one day were selected.

The study is restricted to sdO/Bs, which are not in composite binaries with companions visible in the spectrum. The main reason is that the atmospheric parameters of those double-lined binaries are more complicated to be determined and they are therefore often removed from analyses of larger samples (e.g. Luo et al. 2021). Only few composite sdB binaries have been analysed in detail so far (e.g. Dorsch et al. 2021; Nemeth et al. 2012, 2021). It can also happen that the contribution of the companion is rather weak and not easily apparent when looking at the spectral features alone. The contribution to the continuum flux, however, can introduce significant systematic shifts in the atmospheric parameters usually towards higher temperatures and lower surface gravities. It is therefore important to exclude such a visible companion before performing a spectral analysis.

Known composite systems consisting of sdO/B stars and main-sequence F/G/K companions have therefore been excluded. In a second step we examined the spectral energy distributions (SEDs) of all the stars as described in Heber et al. (2018) to search for yet undetected composite binary systems and excluded them from our sample. This latter method is more sensitive than the inspection of optical spectra and allows to detect cool main sequence companions down late K-type. Our final sample is therefore restricted to single-lined stars. The companions in the detected close binary systems are either M-type main sequence stars, substellar objects, or compact objects such as white dwarfs.

Although the selection functions of the sub-surveys conducted by SDSS and LAMOST are quite complicated, there should be no bias in favour or against RV-variable sdO/B stars within the observed sdO/B samples, because single-lined RV-variable and RV-constant sdO/Bs are indistinguishable in terms

<sup>1</sup> The catalogue contains most likely AGB manqué sdO/B type stars. The hotter sdO stars associated with post-AGB evolution have been excluded. For an early RV variability study of such objects see Reindl et al. (2016).

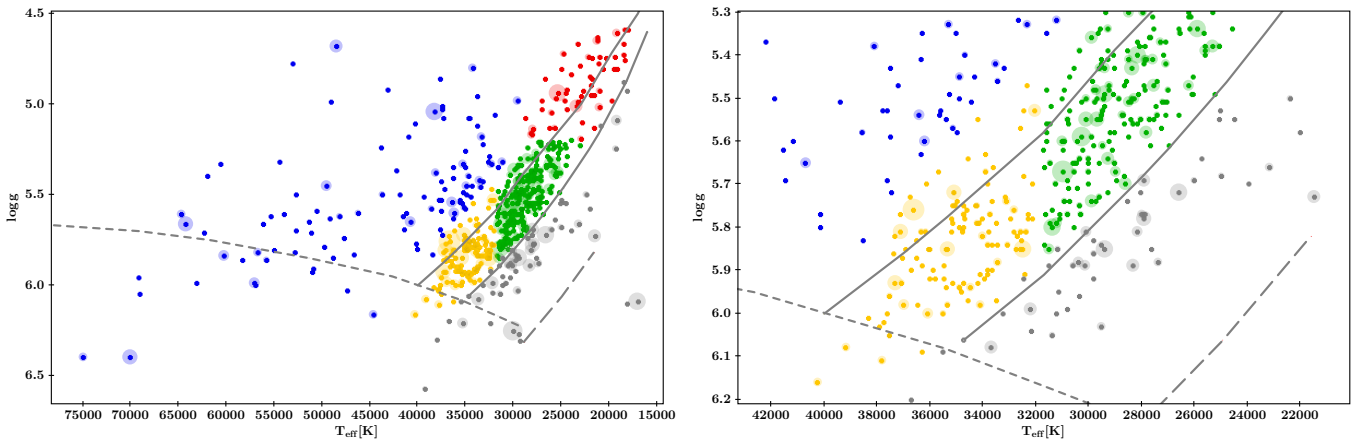


**Fig. 3.** Left panel:  $T_{\text{eff}} - \log g$  diagram similar to Fig. 1 of the sample of He-poor sdO/Bs with different regions marked by colour (EHB1 red, EHB2 green, EHB3 yellow, postEHB blue, bEHB grey) and the size of the symbol encoding  $\Delta RV_{\text{max}}$ . In addition to the canonical EHB for a mass of  $0.47 M_{\odot}$  (Dorman et al. 1993) the EHB for a low mass of  $0.35 M_{\odot}$  (Han et al. 2002) is plotted as long-dashed grey line. Right panel: Close-up of the same diagram showing the division between the regions EHB2 and EHB3 in more detail.

of colour or luminosity. The observing epochs can be considered as randomly distributed and the timespans between single measurements range from one day to several hundred days. Also in this respect the sample is completely unbiased against short or long periods of variability.

Some bias might be introduced by the different exposure times of the LAMOST and SDSS spectra. While the former spectra are exposed for 50 min, the latter ones are exposed for 15 min. For very short period binaries with high RV-variations the LAMOST spectra will be affected by orbital smearing, which should in general lead to an underestimation of the RV shifts. Biases are also introduced by the different sampling of the RV curves and the different number of epochs per object as well as the limited accuracy of our RV measurements (see Sect. 2.3). All those biases, however, should affect the sub-samples we want to study similarly and therefore allow us to compare them in a meaningful way.

## 2.2. Atmospheric parameters

The atmospheric parameters effective temperature  $T_{\text{eff}}$ , surface gravity  $\log g$ , and helium abundance  $\log n(\text{He})/n(\text{H})$  for the hydrogen-rich sdB and sdOB stars ( $\log n(\text{He})/n(\text{H}) < -1.0$ ) have been taken from the literature (Heber et al. 1987; Saffer et al. 1994; Maxted et al. 2001; Edelmann et al. 2003; Lisker et al. 2005; Ströer et al. 2007; Charpinet et al. 2008; Hirsch 2009; Østensen et al. 2010a, 2010b; Nemeth et al. 2012; Geier et al. 2013a, 2014, 2015b, 2017c; Luo et al. 2016, 2019, 2021; Lei et al. 2018, 2019, 2020; Kepler et al. 2019; Hogg et al. 2020), if available.

For the hydrogen-rich sdB and sdOB stars without any parameter determination in the literature, we fitted model spectra to the hydrogen and helium lines of the SDSS, BOSS or LAMOST spectra downloaded from the respective data archives using the SPAS routine (Hirsch 2009) as described in Geier et al. (2011b). To increase the S/N, multiple spectra of one star have been shifted to rest wavelength and coadded.

The quantitative spectral analysis was based on a new grid of model atmospheres and synthetic hydrogen and helium spectra calculated with the ATLAS12 (Kurucz 1996), DETAIL, and SURFACE codes (Giddings 1981; Butler & Giddings 1985) that allowed us

to treat some non-local thermodynamical equilibrium (NLTE) effects. All three codes were updated (Pryzbilla et al. 2011; Irrgang et al. 2018) and a grid covering the parameter range of hot subdwarfs was calculated (e.g. Schaffenroth et al. 2021).

Owing to more pronounced NLTE-effects present in He-sdO/B stars, we re-determined the atmospheric parameters of all helium-enriched ( $\log n(\text{He})/n(\text{H}) \geq -1.0$ ) subdwarfs in our sample as described above using the SPAS routine together with a NLTE grid (Dorsch et al. 2019). For this we computed non-LTE model atmospheres including hydrogen, helium, carbon, nitrogen, and silicon using the TLUSTY and SYNSPEC codes developed by Hubeny (1988) and Lanz & Hubeny (2003).

Finally, sdO stars with temperatures higher than 70 000 K have all been re-fitted with a grid of metal-free NLTE-models (Reindl et al. 2016). For the model calculations we used the Tübingen non-LTE model-atmosphere package (TMAP, Werner et al. 2003; Rauch & Deetjen 2003; Werner et al. 2012).

Our final sample consists of 646 stars with atmospheric parameter determinations and at least two epochs of spectroscopy.

## 2.3. Radial velocities and criterion for variability

The radial velocities of the SDSS<sup>2</sup> and LAMOST spectra provided in the archives are measured by matching template spectra to the data. In addition to the statistical uncertainties provided in the databases, systematic uncertainties have been determined to be about  $5 \text{ km s}^{-1}$  for all three spectrographs (Yanny et al. 2009; Bolton et al. 2012; Gao et al. 2015). The LAMOST spectra have exposure times of 50 min and we downloaded the RVs for the hydrogen-rich sdO/B stars in our sample from the LAMOST DR5 using the VizieR database.

The SDSS spectra taken with the SDSS and the upgraded BOSS spectrograph are co-added from at least three individual integrations with typical exposure times of 15 min. Although in most cases those individual spectra are taken consecutively, sometimes also exposures taken with the same plate at different nights are stacked together to produce a co-added spectrum (Stoughton et al. 2002). While this is not an issue for stars with small or no RV-variability (such as the majority of the main-

<sup>2</sup> <https://www.sdss.org/dr12/algorithms/redshifts/>

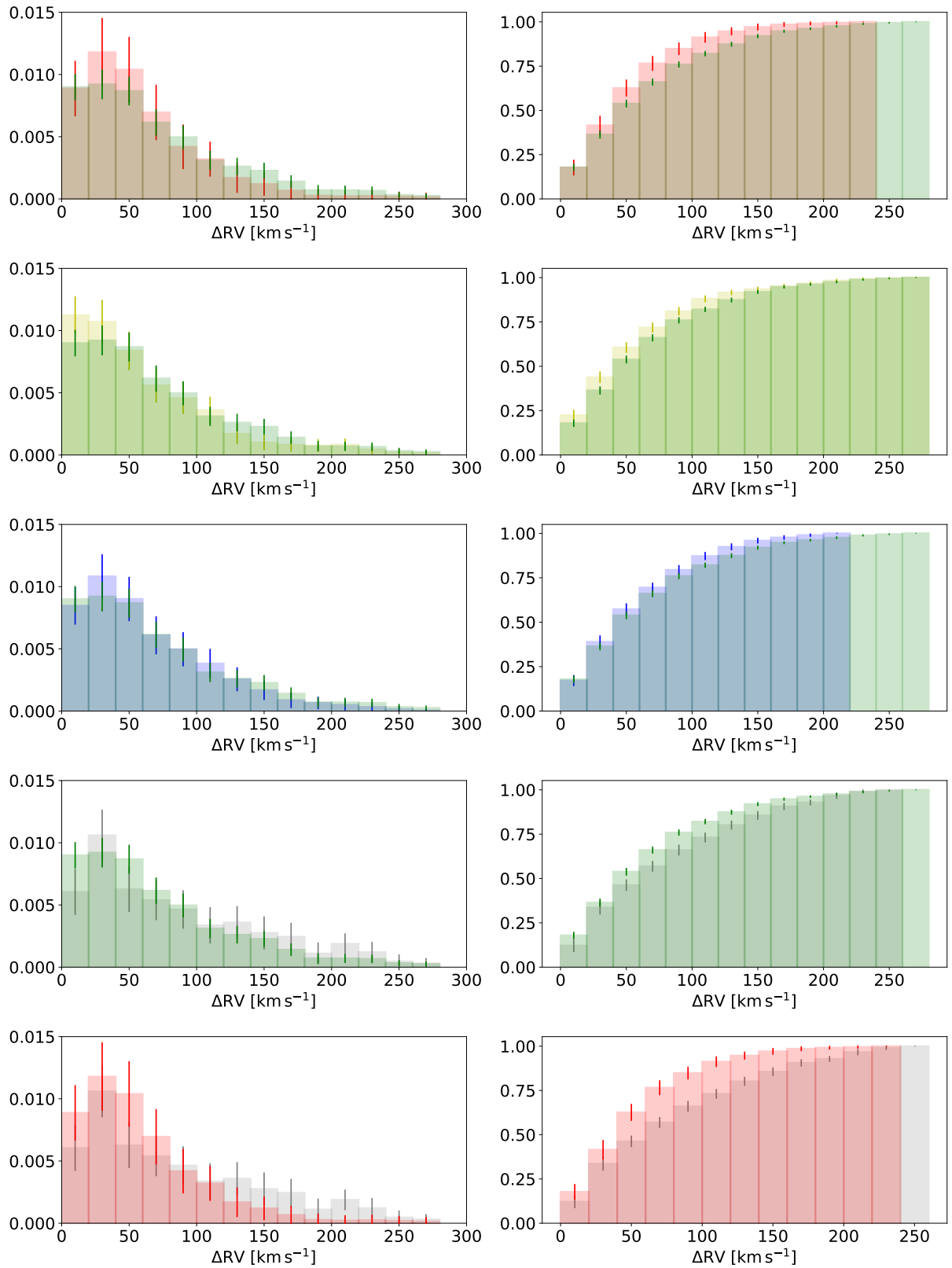


**Fig. 4.** Comparison of the normalised  $\Delta RV_{\max}$  distributions (left panels) and the normalised cumulative  $\Delta RV_{\max}$  distributions (right panels) in the different regions. From top to bottom: EHB1 (red) and EHB2 (green), EHB3 (yellow) and EHB2 (green), postEHB (blue) and EHB2 (green), bEHB (grey) and EHB2 (green), and bEHB (grey) and EHB1 (red). It has to be pointed out that the contribution of stars with high RV shifts tends to be visually overrepresented in the cumulative distributions and is better visible in the normalised distributions.

sequence stars) or extragalactic objects, it can lead to erroneous RV measurements for objects showing high intrinsic RV variability such as close hot subdwarf binaries.

We therefore did not use the RVs from the co-added spectra provided in the SDSS archive. Furthermore, for the helium-rich sdO/B stars in our sample, we could also not rely on the archival RVs, because the template databases do not contain proper He-rich templates. This can lead to a systematic shift in RV especially for hot stars, because the He II lines of the Pickering series are erroneously fitted as hydrogen Balmer lines. The most prominent example for this effect is the hypervelocity He-sdO US 708, where the RV measurement from SDSS is off by more than  $100 \text{ km s}^{-1}$  (Geier et al. 2015a).

We downloaded all the individual SDSS and BOSS spectra as well as the LAMOST spectra of the He-sdO/Bs in the sample and measured the RVs using fixed sets of prominent spectral lines. For the hydrogen-rich sdO/Bs we used the hydrogen Balmer lines  $H_\beta$ ,  $H_\gamma$  and  $H_\delta$ . For the He-sdO/Bs we used the helium lines He I 4472, He I 4922, He II 4541, He II 4686, and He II 5412. The lines were fitted with model spectra (Ströer et al. 2007) by means of chi-squared minimization using the FITSB2 routine (Napiwotzki et al. 2004b), and statistical  $1\sigma$  errors were calculated. A systematic uncertainty of  $5 \text{ km s}^{-1}$  has been added in quadrature to our own measurements and the RVs provided in the LAMOST DR5 to obtain the final uncertainty of each measurement. Highly uncertain RV measurements with errors of more than  $50 \text{ km s}^{-1}$  have been discarded. In total, we measured and compiled 4311 single RVs for the 646 objects in our sample.

The maximum RV variation  $\Delta RV_{\text{max}}$  was calculated as the difference between the maximum and the minimum RV of the star and the associated uncertainty was propagated from the uncertainties of the respective extreme measurements. To estimate the fraction of false detections produced by random outliers and calculate the significance of the measured RV variations we applied the method outlined in Maxted et al. (2001), which was also used in similar studies by Geier et al. (2015b, 2017a), Latour et al. (2018) and Napiwotzki et al. (2020).

For each star we calculate the inverse-variance weighted mean velocity from all measured epochs. Assuming this mean velocity to be constant, we calculate the  $\chi^2$ . Comparing this value with the  $\chi^2$ -distribution for the appropriate number of degrees of freedom we calculate the probability  $p$  of obtaining the observed value of  $\chi^2$  or higher from random fluctuations around a constant value. The detection of RV variability is considered to be significant, if the false-detection probability  $p$  is smaller than 0.01% ( $\log p < -4.0$ ). Stars with false-detection probabilities ranging between 0.01% and 5% ( $\log p = -4.0$  to  $\log p = -1.3$ ) should be regarded as candidates, where follow-up spectroscopy might reveal significant RV variations in the future.

The variability fractions in this study have been determined based on the number of objects with false detection probabilities smaller than 0.01% ( $\log p < -4.0$ ). Given the low-number statistics, the uncertainties of the variability fractions were calculated assuming a binomial distribution and indicate the 68% confidence-level interval (see e.g. Burgasser et al. 2003). It has to be pointed out, that the variability fractions have to be regarded as lower limits only, because the average uncertainty of our RV measurements is  $18 \text{ km s}^{-1}$  and in many cases we cannot exclude variations smaller than that. This is also the reason why we only use them for a differential analysis of the diverse subsamples studied here.

In Table A.1 we provide the atmospheric parameters with literature reference, the number of RV epochs, weighted mean RVs,  $\Delta RV_{\text{max}}$ , and false alarm probabilities  $\log p$  for all the stars

in our sample. The individual RVs will be published in a separate catalogue paper. The sample contains 164 stars with significant RV-variations. Only 19 of them are known binary systems with solved orbits. This sample increases the total number of known RV variable sdO/Bs by about a third.

### 3. Radial velocity variability of hot subdwarfs

Due to its large size, the full sample allows us to study the RV-variability of hot subdwarfs dependent on their location in the  $T_{\text{eff}} - \log g$ - and  $T_{\text{eff}} - \log n(\text{He})/n(\text{H})$  diagrams and therefore dependent on their subtypes and evolutionary stages. Fig. 1 shows the  $T_{\text{eff}} - \log g$  diagram of the full sample, where the size of the symbols scales linearly with  $\Delta RV_{\text{max}}$  ranging from zero up to about  $300 \text{ km s}^{-1}$ , while the colour scales with the helium abundance. It can be clearly seen that the distribution of  $\Delta RV_{\text{max}}$  is far from being isotropic and that rather complicated patterns exist. In the following we try to disentangle those substructures and their dependencies on the atmospheric parameters of the stars. An overview of our results is provided in Table 1.

#### 3.1. Helium abundance

The upper panel of Fig. 2 shows the  $T_{\text{eff}} - \log n(\text{He})/n(\text{H})$  diagram of the full sample. The difference in RV-variability of hot subdwarfs with supersolar and subsolar helium abundance is striking. Many stars with low helium abundances (161 out of 539 objects) show moderate or high RV-variations, while only very few of the iHe- (two out of 60 objects) and eHe-sdO/Bs (one out of 44 objects) show any variation at all. The difference becomes even more striking when the sample is restricted to stars with significant RV variations (middle panel). The difference is also very pronounced when looking at the distribution of the  $\log p$  values of the helium-poor and the helium-rich samples (Fig. 2, lower panel). This is further confirmed when looking at the RV-variability fractions. While the He-poor sdO/Bs have a variability fraction of  $30 \pm 2\%$ , the variability fractions of intermediate He-rich ( $3^{+4}_{-1}\%$ ) and extreme He-rich stars ( $2^{+5}_{-1}\%$ ) are very small.

Our results are in line with the preliminary results from the ESO Supernovae Ia Progenitor Survey (SPY) reported by Napiwotzki et al. (2004a) indicating a similarly low binary fraction for He-sdOs. The somewhat higher RV-variability fraction reported for the He-sdO/Bs from the Massive Unseen Companions to Hot Faint Underluminous Stars from SDSS (MUCHFUSS) survey might be related to the strongly biased selection procedure and the nature of the detected irregular variations (Geier et al. 2015b, 2017a). The preliminary results obtained from the low-resolution sample of Green et al. (2008) are also not consistent with the results presented here.

As can be seen in Fig. 1 the intermediate- and extreme He-sdO/Bs occupy neighbouring regions in the  $T_{\text{eff}} - \log g$ -diagram with effective temperatures ranging from  $\sim 35\,000 \text{ K}$  and  $\sim 55\,000 \text{ K}$  and surface gravities ranging from  $\log g \sim 5.6$  to 6.0. The clear difference in the RV variability with respect to the He-poor sdO/Bs excludes a direct evolutionary connection of those populations in general. He-sdO/Bs do not represent a later stage in the evolution of sdBs. This also means that diffusion processes are unlikely to form He-poor sdO/Bs as the progeny of more He-rich ones as proposed by Miller Bertolami et al. (2008) and Nemeth et al. (2012). Only confirmed single He-poor sdO/Bs might have formed in this way.

The similarities between iHe and eHe-sdO/Bs on the other hand allow for an evolutionary connection. Alternatively, both



**Table 1.** RV variability of the sample and the comparison sample (M&C) of Maxted et al. (2001) and Copperwheat et al. (2011).

Subsample	total	variable	fraction [%]	total (M&C)	variable (M&C)	fraction (M&C) [%]
He-poor	539	161	$30^{+2}_{-2}$	105	50	$48^{+5}_{-5}$
iHe-rich	60	2	$3^{+4}_{-1}$	–	–	–
eHe-rich	44	1	$2^{+5}_{-1}$	–	–	–
EHB1	54	11	$20^{+6}_{-4}$	4	1	$25^{+10}_{-25}$
EHB2	201	68	$34^{+3}_{-3}$	48	29	$60^{+7}_{-7}$
EHB3	116	26	$22^{+4}_{-3}$	17	5	$29^{+8}_{-13}$
postEHB	107	28	$26^{+5}_{-3}$	18	8	$44^{+11}_{-12}$
bEHB	61	28	$46^{+6}_{-6}$	18	7	$39^{+10}_{-12}$

subtypes might just have formed in a similar way. Given that the most recent results of Pelisoli et al. (2020) likely exclude pure single-star formation scenarios for sdO/Bs, the He-WD merger or the CE-merger channel might be a possibility.

Also the fact that no eHe-sdO/B star in a close binary could be confirmed in this region of the  $T_{\text{eff}} - \log g$ -diagram yet points in this direction. This can be seen in Fig. A.1, where we show all known hot subdwarfs in close binary systems with known orbital and atmospheric parameters (Heber et al. 2003; Silvotti et al. 2012; Sener et al. 2014; Kupfer et al. 2015 and references therein; Kawka et al. 2015; Schindewolf et al. 2015; Latour et al. 2014, 2016; Hillwig et al. 2017, priv. comm.; Kupfer et al. 2017a, 2017b, 2020, 2022; Schaffenroth et al. 2018, 2021; Vennes et al. 2018; Bell et al. 2019; Ratzloff et al. 2019, 2020; Löbbling 2020; Reindl et al. 2020; Pelisoli et al. 2021; Pawar et al. priv. comm.).

Among the  $\sim 600$  known He-enriched hot subdwarfs there are only five solved close binaries. PG 1544+488 is a double-lined binary consisting of two extreme He-sdBs with rather low temperatures of 32 800 K and 26 500 K (Sener & Jeffery 2014), Hen 2–428 is a double-lined binary consisting of a iHe-sdOB and an sdOB with subsolar He-abundance (Reindl et al. 2020), and CPD–20 1123 is a single-lined iHe-sdB ( $T_{\text{eff}} \sim 25\,500$  K) with an unseen companion (Naslim et al. 2012; Löbbling 2020). The other two are the closest hot subdwarf binaries known: OW J0741-2948 (Kupfer et al. 2017b) and ZTF J2130+4420 (Kupfer et al. 2020). The latter is currently transferring mass to its WD companion.

The double He-sdO/Bs binaries can only be explained by specific and presumably quite rare formation channels (Justham et al. 2011; Reindl et al. 2020). The iHe-sdOBs in the two very close binaries with WD companions are also peculiar objects, because of their likely quite massive progenitor stars. In this case core-helium burning is ignited under non-degenerate conditions and Kupfer et al. (2020) predicted such stars to be mildly enriched in helium. Due to their lower temperatures, the iHe-sdBs might not be related to the significantly hotter iHe- and eHe-sdOBs and sdOs.<sup>3</sup> We therefore conclude that all He-rich sdO/Bs known in close binary systems likely belong to rare and peculiar sub-populations, whereas the large majority of the iHe- and eHe-sdO/Bs shows no convincing evidence for close binarity, which makes a merger origin very likely.

Fig. 2 (upper panel) also shows that further conclusions about the formation of hot subdwarfs based on their helium abundances are difficult. Luo et al. (2019, 2020) proposed that

<sup>3</sup> The six He-sdO/Bs with significant RV variations discovered by Geier et al. (2015b, 2017a) could not be confirmed to be close binaries and their irregular variations likely have a different, yet unknown origin.

sdBs with  $\log n(\text{He})/n(\text{H}) < -2.2$  are formed via the stable RLOF channel and should therefore not show high RV-variability. In Fig. 2 (upper panel), however, many stars in this parameter range are clearly post-CE systems with high RV-variability.

### 3.2. Position in the $T_{\text{eff}} - \log g$ -diagram

Given that they likely represent a completely different population, we removed He-enriched sdO/Bs from the sample before studying the RV-variability properties along the  $T_{\text{eff}} - \log g$ -diagram. Guided by the structures seen in Fig. 1, we have divided the  $T_{\text{eff}} - \log g$ -diagram in five different regions shown in Fig. 3. The definition of the regions is based on visual inspection of the  $T_{\text{eff}} - \log g$ -diagram. The three regions EHB1 (red), EHB2 (green), and EHB3 (yellow) are located on the EHB. Instead of relying on the uncertain location of the EHB band provided by evolutionary tracks, we took the density of the objects as a proxy to define the EHB assuming that the density is higher on than off the EHB. The region postEHB (blue) covers the stars located above the EHB. Finally, the region bEHB (grey) covers all the objects below the canonical EHB.

#### 3.2.1. Extreme horizontal branch

As can be seen in Fig. 1 and Fig. 3 it turns out that the  $\Delta RV_{\text{max}}$  distribution along the EHB looks quite inhomogeneous.<sup>4</sup> There seems to be a difference between the most populated region EHB2 (201 objects) and the sparsely populated region EHB1 (54 objects), which are divided at an effective temperature of  $\sim 24\,000$  K. Comparing the  $\Delta RV_{\text{max}}$ -distributions as well as the normalised cumulative  $\Delta RV_{\text{max}}$ -distributions of both regions (see Fig. 4 top panel) it can be seen that the RV shifts in region EHB1 are smaller. To assess the statistical significance of this comparison, we performed a Kolmogorov-Smirnow (KS) test. In this way also the uncertainties of the single measurements and the quite different sample sizes are taken into account. We determined a  $p_{\text{KS}}$ -value of 0.12, meaning that the hypothesis that both samples have the same distribution can be rejected with a probability of 88%. However, this value is still lower than the typical 95% threshold, so the difference between both distributions is not significant. The variability fraction in region EHB2 is  $34 \pm 3\%$  compared to only  $20^{+6}_{-4}\%$  in region EHB1.

<sup>4</sup> Green et al. (2008) presented a  $T_{\text{eff}} - \log g$ -diagram (Fig. 3) where the symbols are scaled with standard deviation of RV measurements instead of  $\Delta RV_{\text{max}}$ . The structures seen on the EHB are very similar to our results.



The distinction between the regions EHB2 and EHB3 (116 objects) is shown in Fig. 3 (right panel). There seems to be a region devoid of stars around  $T_{\text{eff}} \sim 33\,000\text{ K}$  and  $\log g \sim 5.7$ . As can be seen in Fig. 4 (second panels from the top) there is a less pronounced difference in the  $\Delta RV_{\text{max}}$  distributions of the regions EHB2 and EHB3. Again the KS-test ( $p_{\text{KS}} = 0.18$ ) provides an indication for a difference between the two regions, which turned out to be not statistically significant. The RV-variability fraction in region EHB3 ( $22^{+4}_{-3}\%$ ) is smaller than in region EHB2, which might be due to a contamination of non-RV-variable iHe-sdOBs with inaccurate helium abundance determinations, which are also located in this region. Alternatively, single iHe-sdOBs might evolve to become sdOBs due to diffusion processes in their atmospheres as proposed by Miller Bertolami et al. (2008).

The differences between regions EHB1 and EHB2 are more pronounced. The higher fraction of apparently single stars and the smaller RV-variations in region EHB1 compared to region EHB2 are indications for lower-mass companions and/or longer orbital periods. The binary population synthesis models of Han et al. (2003) actually predict a desert of RV-variable systems for hot subdwarfs in region EHB1, because neither the first nor the second CE-channel in their simulations are able to form stars with hydrogen envelopes thick enough to correspond to such cool temperatures and low surface gravities (see Sect. 3.2.5). According to their predictions, all those sdBs should come from the stable-RLOF channel and therefore show just small RV-variations undetectable by this study. However, in our pre-selection we discarded sdBs with cool companions detectable in their SEDs, which have been identified as the normal post-RLOF sdB systems. The binary properties in region EHB1 are therefore hard to explain by binary evolution theory and follow-up observations are needed to increase the statistical significance of these results.

### 3.2.2. Above and beyond the extreme horizontal branch

The region postEHB (107 objects) in Fig. 3 is situated above and bluewards of the EHB. The exact location of the terminal age EHB (TAEHB) depends on the metallicity and the core mass of the stars and is therefore not very well defined. The distinction here has therefore to be regarded as a qualitative one only. Most stars in this regions should be evolved post-EHB stars with on-going He-shell burning.

Comparing the  $\Delta RV_{\text{max}}$  distribution we can now probe one of the most important evolutionary connections proposed for hot subdwarfs. Hot subdwarf B stars located on the EHB are proposed to evolve to post-EHB sdOB and sdO stars. In Fig. 4 (middle panels) the  $\Delta RV_{\text{max}}$  distribution of region EHB2 is compared to the one of region postEHB. The distributions look similar. The KS-test with a high  $p_{\text{KS}} = 0.47$  confirms the similarity of both distributions further and the RV variability fraction of region postEHB ( $26^{+5}_{-4}\%$ ) is consistent with the one of region EHB2 within the uncertainties.<sup>5</sup>

### 3.2.3. Below the extreme horizontal branch

The region bEHB (61 objects) is situated below the canonical EHB at somewhat higher surface gravities and covers the whole temperature range (see Fig. 3). It might be populated by sdO/Bs of different origins. Core helium-burning stars slightly below the

canonical ZAEHB for low metallicity populations (such as the thick disk), which is indicated in Fig. 3, might belong to the more metal-rich thin-disk population (e.g. Dorman et al. 1993).

Alternatively, those stars might have masses lower than the canonical mass. Intermediate-mass stars ( $2 - 3 M_{\odot}$ ), which ignite core helium-burning non-degenerately, can evolve to become hot subdwarfs with masses down to  $0.3 M_{\odot}$ , which is the minimum mass for the ignition of He-burning. The EHB for such low-mass stars is also shifted towards higher surface gravities (Han et al. 2002; Bloemen et al. 2014; Wu et al. 2018, see Fig. 3). Due to the higher progenitor masses it is also expected that more massive companions in combination with a deeper spiral-in are necessary to eject the more tightly bound envelopes of the red giants. This scenario was proposed to explain the closest known sdB+WD binaries (e.g. Geier et al. 2013c).

Finally, pre-He-WDs with no active He-burning are also found in this region. Since they are not connected to the EHB at all, they can be situated anywhere in the region bEHB. However, due to the quite different evolutionary timescales, low-mass pre-He-WDs ( $\sim 0.25 M_{\odot}$ ) at the low temperature end shown here should be more frequent than their hotter siblings with higher masses ( $0.3 - 0.35 M_{\odot}$ , Driebe et al. 1998; Althaus et al. 2013; Istrate et al. 2016). However, despite their shorter evolutionary times, the more massive pre-He-WDs might still be present, if more of them are formed in the first place. All pre-He-WDs are expected to be formed by binary mass-transfer and should have companions. The concentration of the hotter bEHB objects ( $> 25000\text{ K}$ ) below the EHB (see Fig. 3) might indicate that most of them are low-mass EHB objects, while the more widely distributed cooler objects might follow the pre-He-WD cooling tracks.

In Fig. 4 (second panels from the bottom) the  $\Delta RV_{\text{max}}$  distribution of region bEHB is compared to the one of region EHB2. The distribution of the bEHB region is similar in terms of the high fraction of RV-variable objects, but somewhat flatter, indicating a higher fraction of binary systems with high RV-amplitudes. However, also in this case the KS-test ( $p_{\text{KS}} = 0.33$ ) does not reveal a statistically significant difference between the two samples. In contrast to that, such a difference is found when comparing region EHB1 and region bEHB ( $p_{\text{KS}} = 0.05$ ) and also the  $\Delta RV_{\text{max}}$  distributions (Fig. 4 bottom panels) look different.

The RV-variability fraction of  $46 \pm 6\%$  in region bEHB is higher than the ones in regions EHB2 and EHB1, consistent with an intrinsically high close binary fraction. If confirmed, the somewhat higher RV-amplitudes would be consistent with a sample of binaries, where the visible primaries are less massive EHB stars or pre-He-WDs probably with higher mass companions and therefore show higher RV-variations. Also shorter orbital periods are possible, because the CE-ejection must have happened before the progenitor reached the tip of the RGB to form a pre-He-WD and the higher binding energy of the envelope favors a deeper inspiral of the companion.

### 3.2.4. Comparison with the RV variability studies in the literature

As can be seen in Appendix A, the results from previous RV variability studies of sdO/Bs yielded quite inhomogeneous results and are due to different systematic biases difficult to be compared in a quantitative way. The sample most similar to the one studied here has initially been published by Maxted et al. (2001) and later been extended and completed by Copperwheat

<sup>5</sup> This is inconsistent with the reported mismatch between the RV-variability fractions of sdBs and sdOBs from the MUCHFUSS project, which was likely caused by selection effects (Geier et al. 2015b, 2017a)

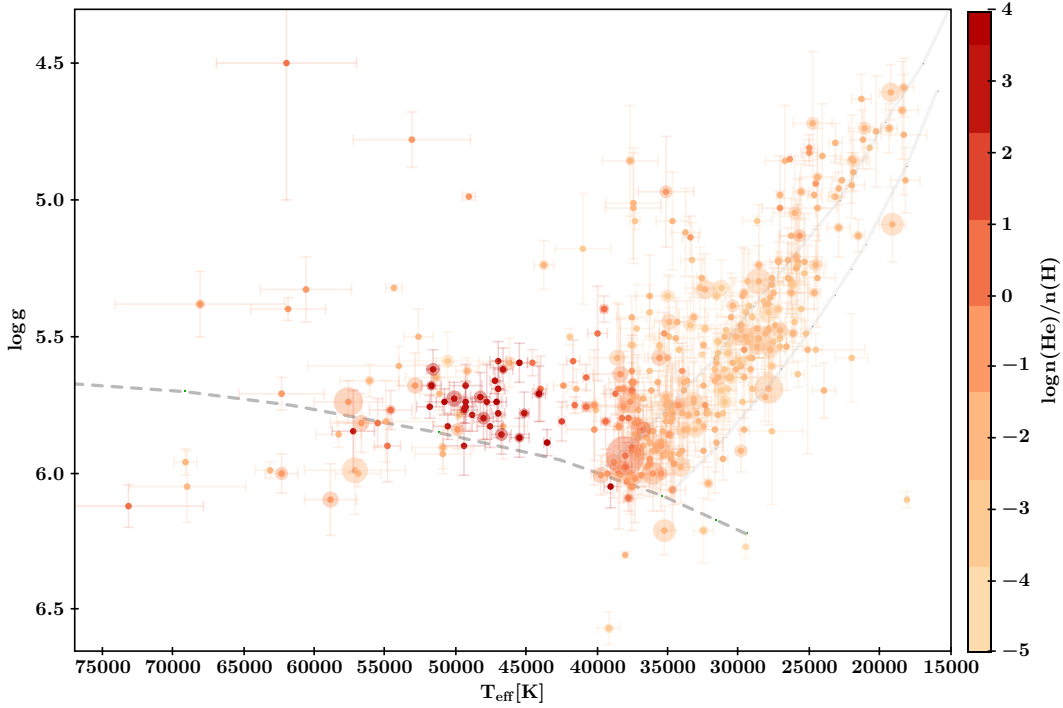


**Fig. 5.**  $T_{\text{eff}} - \log g$  diagram similar to Fig. 1 of the sample of hot subluminescent stars showing no significant RV variations.

et al. (2011). Therefore we refer to it as the M&C sample.<sup>6</sup> The authors used the same method to determine the significance of the RV variations as we did in this study, but their RV accuracy was better (down to  $\sim 2 \text{ km s}^{-1}$ ). The main differences are the smaller sample size (about one fourth of our sample) and the lack of He-rich stars. Apart from that, the M&C sample is well suited as a comparison sample to check whether the inhomogeneities we found for the He-poor sdO/Bs are also present at higher RV accuracy.

Initially, only a subset of the M&C sample had atmospheric parameters published (Saffer et al. 1994; Maxted et al. 2001; Morales-Rueda et al. 2003; Copperwheat et al. 2011). To extent this, we performed a literature research and found atmospheric parameters for two thirds (105 stars) of the M&C sample (Heber et al. 1984; Edelman et al. 2004; Lisker et al. 2005; Østensen et al. 2010b; Geier et al. 2011a, 2013a, 2017c; Nemeth et al. 2012; Luo et al. 2021).

Since a lot of the binaries discovered by M&C were followed-up and the orbital parameters determined, this introduces a bias in the  $\Delta RV_{\text{max}}$  distribution with respect to our sample. This is why we refrained from comparing those. Instead we just determined the RV variability fractions of the M&C sample (after removing the composite binaries) for the He-poor subsamples EHB1, EHB2, EHB3, postEHB and bEHB as defined above (see Table 1). Likely due to the higher RV accuracy, the overall RV variability fraction of the He-poor M&C sample ( $48 \pm 5\%$ ) is significantly higher than the one of our He-poor sample ( $30 \pm 2\%$ ). This is even more pronounced in the region EHB2 (M&C  $60 \pm 7\%$  compared to  $34 \pm 3\%$ ) and also marginally in region postEHB, while the variability fractions of the less populated regions EHB1, EHB3 and bEHB are consistent within the substantial uncertainties. However, there are clear indications

that the binary fraction in region EHB2 of the M&C sample is significantly higher than the one of region EHB3 confirming the trend seen in our sample. The comparison with region EHB1 is less obvious, because of the very small sample size, but also indicates a difference similar to the one in our sample.

### 3.2.5. Comparison with binary population synthesis models

Han et al. (2002, 2003) performed an extensive binary population synthesis (BPS) study of hot subdwarf formation through binary interactions and compared the results to the observed samples of binary sdO/Bs available back then. Assuming that all hot subdwarfs are formed by binary evolution either via CE ejection, stable RLOF or He-WD mergers the distribution of the stars in the  $T_{\text{eff}} - \log g$  diagram depends on the input parameters of the BPS simulations such as the efficiency of the CE ejection.

By comparison with the observed population, Han et al. (2003) favoured a model population with solar metallicity ( $Z = 0.02$ ), a rather high CE ejection efficiency ( $\alpha_{\text{CE}} = 0.75$ ) and an equally high thermal contribution to the binding energy of the envelope ( $\alpha_{\text{th}} = 0.75$ ). Lisker et al. (2005) compared the same simulations to a sample of hydrogen-rich sdBs and sdOBs from the SPY survey and achieved a better match with a model population of subsolar metallicity ( $Z = 0.004$ ) and with lower  $\alpha_{\text{CE}} = 0.5$  as well as  $\alpha_{\text{th}} = 0.5$ .

Due to the inhomogeneous selection of our sample, we refrain from performing a quantitative comparison with the results of Han et al. (2003) and leave that to future studies ideally based on updated BPS models. Instead we focus on obvious features and compare our  $T_{\text{eff}} - \log g$  diagram (Fig. 1) with the models of Han et al. (2003) as visualized in Fig. 17 of Lisker et al. (2005). The model populations are corrected for observational selection effects in the sense that composite systems with MS companions of K- or earlier types have been removed, which matches our selection of single-lined stars very well.

<sup>6</sup> In an additional paper of the series by Morales-Rueda et al. (2003), binary solutions of many stars in the sample were published. However, also binaries discovered in other projects were included.

A prominent and distinctive feature of the models is the extend of the EHB towards low temperatures, which turns out to be very sensitive to the CE ejection parameters. The more efficient the CE ejection, the more objects are found at low temperatures. This corresponds to the low temperature edge of region EHB2 in our sample, while region EHB1 is not populated in the model populations at all. It can be clearly seen that our sample strongly favours models with very few stars cooler than  $\sim 25\,000$  K. This is consistent with the result from Lisker et al. (2005) and indicates low values of  $\alpha_{\text{CE}} = 0.5$ ,  $\alpha_{\text{th}} = 0.5$  and  $Z = 0.004$ .

#### 4. Summary and conclusions

We performed a RV-variability analysis of a large sample of 646 hot subdwarfs with 4311 multi-epoch radial velocities from SDSS and LAMOST spectra. Atmospheric parameters and RVs were taken from the literature, if available and appropriate. For stars with archival spectra and no literature values, we determined the parameters by fitting model atmospheres. In particular, due to the higher systematic uncertainties, we re-determined the atmospheric parameters and RVs for all the He-enriched sdO/Bs. This large sample allowed us to study RV-variability as a function of the location in the  $T_{\text{eff}} - \log g$ - and  $T_{\text{eff}} - \log n(\text{He})/n(\text{H})$  diagrams in a statistically significant way. As diagnostics we used the fraction of RV-variable stars and the distributions of the maximum RV variations  $\Delta RV_{\text{max}}$ . Both indicators turned out to be inhomogeneous across the studied parameters ranges. We discovered 145 new hot subdwarf stars with significant RV variations. The results of this study allowed us to draw several conclusions:

- **Most He-rich sdO/Bs are single stars:** Both iHe- and eHe-sdO/Bs do not show significant RV-variability fractions in contrast to the He-poor sdO/Bs. They are therefore very likely single stars. This confirms preliminary results (Napiwotzki et al. 2004a) for the first time in a statistically significant way.
- **He-poor and He-rich sdO/Bs are not related:** The completely different behaviour of the He-poor and the He-rich hot subdwarfs led us to the conclusion that both subtypes are very likely not evolutionarily related. The iHe- and eHe-sdO/Bs on the other hand likely constitute one population.
- **He-rich sdO/Bs are likely formed by mergers:** Since recent results from the study by Pelisoli et al. (2020) indicate that single star evolution is unlikely for the formation of hot subdwarfs in general, we conclude that this population is formed via the merger channel. The most recent discovery of several hot subdwarf merger candidates is also in line with our conclusion (Vos et al. 2021; Dorsch et al. 2022; Werner et al. 2022).
- **There are indications for inhomogeneous RV-variability of the He-poor sdO/Bs:** Most of the RV-variable post-CE binaries are found in a well defined region on the EHB, which has been predicted by binary population synthesis models. Hot subdwarfs with temperatures cooler than  $\sim 24\,000$  K tend to show smaller RV-variations and a smaller RV-variability fraction. This small number of objects might constitute yet another subpopulation of binaries with longer periods and late-type or compact companions. The RV-variability properties of the EHB and corresponding post-EHB population of the He-poor hot subdwarfs

match and confirm the predicted evolutionary connection between them. Stars found below the EHB show large RV-variations and a significant RV-variability fraction, which is consistent with them being either low-mass EHB stars or non core helium-burning objects and therefore progenitors of He-WDs. Although some of the apparent inhomogeneities of RV-variability in the  $T_{\text{eff}} - \log g$ -diagram turned to be not statistically significant, we still think that they might be real. A comparison with the sample of M&C points in this direction. Comparing the distribution of objects in the  $T_{\text{eff}} - \log g$ -diagram with BPS models by Han et al. (2003), we find indications for a rather low efficiency of CE-ejection. More sophisticated BPS models and a proper treatment of the selection biases are needed to make progress in this direction.

- **Apparently single sdO/Bs are common:** A persistent riddle are the many sdO/B stars, which do not show any significant RV variability ( $> 50\%$  of the single-lined He-poor sdO/Bs and  $\sim 97\%$  of the He-rich sdO/Bs) and also no hints of a cool companion in their SEDs. As can be seen in Fig. 5, those objects are found all over the  $T_{\text{eff}} - \log g$ -diagram. Although a fraction of them might be explainable as binaries with small RV-variations due to long periods or low inclinations, it is very unlikely that all of them are binaries, since many sdO/Bs have been confirmed to be single in the literature based on high-resolution spectroscopy already (e.g. Silvotti et al. 2020). For the iHe- and eHe-sdO/Bs the merger channel provides a convenient formation scenario, which also explains their location in the  $T_{\text{eff}} - \log g$ -diagram. For the cooler He-poor sdO/Bs, other types of stellar mergers might be possible formation channels (Politano 2008; Clausen & Wade 2011; Hall & Jeffery 2016). Some or all of the single He-rich sdO/Bs might still turn into He-deficient stars due to diffusion processes as proposed by Miller Bertolami et al. (2008). Whether the even higher fraction of apparently single sdO/Bs in GCs (Latour et al. 2018) could also be explained along those lines or might be caused by alternative formation channels (e.g. Yi 2008) is still unclear and requires further studies.

Our results open many different routes for more detailed studies. Since the RV accuracy of the medium-resolution survey spectra used here is limited, follow-up studies with high-resolution spectra are needed to estimate the true fractions of non-variable hot subdwarfs and their distribution in the parameter space discussed here. More orbital solutions of binaries at the high and low temperature ends of the EHB as well as the regions below the EHB are needed to characterize those subpopulations. Furthermore, kinematic studies should be performed to determine the Galactic population properties of this sample.

*Acknowledgements.* We would like to thank Thomas Kupfer, Veronika Schaffenroth and Evan Bauer for useful advice. We thank the anonymous referee for helpful comments and suggestions. SG acknowledges funding from the German Academic Exchange Service (DAAD PPP USA 57444366) for this project and would like to thank the host institution Texas Tech University for the hospitality. IP was partially funded by the Deutsche Forschungsgemeinschaft under grant GE2506/12-1 and by the UK's Science and Technology Facilities Council (STFC), grant ST/T000406/1. UH and MD acknowledge funding by the Deutsche Forschungsgemeinschaft (DFG) through grants IR190/1-1, HE1356/70-1 and HE1356/71-1.

This research made use of TOPCAT, an interactive graphical viewer and editor for tabular data Taylor (2005). This research made use of the SIMBAD database, operated at CDS, Strasbourg, France; the VizieR catalogue access tool, CDS, Strasbourg, France.

This work has made use of data from the European Space Agency (ESA) mission *Gaia* (<https://www.cosmos.esa.int/gaia>), processed by the *Gaia* Data Processing and Analysis Consortium (DPAC,

<https://www.cosmos.esa.int/web/gaia/dpac/consortium>). Funding for the DPAC has been provided by national institutions, in particular the institutions participating in the *Gaia* Multilateral Agreement.

Guoshoujing Telescope (the Large Sky Area Multi-Object Fiber Spectroscopic Telescope LAMOST) is a National Major Scientific Project built by the Chinese Academy of Sciences. Funding for the project has been provided by the National Development and Reform Commission. LAMOST is operated and managed by the National Astronomical Observatories, Chinese Academy of Sciences.

Funding for the SDSS and SDSS-II has been provided by the Alfred P. Sloan Foundation, the Participating Institutions, the National Science Foundation, the U.S. Department of Energy, the National Aeronautics and Space Administration, the Japanese Monbukagakusho, the Max Planck Society, and the Higher Education Funding Council for England. The SDSS Web Site is <http://www.sdss.org/>. The SDSS is managed by the Astrophysical Research Consortium for the Participating Institutions. The Participating Institutions are the American Museum of Natural History, Astrophysical Institute Potsdam, University of Basel, University of Cambridge, Case Western Reserve University, University of Chicago, Drexel University, Fermilab, the Institute for Advanced Study, the Japan Participation Group, Johns Hopkins University, the Joint Institute for Nuclear Astrophysics, the Kavli Institute for Particle Astrophysics and Cosmology, the Korean Scientist Group, the Chinese Academy of Sciences (LAMOST), Los Alamos National Laboratory, the Max-Planck-Institute for Astronomy (MPIA), the Max-Planck-Institute for Astrophysics (MPA), New Mexico State University, Ohio State University, University of Pittsburgh, University of Portsmouth, Princeton University, the United States Naval Observatory, and the University of Washington.

Funding for SDSS-III has been provided by the Alfred P. Sloan Foundation, the Participating Institutions, the National Science Foundation, and the U.S. Department of Energy Office of Science. The SDSS-III web site is <http://www.sdss3.org/>. SDSS-III is managed by the Astrophysical Research Consortium for the Participating Institutions of the SDSS-III Collaboration including the University of Arizona, the Brazilian Participation Group, Brookhaven National Laboratory, University of Cambridge, Carnegie Mellon University, University of Florida, the French Participation Group, the German Participation Group, Harvard University, the Instituto de Astrofísica de Canarias, the Michigan State/Notre Dame/JINA Participation Group, Johns Hopkins University, Lawrence Berkeley National Laboratory, Max Planck Institute for Astrophysics, Max Planck Institute for Extraterrestrial Physics, New Mexico State University, New York University, Ohio State University, Pennsylvania State University, University of Portsmouth, Princeton University, the Spanish Participation Group, University of Tokyo, University of Utah, Vanderbilt University, University of Virginia, University of Washington, and Yale University.

## References

- Alam, S., Albareti, F. D., Allende Prieto, C., et al. 2015, *ApJS*, 219, 12
- Althaus, L. G., Miller Bertolami, M. M., & Corsico, A. H. 2013, *A&A*, 557, 19
- Bell, K., Kosakowski, A., Kilic, M., et al. 2019, *Research Notes of the American Astronomical Society*, 3, 81
- Bloemen, S., Hu, H., Aerts, C., et al. 2014, *A&A*, 569, 6
- Bolton, A. S., Schlegel, D. J., Aubourg, E., et al. 2015, *AJ*, 144, 144
- Brown, T. M., Sweigart, A. V., Lanz, T., Landsman, W. B., & Hubeny, I. 2001, *ApJ*, 562, 368
- Burgasser, A. J., Kirkpatrick, J. D., Reid, I. N., et al. 2003, *ApJ*, 586, 512
- Butler, K. & Giddings, J. R. 1985, *Newsletter of Analysis of Astronomical Spectra*, No. 9 (Univ. London)
- Byrne, C. M., Jeffery, C. S., Tout, C. A., & Hu, H. 2018, *MNRAS*, 475, 4728
- Cassisi, S., Schlattl, H., Salaris, M., & Weiss, A. 2003, *ApJ*, 582, L43
- Castellani, M., & Castellani, V. 1993, *ApJ*, 407, 649
- Charpinet, S., van Grootel, V., Reese, D., et al. 2008, *A&A*, 489, 377
- Chen, X., Han, Z., Deca, J., & Podsiadlowski, P. 2013, *MNRAS*, 434, 186
- Clausen, D., & Wade, R. A. 2011, *ApJL*, 733, L42
- Copperwheat, C., Morales-Rueda, L., Marsh, T. R., et al. 2011, *MNRAS*, 415, 1381
- D’Cruz, N. L., Dorman, B., Rood, R. T., & O’Connell, R. W. 1996, *ApJ*, 466, 359
- Dorman, B., Rood, R. T., & O’Connell, R. W. 1993, *ApJ*, 419, 596
- Dorsch, M., Latour, M., & Heber, U. 2019, *A&A*, 630, 130
- Dorsch, M., Jeffery, C. S., Irrgang, A., Woolf, V., & Heber, U. 2021, *A&A*, 653, 120
- Dorsch, M., Geier, S., Reindl, N., et al. 2022, *A&A*, submitted
- Driebe, T., Schoenberner, D., Bloeker, T. & Herwig, F. 1998, *A&A*, 339, 123
- Edelmann, H., Heber, U., Hagen, H.-J., et al. 2003, *A&A*, 400, 939
- Edelmann, H., Heber, U., Lisker, T., & Green, E. M. 2004, *Ap&SS*, 291, 315
- Finch, N., Braker, I. P., Reindl, N., et al. 2019, *ASP Conf. Ser.*, 519, 231
- Gao, H., Zhang, H.-W., Xiang, M.-S., et al. 2015, *RAA*, 15, 2204
- Geier, S., Nesslinger, S., Heber, U., et al. 2007, *A&A*, 464, 299
- Geier, S., Heber, U., Podsiadlowski, P., et al. 2010, *A&A*, 519, A25
- Geier, S., Classen, L., & Heber, U. 2011a, *ApJ*, 733, L13
- Geier, S., Maxted, P. F. L., Napiwotzki, R., et al. 2011b, *A&A*, 526, 39
- Geier, S., & Heber, U. 2012, *A&A*, 543, 149
- Geier, S. 2013, *A&A*, 549, 110
- Geier, S., Heber, U., Edelmann, H., et al. 2013a, *A&A*, 557, 122
- Geier, S., Heber, U., Heuser, C., et al. 2013b, *A&A*, 551, L4
- Geier, S., Marsh, T. R., Wang, B., et al. 2013c, *A&A*, 554, 54
- Geier, S., Østensen, R. H., Heber, U., et al. 2014, *A&A*, 562, 95
- Geier, S., Fürst, F., Ziegerer, E., et al. 2015a, *Science*, 347, 1126
- Geier, S., Kupfer, T., Heber, U., et al. 2015b, *A&A*, 577, 26
- Geier, S., Kupfer, T., Heber, U., et al. 2017a, *A&A*, 602, C2
- Geier, S., Østensen, R. H., Nemeth, P., et al. 2017b, *Open Astronomy*, 26, 164
- Geier, S., Raddi, R., Gentile Fusillo, N. P. & Marsh, T. R. 2019, *A&A*, 621, 38
- Geier, S. 2020, *A&A*, 635, 193
- Giddings, J. R. 1981, PhD thesis, University of London
- Götberg, Y., de Mink, S. E., Groh, J. H., et al. 2018, *A&A*, 615, 78
- Green, E. M., Fontaine, G., Hyde, E. A., For, B.-Q., & Chayer, P. 2008, *ASP Conf. Ser.*, 392, 75
- Hall, P. D., & Jeffery, C. S. 2016, *MNRAS*, 463, 2756
- Han, Z. 2008, *A&A*, 484, 31
- Han, Z., Podsiadlowski, P., Maxted, P. F. L., Marsh, T. R., & Ivanova, N. 2002, *MNRAS*, 336, 449
- Han, Z., Podsiadlowski, P., Maxted, P. F. L., & Marsh, T. R. 2003, *MNRAS*, 341, 669
- Heber, U., Hunger, K., Jonas, G., & Kudritzki, R. P. 1984, *A&A*, 130, 119
- Heber, U. 1986, *A&A*, 155, 33
- Heber, U., & Hunger, K. 1987, *The Messenger*, 47, 36
- Heber, U., Edelmann, H., Lisker, T., & Napiwotzki, R. 2003, *A&A*, 411, L477
- Heber, U. 2009, *ARA&A*, 47, 211
- Heber, U., & Hirsch, H. 2010, *American Institute of Physics Conference Series*, 1314, 79
- Heber, U. 2016, *PASP*, 128, 082001
- Heber, U., Irrgang, A., & Schaffenroth, J. 2018, *Open Astronomy*, 27, 35
- Hillwig, T. C., Frew, D. J., Reindl, N., et al. 2017, *AJ*, 153, 24
- Hirsch, H. 2009, PhD thesis, Friedrich-Alexander University Erlangen-Nürnberg
- Hogg, M. A., Casewell, S. L., Wynn, G. A., et al. 2020, *MNRAS*, 498, 12
- Hu, H., Tout, C. A., Glebbeek, E., & Dupret, M.-A. 2011, *MNRAS*, 418, 195
- Hubeny, I. 1998, *Computer Physics Communications*, 52, 103
- Irrgang, A., Kreuzer, S., Heber, U., & Brown, W. R. 2018, *A&A*, 615, L5
- Istrate, A. G., Marchant, P., Stancliffe, R., et al. 2016, *A&A*, 595, 35
- Justham, S., Podsiadlowski, P., & Han, Z. 2011, *MNRAS*, 410, 984
- Kawka, A., Vennes, S., O’Toole, S. J., et al. 2015, *MNRAS*, 450, 3514
- Kepler, S. O., Pelisoli, I., Koester, D., et al. 2019, *MNRAS*, 486, 2169
- Kramer, M., Schneider, F. R. N., Ohlmann, S., et al. 2020, *A&A*, 642, 97
- Krticka, J., Kubat, J., & Krtickova, I. 2016, *A&A*, 593, 14
- Kupfer, T., Geier, S., Schaffenroth, V., et al. 2015, *A&A*, 576, 44
- Kupfer, T., Ramsay, G., van Roestel, J., et al. 2017a, *ApJ*, 851, 28
- Kupfer, T., van Roestel, J., Brooks, J. et al. 2017b, *ApJ*, 835, 131
- Kupfer, T., Bauer, E., Marsh, T. R., et al. 2020, *ApJ*, 891, 45
- Kupfer, T., Bauer, E., van Roestel, J., et al. 2022, *ApJ*, 925, L12
- Kurucz, R. L. 1996, *ASP Conf. Ser.*, 108, 160
- Lanz, T., & Hubeny, I. 2003, *ApJS*, 146, 417
- Lanz, T., Brown, T. M., Sweigart, A. V., Hubeny, I., & Landsman, W. B. 2004, *ApJ*, 602, 342
- Latour, M., Fontaine, G., Green, E. M., et al. 2014, *ApJ*, 788, 65
- Latour, M., Heber, U., Irrgang, A., et al. 2016, *A&A*, 585, 115
- Latour, M., Randall, S. K., Calamida, A., Geier, S., & Moehler, S. 2018, *A&A*, 618, 15
- Lisker, T., Heber, U., Napiwotzki, R., Christlieb, N., Han, Z., et al. 2005, *A&A*, 430, 223
- Lei, Z., Zhao, J., Nemeth, P., & Zhao, G. 2018, *ApJ*, 868, 70
- Lei, Z., Zhao, J., Nemeth, P., & Zhao, G. 2019, *ApJ*, 881, 135
- Lei, Z., Zhao, J., Nemeth, P., & Zhao, G. 2020, *ApJ*, 889, 118
- Löbbling, L. 2020, *MNRAS*, 497, 67
- Luo, Y.-P., Nemeth, P., Liu, C., Deng, L.-C., & Han, Z. 2016, *ApJ*, 818, 202
- Luo, Y.-P., Nemeth, P., Deng, L.-C., & Han, Z. 2019, *ApJ*, 881, 7
- Luo, Y.-P., Nemeth, P., & Li, Q. 2020, *ApJ*, 898, 64
- Luo, Y.-P., Nemeth, P., Wan, K., Wang, X., & Han, Z. 2021, *ApJS*, 256, 28
- Maxted, P. F. L., Heber, U., Marsh, T. R., & North, R. C. 2001, *MNRAS*, 326, 139
- Michaud, G., Richer, J., & Vick, M. 2011, *A&A*, 534, 18
- Miller Bertolami, M. M., Althaus, L. G., Unglaub, K., & Weiss, A. 2008, *A&A*, 491, 253
- Miller Bertolami, M. M., et al. 2022, *MNRAS*, submitted

- Morales-Rueda, L., Maxted, P. F. L., Marsh, T. R., North, R. C., & Heber, U. 2003, *MNRAS*, 338, 752
- Napiwotzki, R., Karl, C., Lisker, T. et al. 2004a, *Ap&SS*, 291, 321
- Napiwotzki, R., Yungelson, L., Nelemans, G. et al. 2004b, *ASP Conf. Ser.*, 318, 402
- Napiwotzki, R., Karl, C. A., Lisker, T., et al. 2020, *A&A*, 638, 131
- Naslim, N., Geier, S., Jeffery, C. S., et al. 2012, *MNRAS*, 423, 3031
- Naslim, N., Jeffery, C. S., Hibbert, A., & Behara, N. T. 2013, *MNRAS*, 434, 1920
- Nelemans, G., & Tauris, T. M. 1998, *A&A*, 335, L85
- Nemeth, P., Kawka, A., & Vennes, S. 2012, *MNRAS*, 427, 2180
- Nemeth, P., Vos, J., Molina, F., & Bastian, A. 2021, *A&A*, 653, 3
- Østensen, R. H., Green, E. M., Bloemen, S. et al. 2010a, *MNRAS*, 408, 51
- Østensen, R. H., Oreiro, R., Solheim, J.-E., et al. 2010b, *A&A*, 513, 6
- O'Toole, S. J. & Heber, U. 2006, *A&A*, 452, 579
- Paczynski, B. 1971, *Acta Astronomica*, 21, 1
- Pelisoli, I., Vos, J., Geier, S., et al. 2020, *A&A*, 642, 180
- Pelisoli, I., Geier, S., Neunteufel, P., et al. 2021, *Nature Astronomy*, 5, 1052
- Politano, M., Taam, R. E., van der Sluys, M., & Willems, B. 2008, *ApJ*, 687, L99
- Przybill, N., Nieva, M.-F., & Butler, K. 2011, *Journal of Physics Conf. Ser.*, 328, 012015
- Ratzloff, J. K., Barlow, B. N., Kupfer, T., et al. 2019, *ApJ*, 883, 51
- Ratzloff, J. K., Kupfer, T., Barlow, B. N., et al. 2020, *ApJ*, 902, 92
- Rauch, T. & Deetjen, J. L. 2003, *ASP Conf. Ser.*, 288, 103
- Reindl, N., Rauch, T., Werner, K., Kruk, J. W., & Todt, H. 2014, *A&A*, 566, 23
- Reindl, N., Geier, S., Kupfer, T., et al. 2016, *A&A*, 587, 101
- Reindl, N., Schaffenroth, V., Miller Bertolami, M. M. 2020, *A&A*, 638, 93
- Saffer, R. A., Bergeron, P., Koester, D., & Liebert, J. 1994, *ApJ*, 432, 351
- Schaffenroth, V., Geier, S., Heber, U., et al. 2018, *A&A*, 614, 77
- Schaffenroth, V., Barlow, B. N., Geier S., et al. 2019, *A&A*, 630, 80
- Schaffenroth, V., Casewell, S. L., Schneider, D., et al. 2021, *MNRAS*, 501, 3847
- Schindewolf, M., Levitan, D., Heber, U., et al. 2015, *A&A*, 580, 117
- Schindewolf, M., Nemeth, P., Heber, U., et al. 2018, *A&A*, 620, 36
- Schneider, D., Irrgang, A., Heber, U., Nieva, M. F., Przybill, N. 2018, *A&A*, 618, 86
- Sener, H. T. & Jeffery, C. S. 2014, *MNRAS*, 440, 2676
- Silvotti, R., Østensen, R. H., Bloemen, S., et al. 2012, *MNRAS*, 424, 1752
- Silvotti, R., Østensen, & Teltung, J. H. 2020, *Proceedings of the 9th Meeting on Hot Subdwarfs and Related Objects (Hendaye, June 23-28, 2019)*; doi:10.5281/zenodo.3588477 (arXiv:2002.04545)
- Soker, N. 1998, *AJ*, 116, 1308
- Stark, M. A., & Wade, R. A. 2003, *ApJ*, 126, 1455
- Stoughton, C., Lupton, R. H., Bernardi, M., et al. 2002, *AJ*, 123, 485
- Ströer, A., Heber, U., Lisker, T., et al. 2007, *A&A*, 462, 269
- Sweigart, A. V. 1997a, *The Third Conference on Faint Blue Stars*, 3
- Sweigart, A. V. 1997b, *ApJL*, 474, L23
- Taylor, M. B. 2005, *ASP Conf. Ser.*, 347, 29
- Unglaub, K. 2008, *A&A*, 486, 923
- Vennes, S., Kawka, A., & Nemeth, P. 2011, *MNRAS*, 410, 2095
- Vennes, S., Nemeth, P., & Kawka, A., 2018, *Open Astronomy*, 27, 7
- Vos, J., Vuckovic, M., Chen, X., et al. 2018, *MNRAS*, 482, 4592
- Vos, J., Bobrick, A., & Vuckovic, M. et al. 2020, *A&A*, 641, 163
- Vos, J., Pelisoli, I., Budaj, J., et al. 2021, *A&A*, 655, 43
- Webbink, R. F. 1984, *ApJ*, 277, 355
- Werner, K., Deetjen, J. L., Dreizler, S., et al. 2003, *ASP Conf. Ser.*, 288, 31
- Werner, K., Dreizler, S., & Rauch, T. 2012, *TMAP: Tübingen NLTE Model-Atmosphere Package, Astrophysics Source Code Library*
- Werner, K., Reindl, N., Geier, S., & Pritzkeleit, M. 2022, *MNRAS*, 511, L66
- Wu, Y., Chen, X., Li, Z., & Han, Z. 2018, *A&A*, 618, 14
- Xiong, H., Chen, X., Podsiadlowski, Ph., Li, Y., & Han, Z. 2017, *A&A*, 599, 54
- Yanny, B., Rockosi, C., Newberg, H., et al. 2009, *AJ*, 137, 4377
- Yi, S. 2008, *ASP Conf. Ser.*, 392, 3
- Zhang, X., & Jeffery, C. S. 2012, *MNRAS*, 419, 452

## Appendix A: Previous radial velocity variability studies

Since the known companions in close hot subdwarf binaries are either compact objects like WDs, or very cool M-dwarfs and brown dwarfs, they reveal themselves by the Doppler shifts they induce in the spectral lines of the sdO/B primaries. RV variations are therefore one way to detect close binary hot subdwarfs.

The high close binary fraction of sdB stars was initially discovered by Maxted et al. (2001). They observed 36 EHB stars

in total, five of them being composite sdB binaries and 5 more evolved post-EHB stars. The stars were observed over a timespan of 11 nights in total with the single observing epochs usually separated by one or a few days. The accuracy of their RV measurements was  $\sim 2 - 5 \text{ km s}^{-1}$  and they detected significant RV shifts for 21 EHB stars (58%) and one post-EHB star (20%). Excluding the non-variable composite binaries from the counting, the fraction of RV-variable single-lined EHB sdBs was 68%. Assuming a certain period distribution and estimating the detection efficiency, Maxted et al. (2001) concluded that the close binary fraction must be  $69 \pm 9\%$  or more.

Napiwotzki et al. (2004a) observed 46 single-lined sdB stars in the course of the SPY survey and found 18 (39%) of them to be RV variable. Two spectra of each star were taken at random epochs over a few years. The RV accuracy was  $\sim 2 \text{ km s}^{-1}$ . Excluding three post-EHB stars with a binary fraction of 67% (two out of three) from the sample, the binary fraction on the EHB was only 37%. Also corrections similar to the ones performed by Maxted et al. (2001) using an updated period distribution only raised the EHB binary fraction to 40%, significantly different from the one obtained by Maxted et al. (2001). Since the sample of Napiwotzki et al. (2004a) reached down to fainter magnitudes, the authors proposed that a larger fraction of stars from the thick disk or the halo population were observed and that the binary properties of the Galactic populations are different.

Napiwotzki et al. (2004a) also determined the RV-variable fraction of helium-rich sdO stars. Out of 23 single-lined He-sdOs they only found one star (4%) to be variable (5% if corrected as described in Maxted et al. 2001). This provided the first observational hint that the He-sdOs might not be evolutionary related to the sdBs.

Morales-Rueda et al. (2003) and Copperwheat et al. (2011) extended radial-velocity study of Maxted et al. (2001). They obtained multi-epoch RVs of 159 sdBs (two of them in the post-EHB stage), derived binary parameters of 51 close binaries and detected significant RV variations for another 20 stars. The accuracies of their RV measurements are quite inhomogeneous ranging from 2 to more than  $20 \text{ km s}^{-1}$ . Most of the observed stars have RV epochs with timebases of days, which is much longer than the typical orbital periods. However, several stars have been observed within one night only introducing a bias in favor of very short orbital periods. The authors detected significant RV shifts for 64 of the 125 single-lined EHB stars in this sample (51%), while the two post-EHB stars are both close binaries (100%). In addition 32 objects were found to be composite systems and five of them (16%) to be RV-variable. Copperwheat et al. (2011) did not perform simulations, but estimated the true close binary fraction to range from 46% to 56%.

Green et al. (2008) showed preliminary results from a study of 407 sdO/Bs as part of a larger survey of hot stars. Using multi-epoch, low-resolution ( $9 \text{ \AA}$ ), but high-S/N spectra they reported an RV accuracy of  $16 \text{ km s}^{-1}$  and calculated the standard deviation of the single RV measurements. In contrast to Napiwotzki et al. (2004a) they did not detect any significant difference between He-rich and He-poor sdO/Bs in RV variability, which means that variations have been reported in a significant fraction of He-sdO/Bs in their sample.

Kawka et al. (2015) studied 38 hot subdwarfs randomly selected from a sample of UV-bright objects (Vennes et al. 2011; Nemeth et al. 2012). The RV follow-up was performed with several different instruments and the overall accuracy was estimated to be smaller than  $10 \text{ km s}^{-1}$ . Almost all stars have been observed multiple times at random epochs without any bias against longer period systems. Six composite systems were detected by visual

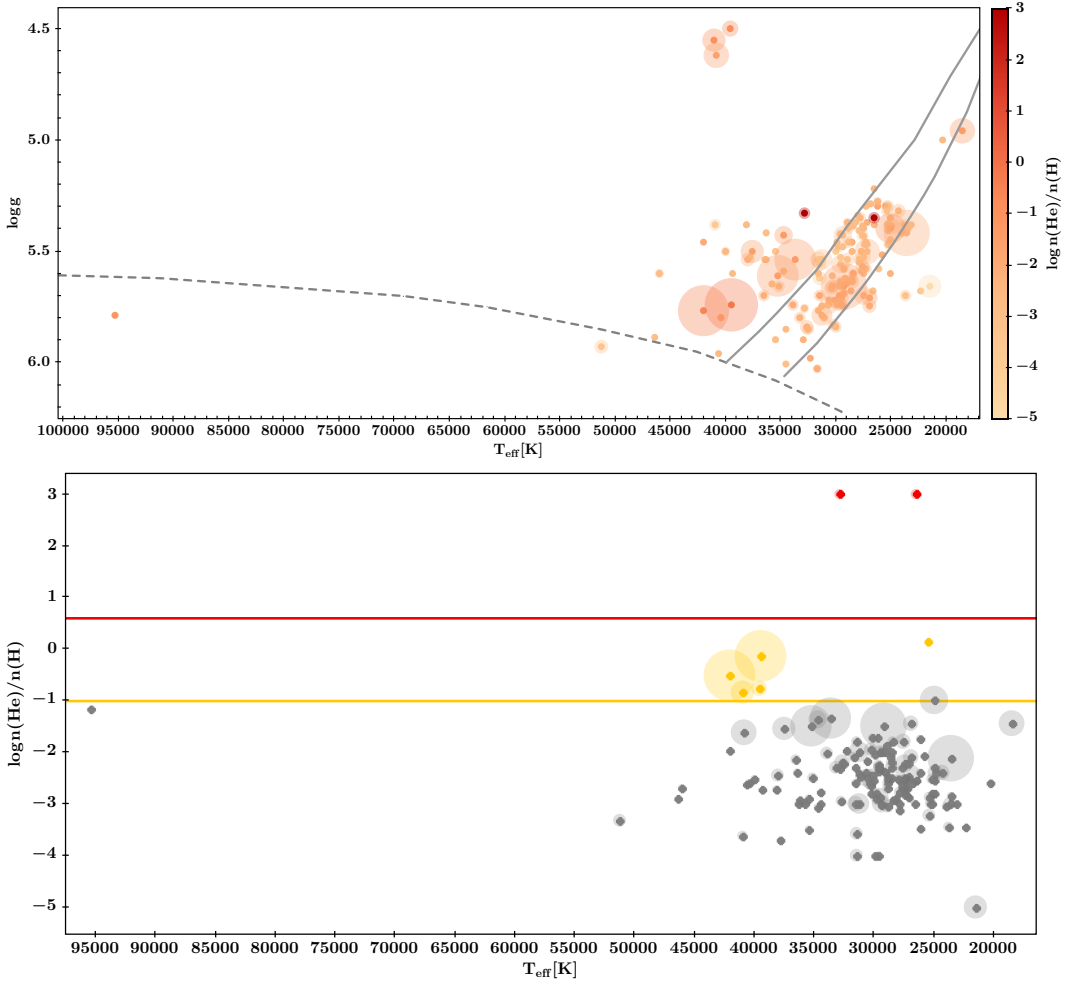


**Fig. 1.** Upper panel:  $T_{\text{eff}} - \log g$  diagram of the sample of solved close hot subdwarf binaries similar to Fig. 1. Lower panel:  $T_{\text{eff}} - \log n(\text{He})/n(\text{H})$  diagram of the solved systems similar to Fig. 2. The scaling of the symbol sizes is different and was chosen for better visualisation.

inspection of the spectra and by fitting their spectral energy distributions, which all did not show significant RV variations (0%). Three stars turned out to be RV-constant He-sdOBs (0%). The sample also included an RV-variable low-mass He-WD progenitor (100%) and a post-EHB sdOB also exhibiting RV variations (100%). From the remaining 27 EHB stars 9 (33%) were found to be RV variable.

Finally, Geier et al. (2015b, 2017a) reported the discovery of 76 new significantly RV-variable hot subdwarfs and 53 candidates in the course of the MUCHFUSS project. However, since this survey aimed at finding short-period binaries with high RV-amplitudes, the target selection was strongly biased and no binary fraction could be derived from this sample. In contrast to other studies, Geier et al. (2015b, 2017a) also targeted 29 He-rich sdOs and sdOBs and discovered six of them to be significantly RV variable. Studying some of those objects in more detail, the authors were not able to determine their orbital parameters and concluded that the irregular RV-variability might be caused by processes other than the presence of close companions. Geier et al. (2015b, 2017a) also reported a mismatch between the RV-variability fraction of sdBs and sdOBs, which should be similar if sdBs are progenitors of sdOBs.

In summary, the previous studies of RV variability in samples of hot subdwarfs found that He-sdO/Bs and sdBs with com-

posite spectra usually do not show significant RV variability, while the variability fractions of EHB and post-EHB stars were rather inconsistent. Selection effects were proposed as possible reason for these inconsistencies.

**Table A.1.** RV variability and spectroscopic parameters for the full sample.  
<sup>a</sup>Helium abundances without uncertainty are upper (if negative) or lower limits (if positive).

Name	Class	ep	$RV_{\text{average}}$ [km s <sup>-1</sup> ]	$\Delta RV_{\text{max}}$ [km s <sup>-1</sup> ]	log p	$T_{\text{eff}}$ [K]	log g	log y <sup>d</sup>	Reference
PG2358+107	sdB	2	31 ± 4	9 ± 10	-0.434	27100 ± 430	5.54 ± 0.07	-2.72 ± 0.11	2016ApJ...818..202L
PG2359+197	sdB+WD	2	-135 ± 4	14 ± 8	-1.0478	31434 ± 500	5.56 ± 0.05	-3.58 ± 0.05	2005A&A...430..223L
SDSSJ00307.06+241211.6	sdB	9	0 ± 4	35 ± 19	-0.1199	27448 ± 481	5.52 ± 0.09	-2.72 ± 0.43	
SDSSJ00607.88-010320.8	He-sdO	6	-242 ± 5	48 ± 21	-0.7693	45456 ± 666	5.87 ± 0.07	3.62 ± 0.72	
PG0009+191	sdB	2	-54 ± 4	73 ± 9	-13.1608	30569 ± 296	5.89 ± 0.06	-2.62 ± 0.15	2019ApJ...881....7L
HS0025+3423	sdOB	2	-32 ± 3	9 ± 7	-0.6737	32320 ± 1430	5.75 ± 0.21	-0.92 ± 0.16	2016ApJ...818..202L
LAMOSTJ003518.97+410658.6	sdB	3	-90 ± 5	101 ± 13	-16.0528	27381 ± 482	5.88 ± 0.08	-2.29 ± 0.11	2019ApJ...881....7L
LAMOSTJ003801.72+343156.2	He-sdOB	2	-64 ± 6	6 ± 13	-0.1758	41705 ± 449	5.59 ± 0.08	-0.07 ± 0.07	
LAMOSTJ004139.06+420713.5	sdOB	2	-37 ± 5	7 ± 28	-0.0917	36447 ± 283	5.98 ± 0.05	-1.82 ± 0.05	2019ApJ...881....7L
SDSSJ004233.42+004717.6	sdB	27	34 ± 3	48 ± 21	-0.0478	31583 ± 600	5.35 ± 0.05	-3.24	
SDSSJ004422.92+425706.4	sdB	2	-39 ± 4	42 ± 8	-6.2867	30003 ± 340	5.65 ± 0.07	-2.68 ± 0.16	2019ApJ...881....7L
SDSSJ004755.27+252027.1	sdO	9	-98 ± 5	141 ± 20	-23.9293	49505 ± 2616	5.45 ± 0.09	-3.08 ± 0.23	
LAMOSTJ004906.06+395021.0	sdB	2	4 ± 8	83 ± 19	-4.6104	31352 ± 139	6.05 ± 0.04	-2.34 ± 0.05	2019ApJ...881....7L
PG0046+207	sdB	3	34 ± 3	47 ± 8	-8.8492	27520 ± 500	5.55 ± 0.07	-2.48 ± 0.23	2012MNRAS.427.2180N
GALEXJ00498+3522	sdOB	2	14 ± 4	39 ± 10	-3.9149	35150 ± 440	5.78 ± 0.06	-1.54 ± 0.06	2018ApJ...868...70L
PG0048+004	sdOB	13	-63 ± 3	53 ± 19	-1.0735	38500 ± 300	5.83 ± 0.07	-1.00 ± 0.10	2015A&A...577A..26G
PG0050+201	sdB	2	64 ± 3	13 ± 7	-1.0303	34156 ± 177	5.93 ± 0.03	-1.88 ± 0.02	2019ApJ...881....7L
FBS0051+377	sdOB	3	2 ± 3	155 ± 13	-77.4162	33680 ± 530	6.08 ± 0.09	-1.87 ± 0.10	2018ApJ...868...70L
SDSSJ010327.84+324033.4	sdOB	3	-74 ± 6	11 ± 30	-0.03	37490 ± 1030	5.43 ± 0.08	-1.69 ± 0.14	2020ApJ...889..117L
FBS0102+362	sdB	3	16 ± 3	4 ± 7	-0.0654	32270 ± 70	5.77 ± 0.02	-1.64 ± 0.02	2018ApJ...868...70L
FBS0104+367	sdB	2	32 ± 4	75 ± 9	-15.5583	29813 ± 186	5.86 ± 0.04	-2.84 ± 0.12	2019ApJ...881....7L
LAMOSTJ010715.60+390416.1	sdB	2	-26 ± 4	11 ± 8	-0.7246	31679 ± 248	5.66 ± 0.04	-1.81 ± 0.05	2019ApJ...881....7L
FBS0106+374	sdB	3	12 ± 3	49 ± 11	-6.6616	29070 ± 160	5.49 ± 0.03	-3.44 ± 0.43	2018ApJ...868...70L
SDSSJ011506.17+140513.5	sdOB	11	-158 ± 7	65 ± 36	-0.0945	37680 ± 2000	4.86 ± 0.20	-1.95 ± 0.40	2009PhDT.....273H
PG0112+142	sdOB	8	-121 ± 3	14 ± 17	-0.0292	40948 ± 2000	5.18 ± 0.20	-3.25 ± 0.40	2009PhDT.....273H
SDSSJ012340.69+300232.16	sdB	3	-139 ± 5	107 ± 23	-16.7156	29260 ± 340	5.34 ± 0.05	-1.97 ± 0.09	2019ApJ...881..135L
PG0112+065	sdOB	11	-47 ± 3	76 ± 39	-0.6315	34707 ± 915	5.77 ± 0.14	-1.80 ± 0.20	2017OAS...26..164G
SDSSJ012739.35+404357.8	sdO	8	-55 ± 6	58 ± 25	-0.8783	56076 ± 2037	5.66 ± 0.06	-1.63 ± 0.06	
LAMOSTJ0134.51+323723.7	sdO	2	-65 ± 7	1 ± 16	-0.0225	63122 ± 1025	5.99 ± 0.03	-1.64 ± 0.12	2019ApJ...881....7L
GALEXJ01509+3107	sdB	2	-42 ± 4	52 ± 13	-4.1554	28520 ± 270	5.74 ± 0.03	-1.73 ± 0.05	2019ApJ...881....7L
LAMOSTJ020201.84+564342.2	sdB	2	-60 ± 4	130 ± 9	-42.0126	30396 ± 178	5.88 ± 0.04	-2.87 ± 0.13	2018ApJ...868...70L
GALEXJ02069+1438	sdB	2	23 ± 4	90 ± 10	-17.3272	30310 ± 660	5.77 ± 0.06	-2.61 ± 0.24	2019ApJ...881....7L
SDSSJ022422.21+000313.5	He-sdOB	80	-230 ± 4	224 ± 61	-1.2186	37949 ± 330	5.94 ± 0.05	-0.07 ± 0.04	2012MNRAS.427.2180N
HS0222+2334	sdO	2	51 ± 3	8 ± 7	-0.5519	46670 ± 1760	5.83 ± 0.12	-2.18 ± 0.24	2012MNRAS.427.2180N
LAMOSTJ023559.85+524549.3	sdB	2	86 ± 6	105 ± 15	-10.7463	29558 ± 415	4.98 ± 0.01	-1.62 ± 0.09	2019ApJ...881....7L
PG0240+066	sdB	2	-14 ± 4	1 ± 10	-0.0341	29530 ± 313	5.84 ± 0.07	-2.42 ± 0.09	2019ApJ...881....7L
SDSSJ030211.57+371109.5	sdO	7	-83 ± 3	52 ± 14	-5.339	48846 ± 2909	5.85 ± 0.12	-2.73 ± 0.30	
LAMOSTJ030236.01+281616.9	sdOB	3	15 ± 3	101 ± 9	-24.7496	39180 ± 434	6.08 ± 0.06	-1.69 ± 0.09	2019ApJ...881....7L
LAMOSTJ030334.75+291355.6	sdB	2	-74 ± 3	78 ± 7	-22.065	19249 ± 68	5.25 ± 0.07	-2.55 ± 0.25	2019ApJ...881....7L
LAMOSTJ030554.72+282908.9	sdB	3	-47 ± 2	21 ± 7	-1.874	24688 ± 515	5.22 ± 0.06	-1.78 ± 0.02	2019ApJ...881....7L
LAMOSTJ031311.81+282735.8	sdOB	2	-82 ± 5	13 ± 12	-0.5474	41417 ± 678	5.69 ± 0.07	-2.53 ± 0.22	2019ApJ...881....7L



LAMOSTJ031319.32+284159.8	sdB	3	-83 ± 3	220 ± 7	-167.6739	25887 ± 415	5.34 ± 0.07	-2.85 ± 0.19	2019ApJ...881...7L
FBS0314+372	sdB	2	-40 ± 4	28 ± 10	-2.1515	31194 ± 206	6.00 ± 0.05	-3.16 ± 0.29	2019ApJ...881...7L
KUV03163+0031	sdB	7	3 ± 6	16 ± 22	-0.0017	21964 ± 1209	4.85 ± 0.16	-2.00 ± 0.20	2017OAJ...26..164G
SDSSJ032101.29+185719.0	sdB	2	48 ± 4	54 ± 8	-9.3461	28634 ± 590	5.68 ± 0.10	-2.39 ± 0.14	2019ApJ...881...7L
SDSSJ032107.05+045150.7	He-sdOB	2	-176 ± 6	4 ± 24	-0.0595	37534 ± 540	5.63 ± 0.09	-0.41 ± 0.06	
PG0319+054	sdB	3	-18 ± 4	68 ± 14	-8.1927	30700 ± 500	5.74 ± 0.06	-2.40 ± 0.10	2015A&A...577A..26G
LAMOSTJ032357.44+421614.8	sdOB	2	-28 ± 3	5 ± 7	-0.2912	37722 ± 327	6.02 ± 0.05	-1.44 ± 0.05	2019ApJ...881...7L
LAMOSTJ033309.34+341230.8	sdOB	2	-25 ± 3	27 ± 7	-3.309	34540 ± 420	5.64 ± 0.05	-1.67 ± 0.04	2018ApJ...868...70L
LAMOSTJ033847.06+413424.2	sdB	2	-7 ± 5	175 ± 10	-67.8438	21457 ± 183	5.73 ± 0.03	-4.30 ± 0.41	2019ApJ...881...7L
LAMOSTJ033946.63+353246.1	sdO	2	77 ± 7	124 ± 15	-14.7455	64650 ± 9600	5.61 ± 0.05	-1.58 ± 0.08	2018ApJ...868...70L
LAMOSTJ034029.29+242956.9	sdB	2	-38 ± 7	16 ± 15	-0.5038	24486 ± 449	5.55 ± 0.06	-3.64 ± 0.29	2019ApJ...881...7L
LAMOSTJ034405.32+220422.7	sdB	4	-20 ± 3	60 ± 15	-4.2384	29251 ± 163	5.72 ± 0.03	-2.71 ± 0.03	2019ApJ...881...7L
LAMOSTJ034422.25+251453.2	sdB	2	-4 ± 4	29 ± 8	-3.0903	29353 ± 1013	6.31 ± 0.17	-3.37 ± 0.11	2019ApJ...881...7L
LAMOSTJ035001.86+324433.0	sdB	2	49 ± 10	28 ± 45	-0.2691	31110 ± 323	5.95 ± 0.08	-2.47 ± 0.13	2019ApJ...881...7L
LAMOSTJ035144.09+365216.7	sdB	2	-12 ± 4	15 ± 8	-1.0795	28170 ± 320	5.37 ± 0.08	-2.58 ± 0.43	2018ApJ...868...70L
SDSSJ035327.61-045427.7	sdB	13	33 ± 4	40 ± 19	-0.1174	32642 ± 1013	5.32 ± 0.15	-3.00 ± 0.20	2017OAJ...26..164G
LAMOSTJ035706.34+362829.4	sdO	2	-19 ± 12	32 ± 37	-0.4029	69159 ± 840	5.96 ± 0.05	-1.50 ± 0.09	2019ApJ...881...7L
LAMOSTJ035710.48+284941.6	sdOB	2	-22 ± 4	32 ± 8	-3.8831	37611 ± 830	5.69 ± 0.12	-4.30 ± 1.83	2019ApJ...881...7L
LAMOSTJ035926.96+270508.6	sdB	2	10 ± 4	2 ± 8	-0.0855	33210 ± 840	5.22 ± 0.14	-2.84 ± 0.49	2020ApJ...889..117L
HS0357+0133	sdB	2	31 ± 3	16 ± 7	-1.5767	30000 ± 800	5.70 ± 0.10	-2.10 ± 0.20	2003A&A...400..939E
LAMOSTJ040242.09+312349.5	sdOB	2	34 ± 3	2 ± 7	-0.104	37500 ± 213	6.05 ± 0.05	-1.58 ± 0.04	2019ApJ...881...7L
LAMOSTJ040422.55+372432.2	sdOB	2	5 ± 4	23 ± 11	-1.4192	34095 ± 237	5.91 ± 0.05	-1.61 ± 0.06	2019ApJ...881...7L
LAMOSTJ040422.89+260754.5	sdB	2	92 ± 5	88 ± 11	-13.0762	30350 ± 180	5.75 ± 0.06	-3.34 ± 0.08	2019ApJ...881..135L
LAMOSTJ041141.69+270918.9	sdB	2	7 ± 5	224 ± 12	-75.4854	29409 ± 267	5.85 ± 0.05	-2.74 ± 0.11	2019ApJ...881...7L
SDSSJ041149.04+152259.1	sdOB	3	-64 ± 5	69 ± 16	-4.9041	37490 ± 520	5.59 ± 0.04	-3.23 ± 0.15	2019ApJ...881..135L
SDSSJ041549.68+303515.3	sdB	4	62 ± 6	48 ± 19	-1.1045	21557 ± 412	5.13 ± 0.06	-2.40 ± 0.07	2019ApJ...881...7L
GALEXJ04158+0154	sdBV	2	14 ± 4	8 ± 8	-0.4489	32920 ± 90	5.78 ± 0.02	-1.71 ± 0.03	2018ApJ...868...70L
LAMOSTJ041737.02+300740.2	sdB	2	-40 ± 3	8 ± 7	-0.5038	31570 ± 190	5.60 ± 0.04	-2.09 ± 0.06	2019ApJ...881..135L
KUV04421+1416	sdBV+dM	2	18 ± 5	76 ± 11	-10.5792	34862 ± 242	5.94 ± 0.04	-2.43 ± 0.05	2021ApJS...256..28L
SDSSJ044715.48+203958.2	sdB	2	3 ± 4	21 ± 9	-1.5574	30250 ± 700	5.51 ± 0.12	-1.88 ± 0.24	2018ApJ...868...70L
LAMOSTJ050252.26+162647.9	sdOB	2	27 ± 4	44 ± 8	-6.1303	41516 ± 624	5.62 ± 0.08	-3.31 ± 0.44	2019ApJ...881...7L
KUV05109+1739	sdB	2	36 ± 4	4 ± 10	-0.1617	30990 ± 200	5.50 ± 0.05	-1.97 ± 0.04	2018ApJ...868...70L
LAMOSTJ052130.82+372146.2	sdB	2	0 ± 3	211 ± 7	-168.2241	26600 ± 300	5.72 ± 0.05	-3.00	2018ApJ...868...70L
LAMOSTJ052354.42-000346.7	He-sdB	2	26 ± 3	15 ± 7	-1.4258	22740 ± 2000	4.47 ± 0.30	-0.45 ± 0.07	
LAMOSTJ053321.16+160647.5	sdB	2	-62 ± 4	22 ± 15	-0.7918	33930 ± 290	5.92 ± 0.05	-1.66 ± 0.05	2018ApJ...868...70L
LAMOSTJ053641.98-033012.4	sdB	2	43 ± 3	1 ± 8	-0.0445	18102 ± 124	6.10 ± 0.03	-3.17 ± 0.48	2019ApJ...881...7L
LAMOSTJ054423.26+381750.0	sdB	2	52 ± 4	42 ± 8	-5.6388	28200 ± 380	5.16 ± 0.06	-2.84 ± 0.24	2019ApJ...881..135L
LAMOSTJ054448.13+153040.2	sdB	2	32 ± 3	9 ± 7	-0.6103	24477 ± 167	4.94	-1.18 ± 0.02	2019ApJ...881...7L
LAMOSTJ055151.32+220437.0	sdB	3	25 ± 3	24 ± 7	-2.4535	29210 ± 190	5.60 ± 0.02	-2.22 ± 0.04	2018ApJ...868...70L
LAMOSTJ055155.40+132352.9	sdB	2	29 ± 3	3 ± 7	-0.1588	32455 ± 187	5.53 ± 0.03	-1.70 ± 0.04	2019ApJ...881...7L
GALEXJ06134+3420	sdOB	2	22 ± 3	4 ± 7	-0.2374	34250 ± 390	5.75 ± 0.10	-1.28 ± 0.08	2012MNRAS.427.2180N
SDSSJ061548.02+344650.2	sdB	2	93 ± 5	106 ± 11	-21.0836	23159 ± 271	5.66 ± 0.05	-3.43 ± 0.12	2019ApJ...881...7L
SDSSJ061754.20+233753.0	sdOB	2	27 ± 4	17 ± 12	-0.7678	36120 ± 470	5.70 ± 0.07	-1.52 ± 0.02	2018ApJ...868...70L
RL54	sdB	5	-4 ± 3	229 ± 14	-69.26	31380 ± 60	5.80 ± 0.02	-2.95 ± 0.08	2018ApJ...868...70L
SDSSJ061927.52+352257.5	sdOB	2	60 ± 4	7 ± 10	-0.2891	35590 ± 210	5.53 ± 0.02	-3.00	2018ApJ...868...70L
GALEXJ06196+3430	sdO	2	6 ± 5	6 ± 15	-0.1605	49063 ± 432	4.99 ± 0.01	-1.13 ± 0.03	2019ApJ...881...7L
LAMOSTJ062049.36+191828.9	sdB	2	67 ± 3	45 ± 7	-8.8871	30420 ± 100	5.71 ± 0.02	-2.05 ± 0.07	2018ApJ...868...70L

LAMOSTJ062442.46+282946.5	sdOB	3	80 ± 3	44 ± 9	-6.562	36680 ± 507	6.20 ± 0.07	-1.99 ± 0.14	2019ApJ...881....7L
SDSSJ062704.91+345809.6	sdB	5	2 ± 2	41 ± 9	-4.1929	25330 ± 540	5.30 ± 0.05	-3.34 ± 0.30	2018ApJ...868...70L
KUV06239+2811	sdB	2	9 ± 3	2 ± 7	-0.0959	22934 ± 540	4.96 ± 0.06	-2.39 ± 0.06	2019ApJ...881....7L
LAMOSTJ063359.35+323314.2	sdB	2	53 ± 4	22 ± 10	-1.5203	28655 ± 454	5.56 ± 0.08	-2.77 ± 0.09	2019ApJ...881....7L
LAMOSTJ063650.09+291925.0	He-sdOB	2	66 ± 8	8 ± 17	-0.194	39902 ± 642	5.49 ± 0.17	-0.06 ± 0.13	2019ApJ...881....7L
SDSSJ064005.18+273553.8	sdOB	2	127 ± 4	116 ± 8	-42.9842	37797 ± 468	6.11 ± 0.08	-1.32 ± 0.07	2019ApJ...881....7L
LAMOSTJ064136.41+334627.1	sdB	3	-18 ± 4	151 ± 14	-28.0578	30149 ± 373	5.89 ± 0.08	-2.14 ± 0.08	2019ApJ...881....7L
FBS0638+428	sdB	2	67 ± 3	37 ± 7	-5.8363	28140 ± 320	5.56 ± 0.06	-2.77 ± 0.14	2018ApJ...868...70L
FBS0646+386	sdB	10	25 ± 3	169 ± 20	-30.7388	32017 ± 15	5.53 ± 0.02	-2.11 ± 0.03	2019ApJ...881....7L
LAMOSTJ065008.84+110749.6	sdOB	2	27 ± 4	29 ± 8	-2.9574	40098 ± 1551	5.80 ± 0.20	-3.51 ± 1.71	2019ApJ...881....7L
SDSSJ065057.12+272335.4	sdB	5	48 ± 5	55 ± 42	-1.3543	20822 ± 741	5.12 ± 0.14	-1.59 ± 0.11	2019ApJ...881....7L
SDSSJ065251.84+290023.3	sdB	4	22 ± 4	35 ± 13	-2.2846	32110 ± 580	5.70 ± 0.13	-1.91 ± 0.12	2016ApJ...818..202L
LAMOSTJ065446.63+244926.8	sdO	2	92 ± 3	0 ± 7	0	54389 ± 541	5.32 ± 0.01	-2.08 ± 0.05	2019ApJ...881....7L
LAMOSTJ065533.05+212339.0	sdB	2	47 ± 5	5 ± 16	-0.1204	32273 ± 324	5.78 ± 0.06	-2.27 ± 0.11	2019ApJ...881....7L
LAMOSTJ065658.95+284457.6	sdB	5	-1 ± 3	197 ± 18	-106.5118	29660 ± 1100	5.55 ± 0.16	-3.20 ± 0.75	2016ApJ...818..202L
FBS0654+366	He-sdB	2	46 ± 3	14 ± 7	-1.2288	24987 ± 532	4.83 ± 0.05	-0.54 ± 0.08	2019ApJ...881....7L
LAMOSTJ065816.72+094343.1	sdOB	2	171 ± 4	148 ± 9	-54.1418	36213 ± 236	5.60 ± 0.04	-1.71 ± 0.04	2019ApJ...881....7L
LAMOSTJ070147.91+283405.3	sdB	3	-5 ± 3	47 ± 8	-7.9354	26070 ± 930	5.49 ± 0.13	-1.88 ± 0.15	2016ApJ...818..202L
LAMOSTJ070514.61+222121.4	sdB	2	54 ± 4	79 ± 8	-18.2068	28837 ± 252	5.50 ± 0.04	-2.87 ± 0.09	2019ApJ...881....7L
LAMOSTJ070615.60+420041.9	sdB	2	-87 ± 13	69 ± 50	-0.7707	29818 ± 360	5.92 ± 0.08	-2.15 ± 0.10	2019ApJ...881....7L
SDSSJ070718.60+140058.3	sdOB	2	11 ± 4	34 ± 8	-4.3161	36280 ± 339	6.09 ± 0.06	-1.92 ± 0.13	2019ApJ...881....7L
LAMOSTJ070828.40+442534.8	He-sdOB	2	-27 ± 9	2 ± 19	-0.036	38992 ± 484	6.05 ± 0.08	4.00 ± 0.50	2019ApJ...881....7L
LAMOSTJ071420.01+262850.9	sdB	2	15 ± 5	40 ± 10	-4.1983	27856 ± 569	5.77 ± 0.09	-2.83 ± 0.23	2019ApJ...881....7L
LAMOSTJ072146.62+233019.6	sdOB	2	-32 ± 24	24 ± 52	-0.1893	38000 ± 13	6.30 ± 0.01	-1.53 ± 0.06	2019ApJ...881....7L
SDSSJ072201.31+403210.2	sdB	6	-19 ± 5	110 ± 26	-2.763	28500 ± 212	5.41 ± 0.04	-2.52 ± 0.06	2018ApJ...868...70L
SDSSJ072351.47+301916.5	sdB	6	3 ± 3	47 ± 7	-6.7001	32400 ± 190	5.91 ± 0.04	-1.53 ± 0.04	2019ApJ...881....7L
LAMOSTJ072454.93+151650.8	sdB	2	91 ± 3	16 ± 7	-1.5092	32721 ± 128	5.85 ± 0.03	-1.78 ± 0.03	2019ApJ...881....7L
SDSSJ072614.69+415748.9	sdB	12	13 ± 4	75 ± 23	-2.4264	29462 ± 463	5.53 ± 0.06	-2.42 ± 0.16	2019ApJ...881....7L
LAMOSTJ073059.10+333706.2	sdOB	3	88 ± 5	87 ± 14	-8.391	36169 ± 345	5.81 ± 0.08	-3.92 ± 0.38	2019ApJ...881....7L
SDSSJ073220.14+270408.5	He-sdOB	7	104 ± 6	38 ± 28	-0.1365	37526 ± 342	5.91 ± 0.07	0.40 ± 0.04	2017OAS...26..164G
SDSSJ073325.61+365257.6	sdB	6	18 ± 3	36 ± 11	-1.3785	33486 ± 876	5.97 ± 0.13	-2.70 ± 0.20	2019ApJ...881....7L
SDSSJ073445.11+302949.5	sdB	2	-8 ± 3	89 ± 7	-32.4533	30340 ± 349	5.64 ± 0.08	-2.80 ± 0.22	2019ApJ...881....7L
TON826	sdB	2	1 ± 3	2 ± 7	-0.1071	27699 ± 316	5.36 ± 0.04	-2.36 ± 0.04	2019ApJ...881....7L
SDSSJ073714.25+250554.6	sdB	2	36 ± 3	14 ± 7	-1.2288	27400 ± 404	5.46 ± 0.06	-2.41 ± 0.06	2019ApJ...881....7L
GALEXJ07380+2624	sdB	4	81 ± 3	127 ± 11	-37.5373	29740 ± 400	5.48 ± 0.06	-3.40 ± 0.87	2012MNRAS.427.2180N
LAMOSTJ073817.49+134427.9	sdB	3	79 ± 8	86 ± 31	-1.8019	28018 ± 453	5.55 ± 0.08	-2.99 ± 0.11	2019ApJ...881....7L
SDSSJ073856.98+401942.0	He-sdO	16	-31 ± 3	89 ± 15	-7.4117	67546 ± 2592	5.45 ± 0.09	2.39 ± 0.18	2017OAS...26..164G
SDSSJ074023.56+204937.0	sdOB	7	73 ± 3	36 ± 16	-0.4293	33988 ± 916	5.78 ± 0.14	-1.70 ± 0.20	2019ApJ...881..135L
SDSSJ074025.12+155155.0	sdOB	8	52 ± 6	63 ± 52	-0.2506	32430 ± 660	6.21 ± 0.12	-3.00	2012MNRAS.427.2180N
SDSSJ074313.25+423334.8	sdB	12	-63 ± 10	114 ± 62	-0.4539	27855 ± 567	5.41 ± 0.10	-2.57 ± 0.38	2017OAS...26..164G
GALEXJ07445+3021	sdB	2	12 ± 5	62 ± 11	-7.702	27910 ± 470	5.42 ± 0.08	-2.75 ± 0.25	2015A&A...577A..26G
SDSSJ074458.09+324259.9	sdOB	9	41 ± 9	80 ± 36	-0.7538	35493 ± 964	6.00 ± 0.14	-1.10 ± 0.20	2019ApJ...881....7L
SDSSJ074551.13+170600.3	sdOB	20	44 ± 3	44 ± 25	-0.0057	35600 ± 400	5.54 ± 0.05	-2.80 ± 0.10	2019ApJ...881....7L
SDSSJ074552.59+255127.3	sdB	2	-27 ± 4	26 ± 9	-2.047	26591 ± 404	5.34 ± 0.05	-2.41 ± 0.08	2015A&A...577A..26G
SDSSJ074613.16+333307.6	He-sdO	12	1 ± 3	45 ± 21	-0.1799	47148 ± 700	5.74 ± 0.07	4.00 ± 1.00	2019ApJ...881....7L
SDSSJ074806.15+342927.7	sdOB	16	-67 ± 5	69 ± 28	-0.1201	35100 ± 800	5.72 ± 0.08	-1.70 ± 0.10	2015A&A...577A..26G
SDSSJ074807.32+193247.7	sdB	9	-56 ± 5	61 ± 31	-0.6182	26183 ± 1262	5.34 ± 0.18	-2.20 ± 0.20	2017OAS...26..164G

SDSSJ074811.33+435239.6	sdB	17	37 ± 3	51 ± 23	-1.0653	26083 ± 851	5.49 ± 0.11	-1.92 ± 0.19	2019MNRAS,486.2169K
SDSSJ074811.70+134349.2	sdB	2	7 ± 3	11 ± 7	-0.8081	25217 ± 363	5.49 ± 0.05	-2.90 ± 0.10	2019ApJ...881....7L
SDSSJ074818.98+482107.7	sdB	12	5 ± 3	35 ± 19	-0.2448	27035 ± 1258	5.03 ± 0.19	-1.20 ± 0.20	2017OAS...26..164G
SDSSJ074852.07+454903.9	sdB	18	87 ± 2	73 ± 19	-6.3093	27217 ± 1129	5.51 ± 0.16	-2.30 ± 0.20	2017OAS...26..164G
GALEXJ07489+3042	sdB	2	137 ± 3	18 ± 8	-1.5548	30760 ± 830	5.71 ± 0.17	-1.85 ± 0.13	2012MNRAS,427.2180N
SDSSJ074902.84+124811.1	sdOB	5	1 ± 6	48 ± 24	-0.4176	37580 ± 840	5.53 ± 0.09	-3.26 ± 0.37	2019ApJ...881..135L
SDSSJ075053.28+144815.0	sdB	9	23 ± 4	95 ± 40	-0.2425	26989 ± 1183	5.48 ± 0.17	-2.40 ± 0.20	2017OAS...26..164G
SDSSJ075108.88+162325.8	sdB	9	18 ± 4	41 ± 17	-0.6879	25936 ± 1235	5.25 ± 0.18	-2.40 ± 0.20	2017OAS...26..164G
LAMOSTJ075139.27+064604.8	He-sdOB	2	-1 ± 8	5 ± 18	-0.1064	40755 ± 203	5.65 ± 0.05	0.03 ± 0.03	
SDSSJ075227.28+194512.2	sdB	11	79 ± 4	92 ± 16	-3.9396	28310 ± 1096	5.56 ± 0.16	-3.00 ± 0.20	2017OAS...26..164G
SDSSJ075236.78+441642.4	sdB	12	-118 ± 4	71 ± 33	-0.115	34234 ± 1046	5.75 ± 0.16	-1.00 ± 0.20	2017OAS...26..164G
SDSSJ075354.22+253109.8	sdB	2	30 ± 3	48 ± 7	-9.2393	33755 ± 320	5.81 ± 0.07	-1.78 ± 0.07	2019ApJ...881....7L
SDSSJ075603.77+222630.9	sdO	4	58 ± 4	19 ± 12	-0.5743	51072 ± 1398	5.71 ± 0.06	-2.13 ± 0.06	
SDSSJ075610.33+410453.6	sdB	11	69 ± 3	34 ± 17	-0.2234	23961 ± 838	5.70 ± 0.10	-2.22 ± 0.15	2019MNRAS,486.2169K
SDSSJ075649.90+231736.5	sdB	25	-39 ± 4	134 ± 34	-1.2889	19140 ± 911	5.09 ± 0.14	-1.94 ± 0.21	
SDSSJ075711.83+134508.4	sdOB	7	50 ± 3	19 ± 20	-0.4881	36907 ± 911	5.85 ± 0.13	-1.50 ± 0.20	2017OAS...26..164G
GALEXJ07581-0432	He-sdOB	3	100 ± 8	17 ± 17	-0.1974	41569 ± 137	5.75 ± 0.03	0.63 ± 0.03	
SDSSJ075847.74+115806.3	sdB	11	141 ± 6	105 ± 33	-0.6712	19163 ± 838	4.61 ± 0.10	-2.33 ± 0.38	
LAMOSTJ075922.99+164601.6	sdOB	3	62 ± 2	16 ± 7	-1.0801	37275 ± 304	5.08 ± 0.03	-3.00 ± 0.07	2019ApJ...881....7L
SDSSJ075944.98+371503.1	He-sdOB	5	22 ± 4	18 ± 15	-0.1509	36826 ± 589	6.01 ± 0.07	-0.88 ± 0.13	
BD-32179	sdO	3	57 ± 5	6 ± 12	-0.0558	62000 ± 5000	4.50 ± 0.50	0.30 ± 0.20	1987Msngr..47...36H
TON299	sdB	5	-31 ± 4	26 ± 15	-0.8044	32450 ± 580	5.92 ± 0.12	-1.36 ± 0.10	2016ApJ...818..202L
SDSSJ080628.65+242057.5	sdB	2	36 ± 3	22 ± 7	-2.6849	28391 ± 262	5.51 ± 0.04	-2.58 ± 0.02	2019ApJ...881....7L
SBSS0803+510	He-sdO	11	-96 ± 3	27 ± 17	-0.0599	50807 ± 615	5.74 ± 0.05	3.59 ± 0.18	
SDSSJ080739.43+384226.5	sdOB	12	-138 ± 6	97 ± 34	-0.6959	35401 ± 564	5.90 ± 0.09	-0.40 ± 0.07	
SDSSJ080758.25+272434.3	sdOB	2	17 ± 5	7 ± 10	-0.2953	41852 ± 264	5.50 ± 0.03	-3.60 ± 0.18	2019ApJ...881....7L
SDSSJ080833.76+180221.8	He-sdO	13	-93 ± 3	41 ± 27	-0.0742	49230 ± 662	5.74 ± 0.08	3.29 ± 0.66	
SDSSJ080921.96+160841.2	sdOB	11	40 ± 2	24 ± 18	-0.0657	36316 ± 967	5.63 ± 0.13	-3.00 ± 0.20	2017OAS...26..164G
SDSSJ081017.91+191749.1	sdOB	9	57 ± 6	53 ± 38	-0.0746	35445 ± 495	5.89 ± 0.09	-1.40 ± 0.08	
SDSSJ081204.81+135204.6	sdB	14	58 ± 3	99 ± 24	-9.0608	27630 ± 460	5.27 ± 0.08	-2.74 ± 0.17	2019ApJ...881..135L
GALEXJ08125+1601	sdB	3	55 ± 3	68 ± 9	-17.4793	31580 ± 490	5.56 ± 0.13	-2.90	2012MNRAS,427.2180N
SDSSJ081342.92+275034.7	sdB	10	-74 ± 3	142 ± 21	-21.9459	25616 ± 1238	5.39 ± 0.18	-2.50 ± 0.20	2017OAS...26..164G
SDSSJ081531.20+245222.6	sdOB	7	1 ± 4	69 ± 15	-5.7209	35360 ± 670	5.55 ± 0.10	-3.00	2019ApJ...881..135L
PG0812+482	sdB	7	-4 ± 2	48 ± 12	-3.5767	23030 ± 1968	5.23 ± 0.29	-2.70 ± 0.20	2017OAS...26..164G
HS0815+4243	sdBV	9	43 ± 3	59 ± 14	-4.1534	33800 ± 800	5.90 ± 0.10	-2.00 ± 0.20	2003A&A...400..939E
SDSSJ081931.22+142756.2	sdB	5	13 ± 3	38 ± 11	-2.1803	19451 ± 3643	4.81 ± 0.42	-2.12 ± 0.32	
SDSSJ082110.89+183924.2	sdOB	13	17 ± 6	92 ± 38	-0.1876	35057 ± 1013	5.75 ± 0.16	-1.80 ± 0.20	2017OAS...26..164G
SDSSJ082159.06+411227.9	sdB	11	-52 ± 5	153 ± 24	-6.4067	27842 ± 328	5.58 ± 0.08	-2.50 ± 0.39	
KUV08191+3951	sdB	5	-4 ± 5	18 ± 16	-0.14	31660 ± 980	5.84 ± 0.23	-2.24 ± 0.19	2016ApJ...818..202L
SDSSJ082332.09+113641.9	sdB+WD	10	45 ± 3	140 ± 21	-37.9199	31200 ± 600	5.79 ± 0.06	-2.00 ± 0.10	2015A&A...577A..26G
PTF1J082340.04+081936.5	sdB	2	41 ± 4	122 ± 9	-36.7241	29526 ± 148	6.03 ± 0.03	-2.72 ± 0.07	2019ApJ...881....7L
SDSSJ082657.29+122818.1	sdOB	10	96 ± 6	54 ± 25	-0.2579	36500 ± 400	5.83 ± 0.12	-1.40 ± 0.10	2015A&A...577A..26G
GALEXJ08275+1753	sdB	2	128 ± 3	8 ± 7	-0.5731	29550 ± 950	5.55 ± 0.09	-1.28 ± 0.10	2012MNRAS,427.2180N
SDSSJ082802.03+404008.9	sdO	13	-169 ± 4	51 ± 27	-0.1724	49214 ± 861	5.63 ± 0.05	-2.10 ± 0.07	
UV0825+15	He-sdOB	2	38 ± 3	11 ± 7	-0.8957	37060 ± 610	5.92 ± 0.10	-0.62 ± 0.08	2012MNRAS,427.2180N
PG0826+480	sdB+WD	18	46 ± 2	173 ± 17	-60.632	25300 ± 600	5.38 ± 0.06	-3.00	2015A&A...577A..26G
SDSSJ083112.95+394730.3	sdB	8	39 ± 7	145 ± 53	-0.8057	28487 ± 1710	5.30 ± 0.28	-2.08 ± 0.43	

SDSSJ083139.68+162316.4	sdB	9	48 ± 5	47 ± 21	-0.3779	19344 ± 538	4.74 ± 0.09	-1.80 ± 0.14	2019ApJ...881....7L
SDSSJ083241.95+483445.1	sdB	11	28 ± 3	49 ± 22	-0.6766	18427 ± 1107	4.67 ± 0.18	-1.70 ± 0.16	2019ApJ...881....7L
TON930	sdB	3	80 ± 4	142 ± 12	-29.3611	28986 ± 118	5.67 ± 0.03	-2.58 ± 0.07	2016ApJ...818..202L
SDSSJ083603.98+155216.4	sdB	6	17 ± 3	122 ± 10	-31.8574	27100 ± 640	5.42 ± 0.07	-2.45 ± 0.17	2019MNRAS...486.2169K
SDSSJ083612.02+191755.8	sdOB	3	139 ± 7	186 ± 20	-17.9672	35097 ± 824	5.72 ± 0.11	-1.92 ± 0.19	2017OAS...26..164G
SDSSJ083842.70+053309.4	sdB	4	111 ± 5	75 ± 15	-7.9841	30932 ± 991	5.60 ± 0.14	-2.50 ± 0.20	
SDSSJ083929.99+391903.4	sdB	9	-185 ± 5	73 ± 41	-0.3279	30353 ± 724	5.39 ± 0.10	-2.38 ± 0.37	
SDSSJ083935.90+030840.8	sdO	13	35 ± 3	53 ± 23	-0.5419	49708 ± 1340	5.79 ± 0.07	-2.77 ± 0.17	
SDSSJ084125.44+610320.7	He-sdO	10	-114 ± 5	51 ± 29	-0.4062	44064 ± 454	5.71 ± 0.10	3.79 ± 1.37	
SDSSJ084328.87+082438.2	sdB	9	-35 ± 4	29 ± 17	-0.0345	25720 ± 430	5.64 ± 0.05	-3.00	2019ApJ...881..135L
SDSSJ084423.12+075306.1	sdO	7	20 ± 6	36 ± 27	-0.0417	73181 ± 5353	6.12 ± 0.08	0.09 ± 0.01	
LB400	sdB	5	59 ± 2	47 ± 7	-10.4298	25258 ± 530	5.21 ± 0.06	-1.64 ± 0.05	2019ApJ...881....7L
SDSSJ084556.15+542357.6	sdB	18	38 ± 6	106 ± 32	-1.0813	32326 ± 759	5.33 ± 0.13	-1.45 ± 0.18	
PG0844+232	sdO	5	-52 ± 4	48 ± 13	-2.8758	52798 ± 2287	5.82 ± 0.09	-1.93 ± 0.07	
SDSSJ085042.50+024546.1	sdB	9	30 ± 3	18 ± 12	-0.0387	25335 ± 1216	5.23 ± 0.17	-2.40 ± 0.20	2017OAS...26..164G
SDSSJ085217.70+211637.5	sdB	4	4 ± 5	34 ± 15	-1.2017	30536 ± 1039	5.43 ± 0.16	-2.50 ± 0.20	2017OAS...26..164G
PG0850+170	sdB+WD	2	54 ± 3	46 ± 7	-8.1666	27100 ± 1000	5.37 ± 0.15	-2.20 ± 0.10	2001MNRAS...326.1391M
SDSSJ085335.09+621642.9	sdOB	12	-170 ± 6	39 ± 36	-0.0029	34530 ± 990	5.97 ± 0.15	-1.00 ± 0.20	2017OAS...26..164G
GALEXJ08568+1701	sdB	4	-14 ± 2	21 ± 8	-1.1502	29270 ± 450	5.39 ± 0.20	-2.81	2012MNRAS...427.2180N
GALEXJ08588+0210	sdO	4	52 ± 2	93 ± 7	-34.7258	48090 ± 1480	5.62 ± 0.06	-1.93 ± 0.14	2018ApJ...868...70L
SDSSJ085900.32+023313.1	sdOB	21	41 ± 3	75 ± 26	-0.1696	33882 ± 917	5.67 ± 0.13	-1.70 ± 0.20	2017OAS...26..164G
PG0856+121	sdB	3	104 ± 3	26 ± 8	-2.1333	25010 ± 1040	5.53 ± 0.11	-3.16	2016ApJ...818..202L
SDSSJ085912.11+025006.6	sdB	18	172 ± 4	41 ± 26	-0.0465	20675 ± 588	4.81 ± 0.08	-3.32 ± 0.47	
SDSSJ090252.46+321316.0	sdB	8	-10 ± 5	94 ± 32	-0.9333	37059 ± 1026	5.93 ± 0.16	-2.00 ± 0.20	2017OAS...26..164G
SDSSJ090318.36+043533.7	sdOB	10	53 ± 6	34 ± 30	-0.0146	40118 ± 398	5.77 ± 0.04	-3.00	
PG0901+309	sdOB	3	6 ± 3	2 ± 10	-0.0098	38400 ± 900	5.69 ± 0.31	-0.57 ± 0.15	2016ApJ...818..202L
SDSSJ090902.40+161207.4	He-sdO	8	62 ± 5	37 ± 21	-0.3144	54824 ± 868	5.90 ± 0.13	0.33 ± 0.16	
PG0905+627	sdO	11	-52 ± 4	47 ± 25	-0.0904	50935 ± 2236	5.91 ± 0.08	-1.67 ± 0.04	
PG0906+597	sdO	2	-95 ± 5	112 ± 41	-2.1394	74935 ± 3876	6.40 ± 0.08	-2.08 ± 0.18	2019ApJ...881....7L
PG0907+123	sdB+WD	2	-13 ± 4	10 ± 8	-0.6051	26200 ± 900	5.30 ± 0.10	-1.70 ± 0.10	2001MNRAS...326.1391M
PG0908+281	sdO	8	76 ± 3	66 ± 23	-3.5785	47386 ± 771	6.03 ± 0.05	-2.61 ± 0.12	
PG0909+164	sdB	3	38 ± 3	98 ± 9	-24.4577	35300 ± 500	5.33 ± 0.05	-2.76 ± 0.10	2013A&A...557A.122G
SDSSJ091225.13+421922.5	sdB	8	-58 ± 5	66 ± 28	-1.6135	29668 ± 1066	5.50 ± 0.17	-3.00 ± 0.20	2017OAS...26..164G
PG0909+276	sdOB	3	35 ± 3	43 ± 8	-5.9941	35500 ± 500	6.09 ± 0.05	-1.00 ± 0.10	2013A&A...557A.122G
PG0912+119	He-sdO	9	61 ± 3	43 ± 15	-2.123	49052 ± 542	5.67 ± 0.06	3.35 ± 0.34	
SDSSJ091544.43+5111338.8	sdOB	9	-22 ± 6	44 ± 30	-0.0332	36668 ± 941	5.90 ± 0.15	-1.80 ± 0.20	2017OAS...26..164G
SDSSJ091615.49+132833.1	sdB	7	-21 ± 6	21 ± 22	-0.0214	30900 ± 400	5.48 ± 0.05	-3.00	2015A&A...577A..26G
SDSSJ091648.02+434704.36	sdB	10	-30 ± 4	51 ± 24	-0.5852	22855 ± 856	5.10 ± 0.11	-2.00 ± 0.18	2019MNRAS...486.2169K
TYC231-972-1	sdB	2	-3 ± 3	7 ± 7	-0.4792	26320 ± 77	4.85	-0.51 ± 0.01	2019ApJ...881....7L
PG0918+029	sdB+WD	2	67 ± 13	40 ± 31	-0.6986	31460 ± 510	5.79 ± 0.12	-2.53 ± 0.14	2016ApJ...818..202L
SDSSJ092206.80+081929.4	sdOB	4	4 ± 4	13 ± 13	-0.1167	32803 ± 917	5.81 ± 0.13	-1.80 ± 0.20	2017OAS...26..164G
PG0919+272	sdB	2	-10 ± 3	27 ± 7	-3.174	33230 ± 240	6.00 ± 0.04	-2.40 ± 0.13	2016ApJ...818..202L
SDSSJ092245.80+214239.0	He-sdO	4	-20 ± 7	24 ± 41	-0.0793	42463 ± 267	5.81 ± 0.07	1.72 ± 0.28	
PG0920+297	sdB	3	37 ± 2	60 ± 7	-17.8072	30810 ± 1430	5.99 ± 0.22	-1.28 ± 0.18	2016ApJ...818..202L
SDSSJ092447.10+231917.6	sdB	2	96 ± 4	46 ± 9	-6.0888	25652 ± 826	5.35 ± 0.10	-2.00 ± 0.09	2019MNRAS...486.2169K
SDSSJ092520.01+273619.7	sdB	12	244 ± 4	203 ± 27	-25.9252	28357 ± 636	5.43 ± 0.10	-2.95 ± 0.48	
SDSSJ092520.70+470330.6	sdB	7	-22 ± 6	107 ± 23	-6.7047	28100 ± 900	5.17 ± 0.15	-2.50 ± 0.20	2015A&A...577A..26G

PG0924+565	sdO	10	-126 ± 3	43 ± 15	-1.1351	6198 ± 2606	5.40 ± 0.04	-1.06 ± 0.04	2012MNRAS.427.2180N
PG0926+065	sdB	4	8 ± 5	18 ± 14	-0.1687	26060 ± 680	5.45 ± 0.08	-2.79 ± 0.46	2017OAst...26..164G
SDSSJ093006.79+314258.4	sdOB	9	78 ± 4	101 ± 20	-6.0273	33427 ± 919	5.88 ± 0.14	-1.70 ± 0.20	2016ApJ...818..202L
PG0927+311	sdB	4	33 ± 2	132 ± 9	-46.8289	28140 ± 490	5.81 ± 0.07	-2.68 ± 0.12	2015A&A...577A..26G
PG0928+031	sdB	3	51 ± 3	81 ± 8	-20.784	30000 ± 600	5.67 ± 0.18	-2.70 ± 0.20	2016ApJ...818..202L
PG0932+314	sdB	10	21 ± 2	57 ± 14	-7.2513	33440 ± 670	5.84 ± 0.14	-1.60 ± 0.13	2016ApJ...818..202L
PG0934+163	He-sdOB	6	111 ± 6	24 ± 21	-0.0752	42320 ± 670	5.68 ± 0.08	-0.23 ± 0.06	2016ApJ...818..202L
PG0934+186	sdB+WD	2	-38 ± 6	9 ± 12	-0.335	34970 ± 1060	5.58 ± 0.14	-2.53	2016ApJ...818..202L
PG0934+553	sdOB	3	67 ± 2	32 ± 7	-4.3653	44340 ± 350	5.37 ± 0.06	-0.43 ± 0.23	2014A&A...562A..95G
PG0941+280	sdB+WD	2	192 ± 4	134 ± 14	-20.7739	29400 ± 500	5.43 ± 0.05	-3.00 ± 0.10	2003A&A...400..939E
HS0941+4649	sdB	7	-144 ± 3	33 ± 16	-1.2373	34700 ± 1500	5.80 ± 0.20	-2.00 ± 0.40	2016ApJ...818..202L
PG0943+043	sdOB	4	67 ± 4	21 ± 14	-0.3703	37110 ± 1020	5.77 ± 0.20	-1.45 ± 0.20	2016ApJ...818..202L
PG0944+275	sdB	12	-10 ± 2	163 ± 20	-24.9678	28320 ± 1720	5.89 ± 0.23	-2.26	2016ApJ...818..202L
SDSSJ094750.71+162731.8	sdB	10	92 ± 4	262 ± 25	-61.3059	30000 ± 700	6.25 ± 0.31	-2.20 ± 0.30	2015A&A...577A..26G
SDSSJ094758.91+091012.3	sdOB	6	-16 ± 7	47 ± 27	-0.195	34839 ± 1009	5.86 ± 0.15	-0.90 ± 0.20	2017OAst...26..164G
SDSSJ094850.47+551631.7	sdOB	7	-36 ± 6	198 ± 35	-11.0786	37295 ± 816	5.93 ± 0.12	-1.49 ± 0.20	
SDSSJ094856.95+334151.0	He-sdO	7	3 ± 6	55 ± 30	-0.2908	51694 ± 652	5.68 ± 0.06	3.66 ± 0.36	
SDSSJ094918.62+144142.6	sdB	8	240 ± 7	52 ± 32	-0.0636	29570 ± 1058	5.34 ± 0.16	-1.60 ± 0.20	2017OAst...26..164G
PG0946+305	He-sdO	4	6 ± 7	13 ± 33	-0.0185	47541 ± 889	5.83 ± 0.08	3.29 ± 0.79	
US1027	sdB	8	-28 ± 4	48 ± 25	-0.2265	28500 ± 500	5.24 ± 0.07	-2.30 ± 0.30	2015A&A...577A..26G
PG0948+187	sdOB	2	197 ± 4	206 ± 10	-81.512	35340 ± 970	5.85 ± 0.19	-1.84 ± 0.20	2016ApJ...818..202L
PG0948+041	sdB+WD	2	161 ± 6	14 ± 15	-0.4316	29800 ± 300	5.48 ± 0.04	-2.80 ± 0.30	2015A&A...577A..26G
SDSSJ095229.62+301553.6	sdB	7	181 ± 6	220 ± 27	-26.4689	38251 ± 1733	5.04 ± 0.19	-2.40	
SDSSJ095254.16+470919.2	sdB	9	-31 ± 6	77 ± 43	-0.1567	33428 ± 1101	5.46 ± 0.12	-3.00	
SDSSJ095854.93+245311.8	He-sdO	6	106 ± 10	153 ± 55	-1.384	50560 ± 1687	5.80 ± 0.13	-0.94 ± 0.12	
KUV09565+3632	sdB	2	-13 ± 4	2 ± 9	-0.0827	27180 ± 230	5.22 ± 0.03	-2.69 ± 0.08	2016ApJ...818..202L
PG0957+037	sdOB	2	125 ± 4	9 ± 10	-0.3898	34300 ± 800	5.45 ± 0.08	-2.50 ± 0.20	2020MNRAS.498...12H
PG0956+359	He-sdO	4	15 ± 6	26 ± 20	-0.1725	47745 ± 1093	5.74 ± 0.14	2.46 ± 1.53	
KUV09577+3700	sdB	11	0 ± 4	43 ± 24	-0.3807	25315 ± 1368	5.27 ± 0.20	-2.70 ± 0.20	2017OAst...26..164G
CBS17	sdB	7	-35 ± 4	69 ± 16	-4.7753	23290 ± 2160	4.67 ± 0.31	-2.14	2016ApJ...818..202L
PG1000+408	sdB+WD	3	23 ± 3	130 ± 13	-22.6157	36400 ± 1000	5.54 ± 0.10	-2.70 ± 0.10	2001MNRAS.326.1391M
SDSSJ100535.76+223952.1	sdB	11	-148 ± 7	45 ± 47	-0.0021	29000 ± 700	5.43 ± 0.13	-2.70 ± 0.20	2015A&A...577A..26G
SDSSJ100621.06-002049.9	sdOB	7	-19 ± 6	73 ± 22	-1.5419	35338 ± 612	5.98 ± 0.08	-1.16 ± 0.13	
PG1009+491	sdB	11	23 ± 4	84 ± 47	-0.0406	28690 ± 1039	5.54 ± 0.16	-2.40 ± 0.20	2017OAst...26..164G
SDSSJ101342.12+260620.0	sdO	12	-22 ± 2	96 ± 26	-5.081	55747 ± 1745	5.86 ± 0.05	-1.75 ± 0.04	
SDSSJ101418.96+521007.5	sdB	12	-180 ± 4	96 ± 21	-9.5174	30803 ± 476	5.55 ± 0.10	-2.72 ± 0.19	2019ApJ...881....7L
SDSSJ101422.92+182849.0	sdB	7	68 ± 9	24 ± 30	-0.0075	31564 ± 908	5.58 ± 0.12	-3.00	2019MNRAS.486.2169K
PG1012+007	sdB	3	53 ± 3	163 ± 7	-119.0972	32200 ± 1000	5.99 ± 0.15	-1.90 ± 0.10	1994ApJ...432..351S
SDSSJ101613.32+240008.3	sdB	2	128 ± 4	13 ± 10	-0.7033	23240 ± 423	4.99 ± 0.01	-4.23 ± 1.05	2019ApJ...881....7L
PG1017+430	sdOB	2	91 ± 3	25 ± 7	-2.9879	40230 ± 1340	5.11 ± 0.10	-2.78 ± 0.25	2016ApJ...818..202L
SDSSJ102120.44+444636.9	He-sdO	5	-89 ± 8	40 ± 31	-0.1099	49242 ± 609	5.76 ± 0.09	2.70 ± 0.57	
SDSSJ102320.36+462026.8	He-sdO	7	62 ± 6	77 ± 23	-1.5295	52763 ± 1579	5.64 ± 0.09	2.97 ± 0.68	
SDSSJ102407.23+392253.5	sdOB	9	159 ± 5	149 ± 24	-16.0958	36962 ± 908	5.98 ± 0.14	-1.10 ± 0.20	2017OAst...26..164G
SDSSJ102439.43+383917.9	sdB	9	41 ± 5	43 ± 23	-0.2338	29800 ± 300	5.61 ± 0.03	-2.10 ± 0.10	
SDSSJ103027.05+152548.28	sdB	8	160 ± 4	49 ± 30	-0.4182	24574 ± 504	5.34 ± 0.06	-2.29 ± 0.06	2021ApJS...256...28L
SDSSJ103104.58-021315.9	sdB	18	184 ± 6	87 ± 45	-0.1638	33063 ± 573	5.84 ± 0.08	-3.00	
PG1032+406	sdB+WD	4	20 ± 2	50 ± 8	-8.9016	31600 ± 900	5.77 ± 0.10	-2.30 ± 0.10	2001MNRAS.326.1391M

SDSSJ103810.94+253204.8	sdB	6	204 ± 5	15 ± 20	-0.0073	21900 ± 200	4.90 ± 0.07	-1.80 ± 0.10	2017OAst...26..164G
SDSSJ103854.02+525847.8	sdB	11	56 ± 4	48 ± 26	-0.0208	26127 ± 1191	5.31 ± 0.17	-2.70 ± 0.20	
PG1038+510	He-sdO	3	110 ± 7	63 ± 25	-1.3203	51644 ± 653	5.66 ± 0.05	3.43 ± 0.26	
GALEXJ10415+1842	sdB	2	33 ± 3	16 ± 7	-1.5767	34890 ± 680	5.80 ± 0.10	-1.68 ± 0.13	2012MNRAS.427.2180N
SDSSJ104312.02+180038.7	He-sdO	5	-40 ± 5	26 ± 19	-0.1873	44611 ± 381	5.60 ± 0.05	0.85 ± 0.07	2019ApJ...881....7L
SDSSJ104620.15+101629.7	sdB	4	-43 ± 8	24 ± 23	-0.1231	23181 ± 514	4.99 ± 0.02	-2.10 ± 0.11	2021ApJS...256...28L
PG1047+003	sdBV	2	-29 ± 4	25 ± 13	-1.1387	35357 ± 143	5.85 ± 0.02	-1.99 ± 0.03	2017OAst...26..164G
SDSSJ105244.44+245925.3	sdOB	4	20 ± 4	27 ± 19	-0.5277	33792 ± 947	5.70 ± 0.15	-1.80 ± 0.20	2003A&A...400..939E
HS1051+2933	sdOB	12	-125 ± 3	45 ± 29	-0.5218	36300 ± 900	5.95 ± 0.10	-0.60 ± 0.20	2001MNRAS.326.1391M
PG1051+501	sdB	3	-115 ± 2	20 ± 7	-2.1376	33800 ± 900	4.96 ± 0.10	-1.40 ± 0.10	2016ApJ...818..202L
SDSSJ105428.85+010514.7	sdB	11	157 ± 3	25 ± 21	-0.0033	27600 ± 2150	5.85 ± 0.27	-2.98 ± 0.79	
SDSSJ110215.45+024034.1	He-sdO	8	58 ± 6	36 ± 31	-0.0166	55556 ± 801	5.82 ± 0.09	0.56 ± 0.10	
PG1100+526	He-sdO	7	-133 ± 4	37 ± 17	-0.8974	51779 ± 891	5.76 ± 0.04	2.83 ± 0.35	
PG1100-008	sdB	2	170 ± 4	110 ± 9	-30.0366	29223 ± 1059	5.47 ± 0.16	-2.40 ± 0.20	2017OAst...26..164G
PG1102+097	sdOB	12	174 ± 3	33 ± 17	-0.2893	37446 ± 2000	5.01 ± 0.20	-2.10 ± 0.40	2009PhDT.....273H
SDSSJ110614.30+180918.6	sdOB	8	93 ± 5	38 ± 23	-0.1559	26588 ± 1164	5.54 ± 0.16	-1.80 ± 0.20	2017OAst...26..164G
PG1104+299	sdB	13	-34 ± 2	25 ± 17	-0.0171	36032 ± 223	5.85 ± 0.05	-1.42 ± 0.05	2019ApJ...881....7L
PG1105+298	sdOB	6	65 ± 3	115 ± 14	-33.8723	34173 ± 1056	4.80 ±	-2.31 ± 0.46	2019MNRAS.486.2169K
PG1106+271	sdO	2	-14 ± 6	93 ± 13	-11.501	43732 ± 1260	5.50 ± 0.07	-3.27 ± 0.31	
SDSSJ111438.57-004024.3	sdO	15	110 ± 8	177 ± 57	-0.7088	57577 ± 2373	5.74 ± 0.08	-0.99 ± 0.05	
SDSSJ11621.61+390254.4	sdB	12	25 ± 4	89 ± 38	-1.9773	27421 ± 1256	5.54 ± 0.18	-2.10 ± 0.20	2017OAst...26..164G
PG1115+275	He-sdO	6	57 ± 3	112 ± 11	-22.7434	44646 ± 747	6.16 ± 0.07	-1.58 ± 0.10	
PG1116+301	sdB+WD	3	-3 ± 3	222 ± 15	-97.6109	32500 ± 900	5.85 ± 0.10	-2.20 ± 0.10	2001MNRAS.326.1391M
PG1117+312	sdOB	5	30 ± 3	34 ± 13	-2.3031	33626 ± 895	5.74 ± 0.13	-2.20 ± 0.20	2017OAst...26..164G
PG1118+099	sdO	19	152 ± 3	47 ± 25	-0.0111	51393 ± 2218	5.65 ± 0.07	-2.54 ± 0.09	
SDSSJ112201.84+242056.8	He-sdO	4	-144 ± 9	85 ± 38	-0.93	39754 ± 510	6.01 ± 0.07	-0.31 ± 0.07	
PG1119+377	sdOB	10	-72 ± 2	46 ± 7	-5.966	37753 ± 1052	5.53 ± 0.14	-2.70 ± 0.20	2017OAst...26..164G
SDSSJ112222.40+072432.4	sdB	9	-113 ± 4	42 ± 23	-0.2032	24436 ± 1352	5.03 ± 0.18	-2.20 ± 0.20	2017OAst...26..164G
GALEXJ11238+2336	sdB	2	50 ± 3	14 ± 7	-1.2288	28080 ± 60	5.38 ± 0.01	-2.36 ± 0.03	2018ApJ...868...70L
SDSSJ112528.47+320628.2	sdB	9	-99 ± 3	120 ± 31	-7.5903	20970 ± 92	5.02 ± 0.06	-2.15 ± 0.11	2019ApJ...881....7L
SDSSJ112555.19+020250.1	sdB	6	218 ± 4	62 ± 33	-4.1566	18488 ± 454	4.73 ± 0.09	-2.43 ± 0.18	
PG1124+123	sdB	8	0 ± 2	112 ± 7	-47.8986	27910 ± 1090	5.14 ± 0.22	-3.57 ± 0.79	2016ApJ...818..202L
SDSSJ112757.48+010044.2	sdB	10	160 ± 4	26 ± 21	-0.0151	27554 ± 454	5.34 ± 0.09	-2.21 ± 0.58	
PG1125+295	sdO	8	41 ± 2	133 ± 43	-3.1378	60248 ± 3700	5.84 ± 0.07	-2.01 ± 0.06	
PG1127+019	He-sdO	3	19 ± 6	38 ± 29	-0.3765	43527 ± 242	5.89 ± 0.05	3.59 ± 0.53	
PG1128+199	sdB	4	-12 ± 5	9 ± 17	-0.0203	29179 ± 1005	5.58 ± 0.16	-3.00 ± 0.20	2017OAst...26..164G
SDSSJ113149.29+344100.9	sdB	11	-121 ± 2	55 ± 11	-5.9551	24001 ± 233	5.20	-1.90 ± 0.21	2019ApJ...881....7L
PG1130+564	sdB	2	-143 ± 5	41 ± 11	-3.6354	31900 ± 1160	5.06 ± 0.24	-2.70 ± 0.49	2016ApJ...818..202L
CBS143	sdOB	8	22 ± 7	21 ± 30	-0.0009	34806 ± 917	5.95 ± 0.14	-2.30 ± 0.20	2017OAst...26..164G
SDSSJ113725.58+051550.7	sdO	8	135 ± 3	160 ± 34	-43.0305	48472 ± 1596	4.68 ± 0.13	-1.03 ± 0.09	
PG1135+585	sdOB	8	12 ± 3	23 ± 15	-0.2125	35158 ± 908	5.81 ± 0.13	-2.00 ± 0.20	
SDSSJ113902.88+065716.8	sdB	10	230 ± 8	74 ± 47	-0.1862	30905 ± 606	5.74 ± 0.10	-2.80 ± 0.37	
PG1137+470	sdB	3	-44 ± 4	6 ± 10	-0.0816	30700 ± 460	5.53 ± 0.09	-3.98	2016ApJ...818..202L
SDSSJ114251.76+111507.9	sdO	4	89 ± 14	8 ± 45	-0.0012	54950 ± 3443	5.81 ± 0.15	-1.59 ± 0.16	
SDSSJ114352.74+660723.4	sdB	12	-91 ± 9	162 ± 55	-1.0562	27899 ± 971	5.69 ± 0.13	-2.00 ± 0.09	2019MNRAS.486.2169K
PG1142-037	sdB	2	21 ± 3	95 ± 7	-38.9079	31170 ± 251	5.85 ± 0.05	-2.64 ± 0.12	2019ApJ...881....7L
SDSSJ115009.48+061042.1	sdO	5	28 ± 9	44 ± 39	-0.28	60602 ± 3257	5.33 ± 0.12	-1.09 ± 0.12	

SDSSJ115101.03+541003.4	sdOB	9	-205 ± 5	23 ± 25	-0.0034	34694 ± 1166	5.08 ± 0.18	-1.90 ± 0.20	2017OAst...26..164G
PG1151+359	sdB	2	-49 ± 7	213 ± 43	-5.8914	29400 ± 500	5.49 ± 0.06	-2.50 ± 0.30	2015A&A...577A..26G
SDSSJ115716.37+612410.7	sdB	10	-178 ± 5	72 ± 24	-0.7232	29900 ± 500	5.59 ± 0.08	-3.20 ± 0.80	2015A&A...577A..26G
PG1201+258	sdOB	2	-55 ± 3	21 ± 7	-2.3343	35440 ± 189	5.92 ± 0.04	-1.78 ± 0.04	2019ApJ...881....7L
SDSSJ120352.24+235343.3	sdOB	11	173 ± 4	54 ± 23	-0.3894	40237 ± 2000	5.75 ± 0.20	-0.36 ± 0.40	2009PhDT.....273H
SDSSJ120427.94+172745.3	sdB	6	138 ± 7	72 ± 30	-2.1815	25100 ± 900	5.25 ± 0.15	-2.60 ± 0.40	2015A&A...577A..26G
SDSSJ120521.48+224702.2	He-sdOB	12	115 ± 7	77 ± 43	-0.1783	49812 ± 977	5.84 ± 0.07	-0.87 ± 0.10	
PG1203+084	He-sdO	9	-49 ± 3	36 ± 18	-0.6531	49235 ± 1155	5.68 ± 0.08	3.00 ± 0.64	2015A&A...577A..26G
SDSSJ120613.40+205523.1	sdOB	20	-15 ± 4	68 ± 30	-0.3332	35000 ± 500	5.35 ± 0.07	-3.00	2012MNRAS.427.2180N
PG1203+574	sdB	4	-62 ± 2	38 ± 7	-5.5946	33620 ± 390	5.90 ± 0.13	-1.88 ± 0.12	
SDSSJ120626.54+663352.5	He-sdO	7	-49 ± 5	49 ± 18	-1.5674	43907 ± 551	5.70 ± 0.08	3.37 ± 0.81	
SDSSJ120855.51+403716.1	sdB	13	144 ± 7	108 ± 43	-0.4672	34100 ± 900	5.98 ± 0.13	-1.50 ± 0.10	2015A&A...577A..26G
SBSS1212+553	sdO	7	-78 ± 6	45 ± 27	-0.1885	56926 ± 1566	6.00 ± 0.05	-1.64 ± 0.06	
SDSSJ122132.17+163256.4	sdOB	6	84 ± 6	37 ± 26	-0.2112	37403 ± 2000	5.03 ± 0.20	-2.31 ± 0.40	2009PhDT.....273H
SDSSJ122541.69+220818.7	sdB	5	95 ± 10	86 ± 50	-1.5647	22886 ± 662	5.19 ± 0.09	-2.56 ± 0.46	
PG1224+583	sdB	7	-193 ± 5	27 ± 21	-0.0397	29637 ± 1129	5.35 ± 0.18	-2.50 ± 0.20	2017OAst...26..164G
PG1233+427	sdB	4	43 ± 2	17 ± 7	-0.8017	26200 ± 1100	5.31 ± 0.12	-2.75 ± 0.10	2013A&A...557A.122G
SDSSJ123613.89+111834.1	He-sdO	7	68 ± 11	94 ± 59	-0.5077	58817 ± 1794	6.10 ± 0.13	-0.54 ± 0.09	
PG1234+505	sdO	2	17 ± 3	57 ± 7	-13.1436	42190 ± 1200	5.37 ± 0.07	-2.22 ± 0.23	2016ApJ...818..202L
SDSSJ123725.20+233954.09	sdB	5	-162 ± 4	30 ± 21	-0.4831	35255 ± 345	5.49 ± 0.08	-1.12 ± 0.04	2021ApJS...256..28L
SDSSJ123731.51+355421.4	sdB	4	-119 ± 6	82 ± 38	-1.9172	25077 ± 880	5.38 ± 0.10	-2.50 ± 0.10	2019ApJ...881....7L
SDSSJ123808.65+053318.2	He-sdO	10	48 ± 6	92 ± 40	-0.545	50046 ± 730	5.73 ± 0.06	3.51 ± 0.44	
PG1236+479	sdB	4	-90 ± 4	60 ± 14	-3.8019	28400 ± 800	5.55 ± 0.10	-2.50 ± 0.20	2003A&A...400..939E
PG1239+439	sdOB	7	15 ± 5	55 ± 25	-0.6439	37400 ± 1720	5.67 ± 0.23	-0.23 ± 0.20	2016ApJ...818..202L
SDSSJ124248.89+133632.6	sdOB	7	-149 ± 4	44 ± 18	-0.9791	36300 ± 600	5.41 ± 0.10	-3.00	
SDSSJ124310.59+343358.4	He-sdOB	8	163 ± 6	31 ± 25	-0.044	37544 ± 496	5.67 ± 0.07	-0.84 ± 0.10	
SDSSJ124520.88+030951.4	sdOB	7	23 ± 11	84 ± 42	-0.3004	38472 ± 2000	6.00 ± 0.20	-0.67 ± 0.40	
SDSSJ124552.82+175112.2	He-sdOB	6	81 ± 9	64 ± 27	-0.7702	37938 ± 413	5.98 ± 0.06	0.13 ± 0.04	
PG1244-004	sdOB	18	-10 ± 4	57 ± 26	-0.0235	39191 ± 845	6.57 ± 0.06	-3.50	
PG1245+041	sdO	8	20 ± 4	57 ± 17	-1.9807	67359 ± 4512	5.74 ± 0.09	-0.99 ± 0.06	
SDSSJ125129.03+164509.9	sdB	5	282 ± 16	93 ± 57	-0.2748	31441 ± 1023	5.65 ± 0.16	-2.51 ± 0.51	
PG1248+066	He-sdO	9	1 ± 3	17 ± 14	-0.0341	48787 ± 1009	5.79 ± 0.06	3.31 ± 0.55	
PG1249-028	sdB	4	70 ± 4	23 ± 14	-0.6937	30780 ± 480	5.69 ± 0.13	-4.50 ± 1.34	2016ApJ...818..202L
PG1250+303	sdB	11	-73 ± 3	80 ± 15	-5.2776	32550 ± 510	5.81 ± 0.10	-2.28 ± 0.17	2016ApJ...818..202L
SDSSJ125410.86-010408.4	sdB	13	73 ± 4	93 ± 24	-3.6881	20979 ± 1191	4.93 ± 0.16	-1.90 ± 0.20	2017OAst...26..164G
PG1254+279	sdB	9	-69 ± 3	27 ± 12	-0.3244	25050 ± 4010	5.55 ± 0.38	-2.52	2016ApJ...818..202L
SDSSJ125702.30+435245.8	sdB	7	-69 ± 8	99 ± 36	-1.4501	28000 ± 1100	5.77 ± 0.17	-3.00	2015A&A...577A..26G
SDSSJ125720.29+584941.2	sdB	9	-155 ± 5	37 ± 27	-0.0349	25739 ± 1349	5.24 ± 0.20	-3.00 ± 0.20	2017OAst...26..164G
SDSSJ125738.33+181724.2	He-sdOB	7	22 ± 8	55 ± 37	-0.1163	37728 ± 343	6.09 ± 0.05	0.31 ± 0.04	
LAMOSTJ125926.03+272122.7	sdB	3	17 ± 3	26 ± 8	-1.9419	18430 ± 390	4.88 ± 0.07	-1.71 ± 0.11	2016ApJ...818..202L
SDSSJ130214.31+120822.1	sdOB	4	49 ± 4	28 ± 14	-1.092	34767 ± 568	5.81 ± 0.06	-1.56 ± 0.14	
PG1300+278	sdB+WD	2	-59 ± 4	11 ± 11	-0.4932	29600 ± 1000	5.65 ± 0.15	-2.30 ± 0.10	2001MNRAS.326.1391M
KUV13023+3145	sdOB	6	-23 ± 6	50 ± 21	-0.7342	38100 ± 600	5.69 ± 0.12	-0.40 ± 0.10	2015A&A...577A..26G
PG1302+284	sdB	3	34 ± 3	19 ± 7	-1.4894	34580 ± 1070	5.76 ± 0.16	-2.84	2016ApJ...818..202L
PG1303+122	sdB	9	-61 ± 2	45 ± 16	-2.2184	30700 ± 200	5.45 ± 0.03	-2.40 ± 0.10	
PG1303+097	sdB	2	45 ± 4	29 ± 10	-2.3887	29800 ± 500	5.83 ± 0.05	-2.17 ± 0.10	2013A&A...557A.122G
PG1304+491	sdB	2	-8 ± 3	8 ± 7	-0.5731	32430 ± 290	5.68 ± 0.04	-1.77 ± 0.05	2016ApJ...818..202L



SDSSJ130839.24+201132.9	sdOB	7	-42 ± 12	86 ± 57	-0.2744	38337 ± 2000	5.64 ± 0.20	-0.18 ± 0.40	2009PhDT.....273H
PG1310+179	sdOB	2	48 ± 5	85 ± 17	-5.7762	34650 ± 486	5.40 ± 0.08	-1.88 ± 0.06	2019ApJ...881....7L
PG1313+165	sdB	11	-25 ± 3	78 ± 20	-3.9297	32371 ± 964	5.81 ± 0.15	-2.10 ± 0.20	2017OAs...26..164G
PG1315+013	sdB	16	59 ± 3	48 ± 15	-1.0878	24393 ± 1282	4.92 ± 0.18	-2.00 ± 0.20	2017OAs...26..164G
SDSSJ131934.62+092947.1	sdB	5	33 ± 4	20 ± 28	-0.0167	25769 ± 1439	5.23 ± 0.21	-2.20 ± 0.20	2017OAs...26..164G
CBS350	sdB	2	-23 ± 4	37 ± 8	-5.0104	30566 ± 223	5.80 ± 0.05	-3.12 ± 0.25	2019ApJ...881....7L
SDSSJ132357.27+261502.5	sdB	11	-7 ± 3	62 ± 15	-3.5932	27330 ± 780	5.21 ± 0.09	-2.21 ± 0.14	2019ApJ...881..135L
PB166	He-sdOB	3	-34 ± 3	36 ± 7	-6.0389	21579 ± 268	4.95 ± 0.03	-1.03 ± 0.06	
SDSSJ132432.37+320420.9	sdB	3	-214 ± 2	26 ± 7	-2.9056	26957 ± 447	5.61 ± 0.07	-2.18 ± 0.07	2019ApJ...881....7L
SDSSJ132526.74+233225.2	sdOB	8	19 ± 8	93 ± 36	-0.4601	33820 ± 966	5.84 ± 0.15	-1.40 ± 0.20	2017OAs...26..164G
SDSSJ132602.78+102522.3	sdB	6	-166 ± 9	81 ± 32	-0.787	24480 ± 635	5.24 ± 0.09	-2.20 ± 0.39	
SDSSJ133040.91-001710.7	sdB	12	-17 ± 3	162 ± 17	-55.8315	28606 ± 305	5.70 ± 0.06	-2.50 ± 0.14	
PG1329+159	sdB+dM	3	-10 ± 3	21 ± 8	-1.2204	29100 ± 1000	5.62 ± 0.15	-2.40 ± 0.10	2001MNRAS.326.1391M
PG1331+591	sdB	3	-83 ± 3	1 ± 9	-0.0048	33400 ± 590	5.14 ± 0.08	-0.99 ± 0.07	2016ApJ...818..202L
SDSSJ133512.81+195155.8	sdOB	11	-22 ± 5	90 ± 24	-5.22	34195 ± 959	5.79 ± 0.16	-1.60 ± 0.20	2017OAs...26..164G
SDSSJ133543.00+330558.4	He-sdO	4	-89 ± 8	25 ± 39	-0.0357	44022 ± 423	5.69 ± 0.12	1.04 ± 0.20	
SDSSJ133555.73+125137.6	sdB	5	-23 ± 13	26 ± 48	-0.0076	34883 ± 990	5.50 ± 0.11	-2.70	
SDSSJ133620.23+180031.7	sdB	9	116 ± 7	107 ± 43	-1.4963	27953 ± 456	5.30 ± 0.07	-3.00	
PG1336-018	sdB V+dM	2	-16 ± 3	111 ± 8	-41.7734	32800 ± 500	5.76 ± 0.05	-2.94 ± 0.14	2008A&A...489..377C
PG1338+481	sdB	4	8 ± 2	83 ± 7	-28.4979	28360 ± 300	5.50 ± 0.05	-2.82 ± 0.13	2016ApJ...818..202L
PG1339+052	sdO	9	78 ± 4	192 ± 23	-38.3576	70000 ± 5000	6.40 ± 0.60	-1.28 ± 0.21	
SDSSJ134133.71+071849.7	sdOB	10	-108 ± 10	93 ± 60	-0.2597	38549 ± 2000	5.58 ± 0.20	-1.70 ± 0.40	2009PhDT.....273H
SDSSJ134600.02+013558.1	sdB	10	13 ± 7	235 ± 37	-9.0121	25285 ± 519	4.94 ± 0.11	-1.68 ± 0.20	
SDSSJ134621.23+224836.7	He-sdOB	7	33 ± 6	21 ± 24	-0.0149	38263 ± 394	5.80 ± 0.07	-0.04 ± 0.06	
SDSSJ134635.67-001804.5	sdB	8	134 ± 10	68 ± 51	-0.0612	21806 ± 893	4.86 ± 0.11	-1.81 ± 0.21	
SDSSJ134748.59+080616.1	sdB	7	-57 ± 9	62 ± 35	-0.3024	29826 ± 469	5.46 ± 0.07	-2.53 ± 0.36	
SDSSJ134947.70+250810.9	sdB	7	-24 ± 3	156 ± 14	-47.7129	29255 ± 828	5.64 ± 0.10	-3.00	2019MNRAS.486.2169K
SDSSJ135059.00+285921.9	sdB	12	7 ± 4	46 ± 29	-0.0955	24671 ± 455	4.98 ± 0.01	-1.56 ± 0.06	2019ApJ...881....7L
PG1349-012	sdB	4	-125 ± 3	275 ± 10	-175.4274	30970 ± 920	5.67 ± 0.19	-2.63	2016ApJ...818..202L
PG1353+162	sdOB	7	-42 ± 3	28 ± 17	-0.3067	37330 ± 915	5.86 ± 0.13	-1.50 ± 0.20	2017OAs...26..164G
PG1353+152	sdB	2	-24 ± 5	48 ± 10	-5.2828	29210 ± 190	5.48 ± 0.04	-2.39 ± 0.06	2019ApJ...881..135L
SDSSJ135728.14+065038.5	sdO	10	76 ± 7	83 ± 42	-0.2542	46220 ± 2191	5.60 ± 0.09	-2.52 ± 0.35	
PG1355+071	sdB	2	0 ± 3	82 ± 7	-27.6925	27680 ± 570	5.36 ± 0.09	-2.95 ± 0.64	2012MNRAS.427.2180N
SDSSJ135920.78+320846.5	sdOB	10	20 ± 7	77 ± 45	-0.1886	38049 ± 2000	5.76 ± 0.20	-0.59 ± 0.40	2009PhDT.....273H
SDSSJ140118.73-012024.8	sdB	10	-114 ± 5	30 ± 27	-0.0045	33651 ± 919	5.84 ± 0.14	-2.20 ± 0.20	2017OAs...26..164G
SDSSJ140453.68+124428.5	He-sdOB	6	-47 ± 6	27 ± 25	-0.0332	38708 ± 321	5.71 ± 0.08	0.35 ± 0.05	
PG1403+019	sdB	10	-36 ± 3	99 ± 16	-10.5954	27300 ± 800	5.37 ± 0.16	-1.90 ± 0.20	2015A&A...577A..26G
SDSSJ140839.10+653124.4	sdB	12	-169 ± 6	54 ± 42	-0.0466	30599 ± 1026	5.65 ± 0.16	-2.40 ± 0.20	2017OAs...26..164G
SDSSJ141259.92+050619.0	sdB	8	106 ± 10	82 ± 52	-0.1564	30466 ± 727	5.65 ± 0.10	-2.70	
PG1412+299	sdB	10	-26 ± 3	72 ± 10	-7.2054	24980 ± 300	5.68 ± 0.04	-3.00	2019ApJ...881..135L
KUV14128+2741	sdB	7	-58 ± 3	35 ± 23	-0.2804	28630 ± 230	5.47 ± 0.03	-2.40 ± 0.13	2019ApJ...881..135L
SDSSJ141558.19-022714.3	sdOB	12	32 ± 7	200 ± 57	-7.0277	37112 ± 1186	5.81 ± 0.09	-2.69 ± 0.28	
PB3580	sdOB	2	-70 ± 3	12 ± 7	-0.8842	34961 ± 907	5.74 ± 0.13	-1.80 ± 0.20	2017OAs...26..164G
PG1423-013	sdO+WD?	9	-42 ± 4	27 ± 19	-0.0492	52662 ± 1000	5.50 ± 0.10	-1.61 ± 0.10	2007A&A...462..269S
SDSSJ142559.17+284715.2	sdOB	3	-138 ± 3	8 ± 7	-0.2321	35647 ± 251	5.67 ± 0.04	-1.86 ± 0.04	2019ApJ...881....7L
SDSSJ142625.09+141200.2	sdB	8	16 ± 4	22 ± 15	-0.1245	18334 ± 1655	4.76 ± 0.22	-1.98 ± 0.38	
PG1425+019	sdB	8	33 ± 3	244 ± 14	-145.9673	30254 ± 250	5.59 ± 0.03	-3.00	

SDSSJ142803.07+055855.4	sdOB	7	-93 ± 7	37 ± 27	-0.0891	40145 ± 2000	5.84 ± 0.20	-0.28 ± 0.40	2009PhDT.....273H
SDSSJ142821.87+135945.2	sdB	6	-213 ± 8	112 ± 49	-2.0261	21267 ± 753	4.65 ± 0.08	-2.18 ± 0.55	
SDSSJ142939.35+152623.6	He-sdOB	6	-90 ± 14	85 ± 58	-0.1746	38741 ± 806	5.96 ± 0.13	-0.17 ± 0.08	
PG1428+513	He-sdO	8	-91 ± 4	39 ± 22	-0.3056	47224 ± 397	5.66 ± 0.05	3.40 ± 0.48	
SDSSJ143026.15+195346.7	sdB	6	51 ± 6	65 ± 21	-1.4724	29069 ± 1159	5.40 ± 0.17	-2.70 ± 0.20	2017Ost...26..164G
SDSSJ143127.88+014416.2	sdB	8	-62 ± 9	102 ± 43	-0.7313	31200 ± 600	5.32 ± 0.10	-2.60 ± 0.30	
SDSSJ143153.06+002824.3	sdOB	8	-4 ± 10	68 ± 35	-0.2878	37300 ± 800	6.02 ± 0.16	-0.80 ± 0.10	2015A&A...577A..26G
LBQS1430+0132	sdB	8	37 ± 4	43 ± 31	-0.1562	29500 ± 500	5.41 ± 0.06	-2.80 ± 0.20	
PG1432+158	sdB+WD	2	11 ± 4	148 ± 8	-63.9136	26210 ± 210	5.47 ± 0.05	-2.52 ± 0.10	2018ApJ...868...70L
SDSSJ143729.14+021506.0	He-sdOB	6	-25 ± 5	30 ± 19	-0.1417	37709 ± 404	5.80 ± 0.09	-0.11 ± 0.07	
SDSSJ143917.64+010251.0	sdB	2	44 ± 3	4 ± 7	-0.2374	27595 ± 236	5.31 ± 0.04	-1.96 ± 0.04	2021ApJS...256...28L
PG1438-029	sdB+dM	2	-32 ± 3	22 ± 7	-2.6418	29280 ± 240	5.41 ± 0.06	-2.89 ± 0.15	2016ApJ...818..202L
PG1439-013	sdO+WD	3	8 ± 4	69 ± 11	-7.4455	43080 ± 2990	4.92 ± 0.16	-2.70 ± 0.54	2016ApJ...818..202L
SDSSJ144301.69+514410.3	sdB	7	-174 ± 4	27 ± 15	-0.2521	21148 ± 893	4.78 ± 0.11	-2.00 ± 0.22	2019MNRAS.486.2169K
SDSSJ144513.66+010112.73	sdB	16	33 ± 2	39 ± 19	-1.4578	19714 ± 221	4.98 ± 0.04	-3.24 ± 0.16	2021ApJS...256...28L
SDSSJ144634.32+191202.8	sdOB	2	79 ± 13	104 ± 40	-1.9681	33311 ± 1149	5.18 ± 0.18	-2.50 ± 0.20	2017Ost...26..164G
SDSSJ144820.93+320956.1	sdB	4	-33 ± 6	33 ± 24	-0.222	27868 ± 639	5.38 ± 0.09	-2.37 ± 0.10	2019ApJ...881....7L
SDSSJ144836.90+230955.5	sdB	4	66 ± 3	33 ± 10	-2.7213	19207 ± 23	4.81 ± 0.02	-3.54 ± 0.18	2019ApJ...881....7L
SDSSJ145049.50+624940.8	sdB	6	-155 ± 7	30 ± 25	-0.0902	29715 ± 583	5.74 ± 0.11	-2.70	
SDSSJ145203.94+453329.6	sdO	7	-209 ± 6	32 ± 23	-0.0448	50951 ± 1927	5.93 ± 0.07	-1.97 ± 0.08	
PG1451+397	sdB	7	-31 ± 4	130 ± 19	-23.4269	30110 ± 470	5.81 ± 0.11	-2.68 ± 0.28	2019ApJ...881..135L
SDSSJ145412.79+213216.0	sdB	6	-21 ± 6	24 ± 21	-0.0535	24420 ± 1293	5.29 ± 0.18	-2.00 ± 0.20	2017Ost...26..164G
SDSSJ145419.32+020323.7	He-sdOB	11	29 ± 6	160 ± 47	-1.9611	37809 ± 511	5.75 ± 0.08	-0.02 ± 0.05	
PG1452+475	sdB	8	44 ± 3	54 ± 20	-2.0907	27233 ± 1102	5.57 ± 0.16	-2.30 ± 0.20	2017Ost...26..164G
SDSSJ145506.86+094204.0	sdB	7	88 ± 5	46 ± 21	-0.8973	34181 ± 956	5.55 ± 0.15	-3.00 ± 0.20	2017Ost...26..164G
SDSSJ145600.56+055904.0	sdO	4	190 ± 7	56 ± 28	-1.6878	55278 ± 3988	5.62 ± 0.16	-1.91 ± 0.17	
SDSSJ150013.05+060410.5	sdB	5	163 ± 10	62 ± 38	-0.5173	35129 ± 1208	5.93 ± 0.16	-2.00 ± 0.42	2019MNRAS.486.2169K
SDSSJ150115.02+053739.4	sdB	2	-38 ± 5	0 ± 11	0	26748 ± 1415	4.86 ± 0.20	-2.40 ± 0.20	2017Ost...26..164G
SDSSJ150150.23+130549.2	sdB	4	-81 ± 5	33 ± 27	-0.4521	21945 ± 907	4.95 ± 0.12	-2.52	2019MNRAS.486.2169K
SDSSJ150222.35+320220.9	sdB	8	-110 ± 6	57 ± 27	-0.32	31400 ± 300	5.52 ± 0.05	-3.00 ± 0.20	
SDSSJ150230.30+091357.3	sdOB	8	23 ± 6	48 ± 30	-0.2406	34711 ± 930	5.75 ± 0.14	-1.50 ± 0.20	
SDSSJ150308.17+405009.1	sdB	8	21 ± 7	68 ± 51	-0.1321	21000 ± 1162	4.74 ± 0.11	-2.03 ± 0.37	
CBS302	sdB+WD	6	-116 ± 7	80 ± 25	-1.4963	29600 ± 600	5.73 ± 0.07	-2.30 ± 0.10	
PG1507-015	He-sdO	15	-128 ± 4	54 ± 18	-0.3325	45150 ± 378	5.78 ± 0.08	3.05 ± 1.07	
SDSSJ151231.28+005317.7	sdOB	15	-80 ± 7	128 ± 61	-0.0665	36075 ± 935	6.00 ± 0.14	-1.00 ± 0.20	
SDSSJ151254.55+150447.0	sdOB	8	-14 ± 7	26 ± 25	-0.0083	38300 ± 600	6.01 ± 0.10	-1.50 ± 0.10	2017Ost...26..164G
SDSSJ151306.71+011439.1	sdB	14	-14 ± 4	159 ± 21	-30.6496	27545 ± 1195	5.47 ± 0.17	-2.30 ± 0.20	2015A&A...577A..26G
PG1512+244	sdB+WD	3	23 ± 3	167 ± 8	-92.7362	29900 ± 900	5.74 ± 0.10	-2.00 ± 0.10	2001MNRAS.326.1391M
SDSSJ151613.21+273854.9	sdO	2	0 ± 4	13 ± 9	-0.7869	58250 ± 1579	5.86 ± 0.05	-1.91 ± 0.10	
PG1515+232	sdB	14	-20 ± 3	147 ± 18	-51.6037	27576 ± 253	5.41 ± 0.08	-2.37 ± 0.14	
SDSSJ151902.41+071535.3	sdB	25	-56 ± 6	121 ± 42	-1.4828	29481 ± 937	5.61 ± 0.14	-2.63 ± 0.35	2019MNRAS.486.2169K
PG1518+299	sdOB	2	-162 ± 3	7 ± 7	-0.4792	37890 ± 480	6.03 ± 0.07	-1.21 ± 0.08	2018ApJ...868...70L
SDSSJ152427.24+120207.6	sdB	5	-85 ± 4	70 ± 16	-9.711	30530 ± 983	5.67 ± 0.14	-2.00 ± 0.20	2017Ost...26..164G
SDSSJ152458.81+181940.5	sdO	12	-17 ± 6	69 ± 28	-0.1196	50549 ± 3422	5.59 ± 0.11	-2.69 ± 0.25	
SDSSJ152607.88+001640.7	He-sdO	14	46 ± 4	48 ± 35	-0.0048	68015 ± 5997	5.38 ± 0.12	-0.63 ± 0.05	
SDSSJ152702.21+420407.1	sdB	4	0 ± 6	34 ± 19	-0.8621	29168 ± 1020	5.58 ± 0.16	-3.00 ± 0.20	2017Ost...26..164G
SDSSJ152707.20+101612.5	sdB	2	-24 ± 6	11 ± 12	-0.433	33744 ± 1072	5.12 ± 0.16	-2.20 ± 0.20	2017Ost...26..164G

PG1525+107	sdOB	5	-93 ± 3	31 ± 13	-1.3635	35120 ± 320	5.75 ± 0.06	-1.36 ± 0.04	2019ApJ...881..135L
SDSSJ152852.27+093144.2	sdB	11	-62 ± 2	60 ± 20	-4.6262	32580 ± 915	5.85 ± 0.13	-1.80 ± 0.20	2017OAS...26..164G
SDSSJ152905.62+002137.5	sdB	9	11 ± 10	53 ± 54	-0.014	34696 ± 972	6.06 ± 0.15	-1.30 ± 0.20	2017OAS...26..164G
PG1528+025	He-sdO	2	29 ± 9	16 ± 22	-0.3196	57258 ± 1470	5.85 ± 0.15	2.98 ± 0.86	
CBS250	sdB	2	-15 ± 3	2 ± 7	-0.1071	32508 ± 85	5.83 ± 0.02	-1.64 ± 0.03	2019ApJ...881....7L
PG1528+104	sdB+WD	2	-21 ± 3	2 ± 7	-0.0992	28954 ± 271	5.69 ± 0.04	-2.63 ± 0.06	2021ApJS...256...28L
SDSSJ153204.35+324152.7	He-sdOB	6	-147 ± 6	60 ± 39	-0.4923	40716 ± 278	5.76 ± 0.02	-0.09 ± 0.06	
SDSSJ153218.00+120243.1	sdOB	6	88 ± 8	120 ± 42	-3.6333	40226 ± 877	6.16 ± 0.15	-1.22 ± 0.21	
PG1532+522	sdB	2	-84 ± 4	17 ± 9	-1.1358	31510 ± 470	5.89 ± 0.11	-2.40 ± 0.17	2016ApJ...818..202L
SDSSJ153529.06+053838.2	sdB	10	47 ± 10	60 ± 49	-0.0108	27665 ± 724	5.61 ± 0.13	-3.00	
SDSSJ153752.95+160201.8	sdB	12	-117 ± 7	64 ± 37	-0.2332	32300 ± 500	5.47 ± 0.07	-3.00	2015A&A...577A..26G
SDSSJ153834.07+030812.9	sdOB	16	30 ± 3	105 ± 20	-16.2657	34469 ± 849	5.94 ± 0.11	-1.77 ± 0.28	2019MNRAS...486.2169K
PG1538+401	sdB	2	-20 ± 4	48 ± 8	-7.5257	33800 ± 1510	5.91 ± 0.19	-2.76	2016ApJ...818..202L
PG1539+442	He-sdO	7	-44 ± 5	31 ± 19	-0.1673	45449 ± 571	5.60 ± 0.07	3.55 ± 0.41	
SDSSJ154227.88+310601.9	He-sdO	16	-185 ± 4	68 ± 25	-0.4524	51627 ± 479	5.62 ± 0.07	3.50 ± 0.13	
SDSSJ154531.01+563944.7	sdB	7	-104 ± 5	31 ± 20	-0.1025	26200 ± 900	5.13 ± 0.14	-2.00 ± 0.20	2015A&A...577A..26G
SDSSJ154720.93+055937.8	sdB	10	14 ± 3	56 ± 14	-2.7787	28570 ± 1240	5.46 ± 0.13	-1.82 ± 0.38	2016ApJ...818..202L
SDSSJ154958.29+043820.2	He-sdOB	7	-135 ± 11	57 ± 42	-0.1613	37073 ± 505	5.81 ± 0.09	-0.94 ± 0.05	
SDSSJ155041.99+294523.5	sdB	5	-4 ± 4	15 ± 13	-0.1311	30422 ± 820	5.60 ± 0.10	-2.10 ± 0.23	2019MNRAS...486.2169K
SDSSJ155128.45-011826.8	sdB	2	-115 ± 5	55 ± 13	-4.2387	28464 ± 781	5.59 ± 0.09	-2.60 ± 0.24	2020MNRAS...498...12H
PG1549+006	sdB	2	-60 ± 3	14 ± 7	-1.1092	33610 ± 1660	5.66 ± 0.29	-1.93 ± 0.25	2016ApJ...818..202L
SDSSJ155202.72+261542.9	He-sdOB	5	-31 ± 5	65 ± 36	-0.3076	36216 ± 662	5.97 ± 0.12	-0.61 ± 0.07	
PG1553+272	sdB	2	92 ± 4	75 ± 10	-13.1951	22100 ± 900	4.74 ± 0.10	-3.00 ± 0.10	2001MNRAS...326.1391M
PG1555+504	He-sdO	9	-39 ± 4	53 ± 26	-1.6179	66853 ± 1163	5.71 ± 0.06	3.52 ± 1.02	
SDSSJ15806.89+254438.2	sdB	5	-12 ± 5	79 ± 26	-2.5379	33718 ± 364	5.77 ± 0.07	-1.87 ± 0.08	2019ApJ...881....7L
SDSSJ15846.44+192219.1	sdO	8	-35 ± 6	46 ± 30	-0.1931	62277 ± 2943	5.71 ± 0.06	-1.12 ± 0.05	
SDSSJ160322.84+093859.4	sdB	12	25 ± 5	46 ± 26	-0.1505	31064 ± 982	5.78 ± 0.14	-3.00 ± 0.20	2017OAS...26..164G
SDSSJ160332.84+514827.9	sdOB	10	-45 ± 4	79 ± 34	-1.6222	36332 ± 961	5.81 ± 0.17	-1.10 ± 0.20	2017OAS...26..164G
SDSSJ160341.45+314322.7	sdB	8	-213 ± 8	113 ± 25	-3.2925	33518 ± 1356	5.42 ± 0.14	-3.00	
SDSSJ160345.26+080153.2	sdB	10	13 ± 7	56 ± 35	-0.0904	34724 ± 800	5.93 ± 0.10	-1.83 ± 0.09	
SDSSJ160453.45+115218.3	sdOB	11	-39 ± 6	68 ± 49	-0.2385	37302 ± 911	5.82 ± 0.15	-1.00 ± 0.20	2017OAS...26..164G
PG1606+388	sdOB	9	-48 ± 5	21 ± 21	-0.0045	34684 ± 968	5.78 ± 0.18	-1.00 ± 0.20	2017OAS...26..164G
PG1605+072	sdBY	2	-30 ± 4	31 ± 16	-1.2107	32550 ± 370	5.29 ± 0.07	-2.51 ± 0.14	2016ApJ...818..202L
SDSSJ160810.17+425845.0	sdB	4	-128 ± 13	200 ± 44	-7.8086	30108 ± 718	5.55 ± 0.12	-3.00	
SDSSJ160835.68+045345.2	He-sdOB	7	-168 ± 12	63 ± 51	-0.0374	39465 ± 287	5.40 ± 0.05	0.48 ± 0.05	
SDSSJ160911.42+314627.6	sdB	9	-31 ± 10	86 ± 48	-0.1247	29438 ± 639	5.50 ± 0.10	-2.32 ± 0.42	2017OAS...26..164G
SDSSJ160911.90+134744.1	sdB	10	-111 ± 8	100 ± 34	-0.6298	34856 ± 1053	5.45 ± 0.17	-2.50 ± 0.20	
SDSSJ161059.80+053625.2	He-sdO	10	-231 ± 5	82 ± 25	-1.0672	48067 ± 669	5.80 ± 0.08	3.37 ± 0.94	
SDSSJ161109.12+105705.6	sdO	4	-89 ± 17	41 ± 50	-0.0538	69000 ± 4182	6.05 ± 0.13	-1.41 ± 0.13	2017OAS...26..164G
SDSSJ161129.89+095004.8	sdOB	11	-7 ± 5	58 ± 44	-0.6496	37520 ± 913	6.05 ± 0.16	-1.00 ± 0.20	2017OAS...26..164G
SDSSJ161132.90+290038.9	sdB	8	-9 ± 3	41 ± 13	-1.9659	28513 ± 1178	5.39 ± 0.17	-3.00 ± 0.20	2017OAS...26..164G
PG1609+195	sdOB	9	-41 ± 4	19 ± 16	-0.0177	33136 ± 918	5.73 ± 0.13	-1.70 ± 0.20	2017OAS...26..164G
PG1610+519	sdOB+WD	2	-16 ± 6	68 ± 12	-7.5496	34620 ± 380	5.08 ± 0.05	-3.00	2018ApJ...868...70L
PG1610+043	He-sdO	10	4 ± 3	30 ± 19	-0.1176	47024 ± 510	5.78 ± 0.09	3.46 ± 0.77	
SDSSJ161400.07+150947.3	sdOB	7	-2 ± 6	46 ± 26	-0.1772	37601 ± 960	6.00 ± 0.15	-1.40 ± 0.20	2017OAS...26..164G
SDSSJ161507.08+105513.5	He-sdO	5	-118 ± 6	56 ± 21	-1.1198	49396 ± 933	5.77 ± 0.05	2.97 ± 0.34	
SDSSJ161603.28+101210.6	He-sdO	8	-87 ± 7	75 ± 36	-0.8794	62302 ± 1197	6.00 ± 0.07	-0.72 ± 0.06	

SDSSJ161921.70+295506.1	sdB	11	-92 ± 3	43 ± 16	-2.256	34115 ± 933	5.79 ± 0.15	-2.00 ± 0.20	2017Ost...26..164G
SDSSJ162250.09+002631.9	sdB	7	-15 ± 6	93 ± 22	-3.2714	29782 ± 1047	5.51 ± 0.16	-2.20 ± 0.20	2017Ost...26..164G
PG1621+476	sdB+BD	7	-62 ± 4	96 ± 20	-9.765	29000 ± 600	5.65 ± 0.06	-1.90 ± 0.10	2015A&A...577A..26G
SDSSJ162411.53+312252.6	He-sdO	10	-154 ± 5	64 ± 28	-0.6984	54614 ± 1536	5.77 ± 0.07	1.06 ± 0.31	
SDSSJ162429.73+333408.1	sdB	7	28 ± 8	58 ± 38	-0.0883	18339 ± 677	4.59 ± 0.11	-2.34 ± 0.41	
PG1622+411	sdB	2	-7 ± 3	6 ± 7	-0.358	27590 ± 430	5.29 ± 0.06	-2.53 ± 0.30	2012MNRAS.427.2180N
SDSSJ162435.66+150355.5	He-sdO	10	-35 ± 5	73 ± 41	-1.1169	46765 ± 732	5.86 ± 0.07	3.31 ± 1.15	
SDSSJ162535.78+362039.2	sdB	7	-22 ± 9	146 ± 51	-0.7821	28484 ± 429	5.51 ± 0.07	-2.30 ± 0.28	
SDSSJ162554.94+315435.2	sdB	11	-245 ± 5	92 ± 32	-5.3945	27128 ± 663	5.21 ± 0.12	-2.27 ± 0.45	
SDSSJ162610.34+130401.6	sdB	5	-358 ± 18	24 ± 58	-0.0021	33900 ± 500	5.63 ± 0.10	-1.00 ± 0.10	2015A&A...577A..26G
SDSSJ162730.30+203416.9	sdB	8	15 ± 4	18 ± 19	-0.0252	18150 ± 1011	4.93 ± 0.12	-1.90 ± 0.17	
SDSSJ162825.87+353205.1	sdO	4	-315 ± 14	116 ± 40	-1.9064	61915 ± 2669	5.82 ± 0.15	-0.92 ± 0.13	
SDSSJ162936.86+312411.9	sdO	6	-134 ± 10	145 ± 50	-1.2032	57100 ± 3569	5.99 ± 0.16	-2.21 ± 0.26	
SDSSJ163027.19+180233.2	He-sdO	10	-50 ± 6	80 ± 44	-0.3543	48202 ± 749	5.72 ± 0.09	3.41 ± 0.46	
SDSSJ163119.12+114618.0	sdB	9	-22 ± 6	43 ± 28	-0.1127	24013 ± 1378	4.84 ± 0.19	-1.80 ± 0.20	2017Ost...26..164G
PG1629+081	sdOB	4	10 ± 3	100 ± 18	-26.6836	38110 ± 680	5.38 ± 0.09	-2.71 ± 0.29	2012MNRAS.427.2180N
SDSSJ163205.75+172241.3	sdB	8	-155 ± 4	218 ± 19	-64.5515	28160 ± 298	5.40 ± 0.04	-2.72 ± 0.54	
PG1629+179	sdB	8	50 ± 3	30 ± 14	-0.923	37440 ± 2100	5.72 ± 0.19	-3.20 ± 0.69	2016ApJ...818..202L
SDSSJ163213.05+205124.0	sdB	8	-247 ± 6	37 ± 24	-0.1059	29035 ± 1110	5.58 ± 0.16	-1.40 ± 0.20	2017Ost...26..164G
SDSSJ163306.58+003216.2	sdB	12	-72 ± 5	15 ± 29	0	31688 ± 1013	5.62 ± 0.15	-2.70 ± 0.20	2017Ost...26..164G
SDSSJ163310.21+233949.1	sdB	10	-56 ± 7	62 ± 32	-0.2674	33487 ± 944	5.79 ± 0.15	-1.90 ± 0.20	2017Ost...26..164G
SDSSJ163356.54+265538.1	sdOB	2	15 ± 7	23 ± 15	-0.8854	34414 ± 1623	5.51 ± 0.15	-1.81 ± 0.42	
SDSSJ163435.32+262101.7	sdO	2	21 ± 5	32 ± 14	-1.6071	52738 ± 2473	5.70 ± 0.07	-2.21 ± 0.12	
SDSSJ163509.13+000235.0	sdB	12	47 ± 7	61 ± 39	-0.0132	27157 ± 1051	5.40 ± 0.14	-3.00	2019MNRAS.486.2169K
SDSSJ163511.58+291240.5	sdB	8	-115 ± 4	64 ± 23	-1.9427	18035 ± 520	4.59 ± 0.06	-1.71 ± 0.29	
SDSSJ163605.36+130404.1	He-sdOB	13	-168 ± 8	129 ± 56	-0.3693	37616 ± 392	5.74 ± 0.06	-0.22 ± 0.04	
SDSSJ163702.78-011351.7	He-sdO	11	-6 ± 5	50 ± 34	-0.0182	46588 ± 688	5.62 ± 0.08	2.30 ± 0.70	
SDSSJ163715.18+142324.9	sdB	9	-271 ± 6	74 ± 39	-0.7121	26049 ± 1500	5.05 ± 0.21	-2.30 ± 0.20	2017Ost...26..164G
SDSSJ163834.68+265110.2	sdOB	9	-34 ± 5	41 ± 26	-0.0597	36000 ± 300	5.92 ± 0.09	-1.40 ± 0.10	2015A&A...577A..26G
SDSSJ163842.70+224115.6	sdB	8	-111 ± 7	55 ± 35	-0.1798	25542 ± 600	4.97 ± 0.10	-1.75 ± 0.20	
SDSSJ163845.10+295437.2	sdB	5	6 ± 11	161 ± 41	-3.1614	29893 ± 740	5.36 ± 0.12	-3.00	
SDSSJ163932.15+232248.8	sdB	10	-84 ± 4	83 ± 19	-2.0476	22369 ± 1334	5.50 ± 0.13	-3.00	2019MNRAS.486.2169K
SDSSJ164050.80+363650.9	sdO	8	-241 ± 5	51 ± 29	-0.369	43768 ± 719	5.24 ± 0.09	-2.17 ± 0.08	
SDSSJ164125.48+364116.1	sdB	13	-257 ± 8	92 ± 38	-0.5017	31230 ± 1094	5.70 ± 0.16	-2.70 ± 0.20	2017Ost...26..164G
SDSSJ164236.24+351432.3	sdB	16	-229 ± 5	73 ± 41	-0.7312	25688 ± 1351	5.13 ± 0.21	-1.20 ± 0.20	2017Ost...26..164G
SDSSJ164419.44+452326.7	sdB	7	-310 ± 6	23 ± 25	-0.0225	32100 ± 300	5.78 ± 0.05	-3.00	
SDSSJ164453.34+213711.5	sdB	14	-43 ± 5	59 ± 34	-0.0615	25868 ± 1437	5.21 ± 0.21	-2.20 ± 0.20	2017Ost...26..164G
PG1643+209	sdB	11	51 ± 3	19 ± 18	-0.0038	30200 ± 1000	5.62 ± 0.15	-1.60 ± 0.10	1994ApJ...432..351S
PG1644+403	sdB	2	50 ± 4	82 ± 10	-15.6191	29990 ± 300	5.64 ± 0.07	-1.92 ± 0.08	2016ApJ...818..202L
SDSSJ164706.94+345655.9	sdOB	7	-242 ± 10	81 ± 36	-0.6057	35150 ± 2000	4.97 ± 0.20	-0.88 ± 0.40	2009PhDT.....273H
PG1646+250	sdB	14	-3 ± 3	31 ± 17	-0.0089	22001 ± 1143	5.58 ± 0.16	-2.70 ± 0.20	2017Ost...26..164G
PG1648+536	sdB+WD	2	-94 ± 4	141 ± 8	-55.947	31000 ± 740	5.60 ± 0.12	-3.00	2018ApJ...868...70L
SDSSJ165325.75+205659.1	sdB	14	-67 ± 3	31 ± 20	-0.0257	30968 ± 1014	5.62 ± 0.14	-2.70 ± 0.20	2017Ost...26..164G
SDSSJ165446.26+182224.6	sdB	9	-223 ± 8	100 ± 45	-0.5373	30100 ± 500	5.50 ± 0.08	-1.70 ± 0.10	2015A&A...577A..26G
PG1653+131	sdB	2	13 ± 3	3 ± 7	-0.164	25600 ± 900	5.40 ± 0.10	-2.70 ± 0.10	2001MNRAS.326.1391M
SDSSJ165732.52+215660.0	sdOB	6	-164 ± 11	132 ± 50	-0.783	35268 ± 408	6.21 ± 0.09	-1.47 ± 0.07	
SDSSJ165809.14+214046.4	sdB	7	-18 ± 3	49 ± 17	-0.8592	32140 ± 206	6.04 ± 0.06	-1.81 ± 0.04	

SDSSJ165837.43+384748.2	sdB	12	-264 ± 7	86 ± 34	-0.4625	27692 ± 1030	5.55 ± 0.13	-2.00 ± 0.31	2019MNRAS,486.2169K
SDSSJ165939.69+214704.9	sdOB	9	-33 ± 7	42 ± 38	-0.0151	36501 ± 924	5.87 ± 0.14	-1.40 ± 0.20	2017OAJ...26..164G
SDSSJ165957.59+434136.8	sdOB	2	-115 ± 30	143 ± 61	-1.6985	40688 ± 1586	5.65 ± 0.15	-2.67 ± 0.39	
PG1658+337	sdB	5	21 ± 5	75 ± 15	-8.0385	26540 ± 940	5.35 ± 0.16	-3.04 ± 0.39	2016ApJ...818..202L
PG1700+247	sdB	5	-72 ± 4	24 ± 15	-0.5072	26420 ± 620	5.29 ± 0.13	-2.39 ± 0.21	2016ApJ...818..202L
SDSSJ170256.38+241757.9	sdB	8	-26 ± 8	112 ± 45	-1.3368	26400 ± 1000	5.25 ± 0.16	-1.80 ± 0.30	
SDSSJ170406.88+285416.1	sdB	19	23 ± 3	69 ± 23	-2.0936	32676 ± 934	5.82 ± 0.14	-1.90 ± 0.20	2017OAJ...26..164G
SDSSJ170411.22+293546.7	sdB	16	-132 ± 3	80 ± 21	-3.2917	29506 ± 1050	5.54 ± 0.16	-2.50 ± 0.20	2017OAJ...26..164G
SDSSJ170534.62+245326.9	sdOB	5	-46 ± 4	93 ± 17	-13.5382	35140 ± 1090	5.57 ± 0.16	-1.43 ± 0.12	2016ApJ...818..202L
SDSSJ170540.02+292041.2	sdOB	8	-242 ± 6	61 ± 31	-0.346	37553 ± 2000	5.70 ± 0.20	-0.09 ± 0.40	2009PhDT.....273H
SDSSJ170556.15+363221.8	sdO	8	-133 ± 4	30 ± 27	-0.1569	53049 ± 4125	4.78 ± 0.10	-1.19 ± 0.08	
SDSSJ170802.61+220552.6	sdB	7	87 ± 8	52 ± 32	-0.1134	30732 ± 826	5.56 ± 0.09	-2.85 ± 1.02	
SDSSJ170810.97+244341.6	sdOB	7	-92 ± 10	87 ± 39	-0.6135	35600 ± 800	5.58 ± 0.14	-0.80 ± 0.10	2015A&A...577A..26G
SDSSJ170957.39+222745.0	He-sdO	2	-519 ± 9	72 ± 20	-3.4527	56668 ± 612	5.71 ± 0.04	3.50 ± 0.17	
SBSS1709+535	sdB	2	13 ± 3	96 ± 7	-39.71	26028 ± 228	5.69 ± 0.04	-2.38 ± 0.04	2019ApJ...881....7L
SDSSJ171142.45+380525.2	He-sdO	10	-163 ± 5	64 ± 17	-1.3391	46717 ± 510	5.74 ± 0.09	2.81 ± 0.80	
SDSSJ171314.08+404108.9	He-sdO	6	-212 ± 10	99 ± 48	-0.8174	52905 ± 1188	5.68 ± 0.12	-0.49 ± 0.10	
SDSSJ171424.16+614710.9	sdB	9	-25 ± 7	59 ± 39	-0.1852	33170 ± 1012	5.43 ± 0.15	-2.40 ± 0.20	2017OAJ...26..164G
SDSSJ171533.84+365214.7	sdB	12	159 ± 4	40 ± 21	-0.108	22700 ± 700	4.93 ± 0.06	-2.00 ± 0.30	
SDSSJ172119.36+374538.5	sdOB	7	35 ± 5	85 ± 22	-3.0702	37494 ± 913	5.96 ± 0.12	-1.43 ± 0.24	2019MNRAS,486.2169K
SDSSJ173033.53+451537.3	sdO	3	-243 ± 17	189 ± 46	-4.4155	64228 ± 6517	5.66 ± 0.18	-1.13 ± 0.19	
SDSSJ173110.56+530512.5	sdB	2	-83 ± 5	101 ± 38	-2.0426	28746 ± 429	5.54 ± 0.06	-2.76 ± 0.08	2019ApJ...881....7L
PG1733+326	sdOB	6	-57 ± 3	50 ± 13	-5.5089	31350 ± 926	5.76 ± 0.13	-1.80 ± 0.20	2017OAJ...26..164G
SDSSJ174408.22+251657.5	He-sdOB	5	20 ± 7	53 ± 21	-1.2323	39370 ± 367	5.81 ± 0.10	-0.11 ± 0.06	
HS1831+6432	sdOB	5	-100 ± 5	24 ± 19	-0.133	36000 ± 900	5.85 ± 0.10	-1.60 ± 0.20	2003A&A...400..939E
LAMOSTJ184134.30+411535.9	sdB	2	1 ± 3	5 ± 7	-0.3116	24972 ± 365	4.81 ± 0.05	-1.08 ± 0.13	
BD+423250	sdB	5	-10 ± 2	17 ± 7	-0.7083	28700 ± 1000	5.08 ± 0.02	-2.60 ± 0.10	2010A&A...513A..60
TYC3133-2416-1	sdB	5	19 ± 2	22 ± 11	-1.2937	28049 ± 662	5.72 ± 0.09	-2.44 ± 0.16	2019ApJ...881....7L
KBS13	sdB+dM	3	3 ± 3	29 ± 7	-3.4042	31075 ± 111	5.77 ± 0.02	-1.60 ± 0.02	2021ApJS...256..28L
KIC8754603	sdB	2	21 ± 5	215 ± 13	-58.6685	17001 ± 94	6.09 ± 0.02	-2.43 ± 0.13	2019ApJ...881....7L
Kepler-451	sdBV+dM	3	7 ± 3	103 ± 7	-46.3711	29600 ± 500	5.43 ± 0.05	-2.36 ± 0.06	2010MNRAS,408L...510
KIC9543660	sdOB	3	-78 ± 3	35 ± 8	-5.2654	39380 ± 420	5.51 ± 0.03	-3.27 ± 0.51	2018ApJ...868...70L
KIC8054179	He-sdOB	2	-26 ± 3	2 ± 7	-0.1071	39231 ± 570	6.00 ± 0.07	-0.95 ± 0.12	
SDSSJ204358.55-065025.8	He-sdOB	9	-309 ± 11	94 ± 36	-0.5707	36670 ± 644	5.84 ± 0.09	-0.09 ± 0.05	2017OAJ...26..164G
SDSSJ204726.94-060325.7	sdOB	7	14 ± 8	40 ± 34	-0.0367	35133 ± 984	5.79 ± 0.16	-1.40 ± 0.20	2017OAJ...26..164G
SDSSJ210823.60+010155.3	sdB	4	-6 ± 5	157 ± 14	-36.909	23398 ± 1339	5.01 ± 0.18	-2.30 ± 0.20	2017OAJ...26..164G
SDSSJ211045.16+000142.0	sdOB	10	-100 ± 4	44 ± 20	-0.0887	36268 ± 1037	5.35 ± 0.15	-2.10 ± 0.20	2017OAJ...26..164G
PG2110+001	He-sdO	11	23 ± 3	38 ± 21	-0.1557	47035 ± 468	5.69 ± 0.10	2.43 ± 0.78	
SDSSJ211340.26+204256.5	sdB	2	-82 ± 7	12 ± 14	-0.3873	26520 ± 310	5.29 ± 0.03	-2.58 ± 0.08	2018ApJ...868...70L
SDSSJ211440.06+205441.5	sdB	2	-1 ± 5	24 ± 21	-0.5807	30922 ± 283	5.74 ± 0.06	-3.38 ± 0.25	2019ApJ...881....7L
SDSSJ211651.96-003328.5	sdB	10	-64 ± 6	202 ± 31	-34.6154	27900 ± 800	5.78 ± 0.15	-3.90 ± 0.70	2015A&A...577A..26G
PG2116+008	He-sdO	10	-20 ± 3	27 ± 16	-0.0912	47022 ± 585	5.59 ± 0.07	3.29 ± 0.68	
SDSSJ211924.56-004955.5	sdOB	7	-128 ± 10	49 ± 40	-0.051	37035 ± 980	5.87 ± 0.16	-1.10 ± 0.20	2017OAJ...26..164G
SDSSJ212149.44+202216.8	sdOB	2	52 ± 3	26 ± 7	-3.1936	41141 ± 260	5.60 ± 0.04	-2.94 ± 0.15	2019ApJ...881....7L
SDSSJ212300.31+043453.0	sdOB	4	-239 ± 14	283 ± 41	-12.9478	36600 ± 1000	5.76 ± 0.25	-1.20 ± 0.10	
SDSSJ212330.46+004238.8	He-sdOB	4	-65 ± 7	24 ± 23	-0.1599	36267 ± 346	5.85 ± 0.03	-0.65 ± 0.05	
SDSSJ212504.92-000207.0	sdOB	8	-4 ± 5	31 ± 26	-0.0714	36740 ± 580	5.73 ± 0.08	-1.43 ± 0.07	2019ApJ...881...135L

SDSSJ212749.34+002924.1	sdO	8	-69 ± 10	165 ± 35	-5.0654	67202 ± 3019	6.26 ± 0.11	-0.99 ± 0.12	2019ApJ...881....7L
SDSSJ213128.85-003823.0	sdB	8	6 ± 5	27 ± 20	-0.1592	26409 ± 496	5.22 ± 0.12	-1.70 ± 0.19	2017Ost...26..164G
SDSSJ213229.40-004831.3	sdB	8	-5 ± 4	31 ± 20	-0.2053	27048 ± 232	4.98 ± 0.01	-2.35 ± 0.07	2015A&A...577A..26G
SDSSJ213355.34-004512.5	sdB	14	-12 ± 4	41 ± 21	-0.0735	21231 ± 736	4.63 ± 0.09	-2.12 ± 0.23	2015A&A...577A..26G
SDSSJ215049.19+010338.3	sdOB	17	1 ± 6	63 ± 32	-0.1543	35848 ± 970	5.90 ± 0.16	-1.40 ± 0.20	2015A&A...577A..26G
SDSSJ215307.34-071948.3	sdB	13	-2 ± 5	117 ± 39	-1.1397	33100 ± 1300	5.74 ± 0.15	-2.00 ± 0.20	2015A&A...577A..26G
SDSSJ215631.55+121237.6	He-sdO	6	-52 ± 5	21 ± 16	-0.0648	50549 ± 1093	5.83 ± 0.05	3.51 ± 0.21	2015A&A...577A..26G
SDSSJ215648.71+003620.7	sdB	11	-149 ± 5	97 ± 28	-1.4951	30800 ± 800	5.77 ± 0.12	-2.20 ± 0.30	2019MNRAS.486.2169K
SDSSJ215722.90+115908.3	sdOB	2	-88 ± 4	8 ± 12	-0.2882	35382 ± 837	5.94 ± 0.11	-2.22 ± 0.25	2019ApJ...881..135L
SDSSJ215854.10+212432.5	sdB	7	-48 ± 4	21 ± 22	-0.0355	29350 ± 310	5.30 ± 0.10	-2.78	2013A&A...557A.122G
SDSSJ220048.67+123612.4	sdO	4	-349 ± 12	101 ± 40	-1.0732	56708 ± 2174	5.82 ± 0.11	-1.21 ± 0.10	2015A&A...430..223L
HE2201-0001	sdB	8	-100 ± 3	45 ± 22	-0.3276	27062 ± 500	5.51 ± 0.05	-3.29 ± 0.05	2019ApJ...881....7L
LAMOSTJ220427.80+045612.0	sdB	7	-26 ± 3	20 ± 7	-2.0638	30354 ± 194	5.96 ± 0.05	-2.51 ± 0.12	2017Ost...26..164G
SDSSJ220429.52+211610.8	He-sdO	7	-262 ± 6	22 ± 33	-0.0027	49388 ± 1461	5.90 ± 0.11	3.00 ± 1.01	2003A&A...400..939E
SDSSJ220745.48+221640.6	sdOB	8	-57 ± 5	17 ± 21	-0.001	37174 ± 1096	5.47 ± 0.16	-3.00 ± 0.20	2017Ost...26..164G
SDSSJ220759.08+204505.9	sdB	12	-338 ± 3	31 ± 19	-0.0366	23100 ± 500	4.79 ± 0.07	-2.10 ± 0.50	2013A&A...557A.122G
PG2205+023	sdB	2	0 ± 5	15 ± 11	-0.7582	27100 ± 500	5.51 ± 0.05	-4.00	2015A&A...577A..26G
SDSSJ220810.05+115913.9	sdB	11	-52 ± 4	45 ± 24	-0.0988	27200 ± 600	5.23 ± 0.07	-2.30 ± 0.30	2003A&A...400..939E
SDSSJ220922.17+010308.0	sdOB	11	-199 ± 4	16 ± 23	-0.0001	37580 ± 399	5.92 ± 0.09	-0.23 ± 0.07	2017Ost...26..164G
SDSSJ221003.91+123614.6	sdB	14	-151 ± 3	67 ± 16	-5.1445	21741 ± 899	4.75 ± 0.12	-1.94 ± 0.14	2012MNRAS.427.2180N
HS2213+1336	sdB	6	-19 ± 3	32 ± 12	-1.1633	20300 ± 1000	4.75 ± 0.20	-2.30 ± 0.20	2017Ost...26..164G
PG2220+006	sdO	9	-99 ± 3	46 ± 13	-3.2284	47670 ± 1425	5.74 ± 0.06	-2.97 ± 0.23	2005A&A...430..223L
SDSSJ222411.66+393931.3	sdB	8	-45 ± 4	28 ± 15	-0.1094	27895 ± 1067	5.47 ± 0.16	-2.40 ± 0.20	2017Ost...26..164G
HS2225+2220	sdB	12	-29 ± 3	144 ± 18	-21.9139	31500 ± 800	5.85 ± 0.10	-1.60 ± 0.20	2003A&A...400..939E
SDSSJ222932.80-004822.6	sdOB	9	-19 ± 4	40 ± 24	-0.0867	36271 ± 909	5.89 ± 0.13	-1.50 ± 0.20	2017Ost...26..164G
PG2223+143	sdB	2	-20 ± 3	38 ± 7	-6.0313	35020 ± 820	5.26 ± 0.15	-2.72 ± 0.40	2017Ost...26..164G
PG2236+134	sdB	6	-28 ± 3	46 ± 16	-2.426	31566 ± 995	5.48 ± 0.14	-3.00 ± 0.20	2017Ost...26..164G
PG2237+018	sdB	2	-65 ± 4	44 ± 10	-4.8791	25606 ± 500	5.38 ± 0.05	-1.92 ± 0.05	2005A&A...430..223L
SDSSJ224311.68-000442.0	sdB	8	-24 ± 4	35 ± 18	-0.3962	27870 ± 1117	5.48 ± 0.16	-2.20 ± 0.20	2017Ost...26..164G
SDSSJ224518.65+220746.5	sdB	17	-18 ± 3	121 ± 22	-19.5818	34000 ± 800	5.82 ± 0.07	-2.20 ± 0.10	2015A&A...577A..26G
SDSSJ224622.46+220549.4	sdB	13	-164 ± 4	72 ± 35	-0.1779	24786 ± 1389	4.72 ± 0.26	-2.28 ± 0.31	2017Ost...26..164G
SDSSJ224635.23+304812.9	sdB	5	-137 ± 6	35 ± 19	-0.6377	29380 ± 1043	5.52 ± 0.16	-2.70 ± 0.20	2017Ost...26..164G
SDSSJ224733.66+311932.9	sdB	3	-7 ± 4	4 ± 13	-0.0206	28099 ± 1079	5.49 ± 0.16	-2.20 ± 0.20	2017Ost...26..164G
SDSSJ224856.10+300900.8	sdOB	5	-68 ± 8	40 ± 29	-0.2374	35765 ± 926	5.92 ± 0.14	-1.80 ± 0.20	2017Ost...26..164G
SDSSJ225854.98+060546.2	sdB	16	-251 ± 6	115 ± 30	-3.346	27823 ± 541	5.41 ± 0.11	-2.02 ± 0.17	2018ApJ...868....70L
GALEXJ23056+3441	sdB	2	-6 ± 4	138 ± 12	-28.5382	28260 ± 160	5.50 ± 0.01	-2.34 ± 0.03	2019ApJ...881....7L
SDSSJ232110.36+191430.5	sdB	2	-40 ± 3	15 ± 7	-1.4258	29498 ± 337	5.42 ± 0.06	-2.77 ± 0.09	2021ApJS...256...28L
SDSSJ232337.12+183504.47	sdB	5	0 ± 5	41 ± 19	-0.5199	29413 ± 243	6.27 ± 0.04	-4.13 ± 1.42	2009PhDT.....273H
SDSSJ233541.47+000219.4	He-sdO	12	9 ± 2	39 ± 14	-1.4634	71388 ± 7000	5.45 ± 0.20	1.14 ± 0.40	2019ApJ...881....7L
LAMOSTJ235643.27+394250.8	sdB	2	-18 ± 22	2 ± 47	-0.0158	32576 ± 282	5.57 ± 0.08	-4.30 ± 2.49	2019ApJ...881....7L
PG2355+242	sdOB	5	1 ± 6	21 ± 23	-0.079	53970 ± 6490	5.61 ± 0.07	-2.40 ± 0.19	2019ApJ...881..135L